NOTE TO USERS

This reproduction is the best copy available.

UMI®

uOttawa

L'Université canadienne
Canada's university

FACULTÉ DES ÉTUDES SUPÉRIEURES ET POSTOCTORALES

uOttawa

L'Université canadienne
Canada's university

FACULTY OF GRADUATE AND POSDOCTORAL STUDIES

Darren Hutt

AUTEUR DE LA THÈSE / AUTHOR OF THESIS

Ph.D. (Neuroscience)

GRADE / DEGREE

Department of Cellular and Molecular Medicine

FACULTÉ, ÉCOLE, DÉPARTEMENT / FACULTY, SCHOOL, DEPARTMENT

PRA1 and Synaptotagmin VIII: Regulators of Vesicle Trafficking and Fusion

TITRE DE LA THÈSE / TITLE OF THESIS

Johnny Ngsee

DIRECTEUR (DIRECTRICE) DE LA THÈSE / THESIS SUPERVISOR

Jay Baltz

CO-DIRECTEUR (CO-DIRECTRICE) DE LA THÈSE / THESIS CO-SUPERVISOR

EXAMINATEURS (EXAMINATRICES) DE LA THÈSE / THESIS EXAMINERS

Harvey Florman

Christopher Kennedy

William Staines

Nongnuj Tanphaichitr

Gary W. Slater

LE DOYEN DE LA FACULTÉ DES ÉTUDES SUPÉRIEURES ET POSTDOCTORALES /
DEAN OF THE FACULTY OF GRADUATE AND POSTDOCORAL STUDIES

PRA1 and Synaptotagmin VIII: Regulators of Vesicle Trafficking and Fusion

Darren Hutt

665028

This thesis is submitted to the faculty of Graduate and Postdoctoral studies as a partial fulfillment of the Ph.D. program in Neuroscience

Submitted on May 3, 2005

Department of Cellular and Molecular Medicine

Faculty of Medicine

University of Ottawa

© Darren Hutt, Ottawa, Canada 2005

Library and Archives Canada

Published Heritage Branch

395 Wellington Street
Ottawa ON K1A 0N4
Canada

Bibliothèque et Archives Canada

Direction du Patrimoine de l'édition

395, rue Wellington
Ottawa ON K1A 0N4
Canada

Your file Votre référence
ISBN: 0-494-10977-7
Our file Notre référence
ISBN: 0-494-10977-7

NOTICE:
The author has granted a non-exclusive license allowing Library and Archives Canada to reproduce, publish, archive, preserve, conserve, communicate to the public by telecommunication or on the Internet, loan, distribute and sell theses worldwide, for commercial or non-commercial purposes, in microform, paper, electronic and/or any other formats.

The author retains copyright ownership and moral rights in this thesis. Neither the thesis nor substantial extracts from it may be printed or otherwise reproduced without the author's permission.

AVIS:
L'auteur a accordé une licence non exclusive permettant à la Bibliothèque et Archives Canada de reproduire, publier, archiver, sauvegarder, conserver, transmettre au public par télécommunication ou par l'Internet, prêter, distribuer et vendre des thèses partout dans le monde, à des fins commerciales ou autres, sur support microforme, papier, électronique et/ou autres formats.

L'auteur conserve la propriété du droit d'auteur et des droits moraux qui protège cette thèse. Ni la thèse ni des extraits substantiels de celle-ci ne doivent être imprimés ou autrement reproduits sans son autorisation.

In compliance with the Canadian Privacy Act some supporting forms may have been removed from this thesis.

While these forms may be included in the document page count, their removal does not represent any loss of content from the thesis.

Conformément à la loi canadienne sur la protection de la vie privée, quelques formulaires secondaires ont été enlevés de cette thèse.

Bien que ces formulaires aient inclus dans la pagination, il n'y aura aucun contenu manquant.

Canada

Abstract

The work described within my doctoral thesis examines the localization and functional role of the prenylated Rab acceptor 1 (PRA1) in the Rab GTPase cycle and the expression, localization and functional role of synaptotagmin VIII in the mouse sperm acrosome reaction. My work began with the examination of both PRA1 and synaptotagmin VIII. The PRA1 project was taken over by other graduate students while my interests remained focused on elucidating the role of synaptotagmin VIII in sperm.

Rab is a family of small Ras-like GTPases regulating intracellular vesicle transport. Prenylated Rab Acceptor (PRA1) has previously been shown to interact with Rab GTPases and VAMP2. I have examined the subcellular localization of PRA1 and examined the functional significance of its interaction with Rab3A. PRA1 is localized to the Golgi complex while truncation of the carboxy-terminus results in a mislocalization to the ER. I also observed that PRA1 is able to bind weakly to GDP dissociation inhibitor (GDI), a protein involved in the solubilization of membrane-bound Rab GTPases. Furthermore, the addition of PRA1 inhibited the extraction of membrane-bound Rab3A by GDI, suggesting that membrane localization of Rab GTPases is dependent on the opposing action of PRA1 and GDI.

The sperm acrosome is a large secretory granule that undergoes calcium-stimulated exocytosis by a mechanism analogous to neuronal secretion. In neurons, the core SNARE complex, composed of syntaxin (Stx), SNAP-25 and VAMP2, mediates vesicle fusion, while calcium regulation is thought to be accomplished by the synaptotagmin (Syt) family via calcium-dependent binding to syntaxin and SNAP-25. I examined the expression, localization and function of Syt VIII in mouse sperm. I found that Syt VIII is

expressed in spermatozoa and localizes to the acrosome. In addition, the introduction of Syt VIII antibodies and recombinant protein into Streptolysin O permeabilized sperm, resulted in inhibition of the acrosome reaction (AR), suggesting a critical function for this protein. Syt VIII also exhibited Ca^{2+}-dependent binding to Stx2 with an EC_{50} that closely matches the calcium requirement of the AR. Taken together, our data suggest a critical role for Syt VIII and Stx2 in the acrosome reaction.

Table of Contents

Introduction.....1
Rab proteins and vesicle trafficking.....2
Rab GTPases as molecular switches.....2
Rab 1, 5, 27a and 3A as examples of different Rab activities.....7
PRA1 project objectives.....11
SNARE protein and vesicle fusion.....14
The vesicle membrane SNARE (v-SNARE) VAMP.....15
Target membrane SNAREs (t-SNAREs) syntaxin and SNAP-25.....17
SNARE complex.....20
Assembly of the SNARE complex.....22
SNARE complex disassembly by ✔-SNAP and NSF.....26
Synaptotagmin.....27
Synaptotagmin is essential for Ca^{2+}-mediated release.....27
Properties of synaptotagmin.....29
Sperm.....34
The acrosome as a secretory vesicle.....36
SNARE proteins in sperm.....37
Synaptotagmins in sperm.....37
Synaptotagmin VIII.....38
Synaptotagmin VIII project objectives.....40
Materials & Methods.....41
Results.....57
PRA1 Project:
PRA1 localizes primarily to the Golgi complex.....57
GDI1 co-precipitates with PRA1.....57
PRA1 inhibits GDI1-mediated extraction of Rab3A from the membrane.....61
Synaptotagmin VIII Project:
Synaptotagmin VIII is expressed in the testis.....65
Synaptotagmin VIII is present in sperm and localizes to the acrosome.....68
Synaptotagmin VIII is shed upon acrosome reaction.....71
Ca^{2+}-dependence of the acrosome reaction.....74
Ca^{2+}-dependent binding between synaptotagmin and syntaxin isoforms.....76
Inhibition of acrosome reaction by anti-synaptotagmin VIII in capacitated sperm.....85
Inhibition of acrosome reaction by anti-synaptotagmin VIII and anti-syntaxin2 in non-capacitated sperm.....91
Inhibition of acrosome reaction by recombinant synaptotagmins.....94
Inhibition of acrosome reaction by recombinant syntaxins.....94
Discussion.....99
PRA1 Project:
PRA1 is associated with the Golgi complex.....99
GDI1 binds to PRA1.....100
PRA1 inhibits the GDI1-mediated extraction of Rab3A.....101

Conclusions of PRA1 Project.....104
Synaptotagmin VIII Project:
Synaptotagmin VIII is present in sperm.....106
Ca^{2+}-dependence of the acrosome reaction.....109
Ca^{2+} titration of synaptotagmin binding to syntaxin.....111
Anti-synaptotagmin VIII antibodies inhibit the acrosome reaction.....113
Recombinant synaptotagmin inhibits the acrosome reaction.....113
Anti-syntaxin2 does not inhibit acrosome reaction in capacitated sperm.....115
Recombinant syntaxin inhibits the acrosome reaction.....115
Anti-syntaxin2 inhibits the acrosome reaction in non-capacitated sperm.....116
Model of synaptotagmin action in the acrosome reaction.....117
Conclusion of the Synaptotagmin VIII Project.....118
References.....121

List of Figures

Figure 1: Summary of the intracellular localization of Rab isoforms 4
Figure 2: Rab GTPase cycle 6
Figure 3: Rab5 effector scaffold 9
Figure 4: PRA1 structure and amino acid composition 12
Figure 5: PRA isoforms sequence alignment 13
Figure 6: Schematic diagram of the domain arrangement of VAMP 16
Figure 7: Schematic diagram of syntaxin domain arrangement 19
Figure 8: Schematic diagram of the domain arrangement of SNAP-25 21
Figure 9: Ribbon diagram of the SNARE 4-helix bundle 23
Figure 10: Ionic layer of the SNARE core complex 24
Figure 11: SNARE core complex assembly 25
Figure 12: Ribbon diagram of Synaptotagmin with Ca^{2+} coordination sites 28
Figure 13: Sequence alignment of the C2A and C2B of synaptotagmin I and VIII 31
Figure 14: Schematic diagram of the hypothetical Ca^{2+}coordination scheme for the C2A of synaptotagmin I and VIII 33
Figure 15: Membrane regions of the sperm head 35
Figure 16: Immunocytochemical analysis of PRA1 58
Figure 17: In vitro binding analysis of PRA1 and GDI1 60
Figure 18: Western blot analysis of the inhibition of GDI1-mediated extraction of Rab3A by PRA1 62
Figure 19: Quantitative analysis of the inhibition of GDI1-mediated extraction of Rab3A by PRA1 63
Figure 20: Southern blot analysis of synaptotagmin I and VIII 66
Figure 21: Analysis of the specificity of the synaptotagmin VIII antibody 67
Figure 22: Western immunoblot of brain and sperm homogenate 69
Figure 23: Western immunoblot of sperm membrane fractions 70
Figure 24: Immunocytochemical localization of synaptotagmin VIII 72
Figure 25: Synaptotagmin VIII is shed following the acrosome reaction 73
Figure 26: Western blot analysis of synaptotagmin VIII following the acrosome reaction 75
Figure 27: Model of the streptolysin O-mediated permeabilization 77
Figure 28: Calcium titration of the acrosome reaction 78
Figure 29: Western blot of the in vitro binding assay of Syntaxin and synaptotagmin 81
Figure 30: Quantitative analysis of the in vitro binding assay of syntaxin and synaptotagmin 83
Figure 31: Hill plots for the syntaxin and synaptotagmin in vitro binding assay 86
Figure 32: Titration of recombinant streptolysin O in capacitated sperm 89
Figure 33: Inhibition of the acrosome reaction by anti-synaptotagmin VIII 90
Figure 34: Titration of recombinant streptolysin O in non-capacitated sperm 92
Figure 35: Inhibition of the acrosome reaction by anti-syntaxin2 in non-capacitated sperm 93
Figure 36: Inhibition of the acrosome reaction by recombinant synaptotagmins 95
Figure 37: Inhibition of the acrosome reaction by recombinant syntaxins 97

Figure 38: Inhibition of the acrosome reaction by native and denatured recombinant syntaxin and synaptotagmin isoforms 98
Figure 38: Model of the streptolysin O-mediated permeabilization 119
Figure 39: Model of the action of synaptotagmins VI and VIII in mouse sperm 139

List of Tables

Table 1: Function and localization of Rab isoforms 3
Table 2: Function and localization of mammalian syntaxin isoforms 18
Table 3: Function and cellular distribution of yeast syntaxin orthologs 18

List of Abbreviations

AR = acrosome reaction
BHK = baby hamster kidney
BoNT = Botulinum neurotoxin
BSA = bovine serum albumin
CM = crude membrane
DMSO = dimethyl sulfoxide
DTT = dithiothreitol
EC_{50} = half maximal excitatory concentration
ECL = enhanced chemiluminescence
EEA1 = early endosome antigen 1
ER = endoplasmic reticulum
GAP = GTPase activating protein
GDI = GDP dissociation inhibitor
GEF = guanine nucleotide exchange factor
GST = glutathione S-transferase
HA = hemagglutinin
HD = hydrophobic domain
HRP = horse radish peroxidase
IAM = inner acrosomal membrane
IgG = immunoglobulin G
IPTG = isopropyl-beta-D-thiogalactopyranoside
KRB = Krebbs Ringer Bicarbonate
LDVC = large dense core vesicle
NSF = N-ethyl maleimide sensitive factor
OAM = outer acrosomal membrane
PBS = phosphate buffered saline
pfu = plaque forming units
PI3,4P = phosphatidylinositol 3, 4 bisphosphate
PI3K = phosphatidylinositol 3 kinase
PI3P = phosphatidylinositol 3 phosphate
PL = phospholipids
PM = plasma membrane
PMSF = phenyl methyl sulfonyl fluoride
PRA1 = prenylated rab acceptor 1
PS = pachytene spermatocytes
PS = phosphatidyl serine
RIM = Rab interacting molecule
RS = round spermatids
SDS = sodium dodecyl sulphate
SDS-PAGE = sodium dodecyl sulphate polyacrylimide gel electrophoresis
SLO = streptolysin O
SNAP = soluble NSF attachment protein
SNAP-25 = synaptosome associated protein of 25 kDa
SNARE = soluble NSF attachment protein receptors
Stx = syntaxin

SV = synaptic vesicles
Syt = synaptotagmin
TBS = Tris-buffered saline
TeNT = tetanus neurotoxin
TGN = trans Golgi network
TM = transmembrane
TS = Tris Sucrose
VAMP = vesicle associated membrane protein
ZP = zona pellucida

Aknowledgements

I would like to dedicate this work to my parents, Janine and Ronald and my sister Lise-Anne, whose patience and support were instrumental in my ability to complete this journey. Your encouragement gave me the strength I needed to overcome the hurdles that I encountered. I am forever grateful to you. I would like to thank my friends who stood by me and provide me with support when I needed it the most.

Lastly and most importantly, I would like to thank my supervisors, Dr Johnny K Ngsee and Dr Jay M Baltz. You gave me the opportunity to work under your tutelage, and it has been a learning experience that I will take with me throughout my career. You taught me more than how to run an experiment, you taught me how to think about problems and to come up with solutions. These are skills that I will not only use in my future research endeavours, but in my everyday life.

Introduction

Exocytosis is a term utilized to describe both the delivery of lipid and protein components to the plasma membrane (PM) and the release of the content of secretory vesicles into the extracellular milieu. The cells employ two pathways to accomplish these tasks, the constitutive and the regulated secretory pathways. The constitutive secretory pathway is the default track and all of the proteins will be directed to this pathway unless a sorting signal contained within its amino acid sequence dictates its redirection to the regulated secretory pathway. These sorting signals can direct digestive enzymes to the lysosomes, and secreted molecules, such as hormones and neurotransmitters, to secretory vesicles. The idea of synaptic vesicles as an intracellular membrane bound organelle was originally proposed by Fatt & Katz to explain the quantal release of acetylcholine at the neuromuscular junction (Fatt and Katz, 1952). It is now understood that secretory vesicles (SV) are found in a number of specialized cell types, which exhibit regulated secretion such as neuronal and neuroendocrine cells. Following their formation in the *trans* Golgi network (TGN), these secretory vesicles are sequestered near the PM by association with the cytoskeleton until the appropriate signal directs their relocation to the active zone and a subsequent stimulus triggers the docking and fusion at the site of release, known as the active zone. The divergence within the constitutive and regulated pathways occurs within the TGN where cargo molecules and lipid components are concentrated together for assembly into the appropriate type of trafficking vesicle. It is now accepted that membrane-bound vesicles are the transfer units responsible for the exchange of materials between the various subcellular organelles and not just for the regulated delivery of signaling molecules. To date a number of the proteins involved in vesicle formation, trafficking, docking, priming and fusion of these lipid bound organelles to their

site of fusion have been identified and characterized. However, the complete set of proteins is not known and the interplay between the known components remains unclear. The majority of the known information has been derived from studying the trafficking and fusion of synaptic and large dense core vesicles since these pathways have an identifiable endpoint to allow monitoring of the fusion reaction. However, it is of note that most of the proteins shown to have a critical role in the trafficking and fusion of secretory vesicles have homologs involved in other forms of regulated secretion as well as in the constitutive secretory pathway and intracellular trafficking. Much of the research pertaining to intracellular trafficking centers on the identification of novel effectors of vesicle trafficking and fusion as well as elucidation of the function of known components involved in the vesicle cycle.

Rab Proteins and Vesicle Trafficking

Rab GTPases as molecular switches

With over 60 mammalian isoforms, Rab GTPases represent the largest of the 5 subfamilies of the Ras superfamily of proteins. The Rabs are evolutionarily conserved with 11 yeast orthologs having been identified. In both yeast and mammalian cells the Rab isoforms are localized to the various subcellular organelles (Table 1 and Figure 1) making them ideal candidates to mediate the trafficking of a given class of vesicle to the appropriate subcellular compartment. The greater number of Rab isoforms found in mammalian cells could represent the increased complexity within individual trafficking pathways and the emergence of specialized cell types, which require distinct trafficking characteristics. Rab GTPases, as their Ras counterparts, cycle between an active GTP-bound and inactive GDP-bound state and are therefore ideal molecular switches for regulating the orderly progression

Rab	Human chromosomal localization[a]	Rab localization	Possible function
Rab1a	2p14	ER–Golgi intermediate compartment, *cis*-Golgi	ER–Golgi and intra-Golgi transport
Rab1b	11q12	ER–Golgi intermediate compartment, *cis*-Golgi	ER–Golgi and intra-Golgi transport
Rab2a	8p22–q21.3	ER–Golgi intermediate compartment, *cis*-Golgi	Golgi–ER retrograde transport
Rab2b	14		
Rab3a	19p13.2	SV, secretory granules, PM	Regulated neurotransmitter release and other forms of regulated secretion
Rab3b	1p32–p31	Epithelial tight junctions, secretory granules, PM	Regulated secretion
Rab3c	5	SV, PM	Regulated secretion
Rab3d	19p13.2	Secretory granules, PM	Regulated secretion
Rab4a	1q42–q43	EE, RE, PM	EE–PM sorting/recycling
Rab4b	19q13.2		
Rab5a	3p24–p22	EE, CCV, PM, SV	PM–EE transport and EE–EE fusion; EE motility
Rab5b	12q13	EE, CCV, PM	Same as Rab5a?
Rab5c	17q21.2	EE, CCV, PM	Same as Rab5a?
Rab6a	2q14–q21	ER, Golgi, TGN	Retrograde Golgi–ER and intra-Golgi traffic; motility of Golgi–ER vesicles
Rab6b	3q21–q23	ER, Golgi	Golgi–ER transport?
Rab6c	2q31		
Rab7	3q21	LE	EE–LE, LE–lysosome
Rab8a	19p13.1	TGN, post-Golgi secretory vesicles, PM	Polarized secretion; TGN–basolateral PM transport
Rab8b	15q11.2	Secretory granules, PM	Regulated secretion
Rab9a	Xp22.2	LE, TGN	LE–TGN transport
Rab9b	Xq22.1–q22.3		
Rab10	2p24.3–p24.1	TGN	
Rab11a	15q21.3–q22.31	RE, TGN, PM	Endocytic recycling via RE and TGN
Rab11b	19pter–p13.3	RE, TGN, PM	Endocytic recycling via RE and TGN
Rab12	18p11.3	Golgi, secretory granules	
Rab13	12q13	Epithelial tight junctions	Formation of tight junctions
Rab14	9q32–q34.11	Phagosome	
Rab15	14	EE, RE, PM	E–PM recycling
Rab17	2q37.3	Apical EE and basolateral PM	Transcytosis
Rab18	10	EE, RE, PM	E–PM recycling
Rab19	7		
Rab20	13	Apical EE	
Rab21	12q15–12q21.1	TGN, apical PM	TGN apical PM polarized secretion
Rab22a	20p11.23–p11.21	E, PM	
Rab22b	18p11.3	E	
Rab22c			
Rab23	6p11.2–p12.3		Neural patterning (*open brain* mouse)
Rab24	5	ER, ER–Golgi intermediate compartment, LE; soluble?	
Rab25	1	E	
Rab26	16p13.3	Secretory granules	Regulated secretion
Rab27a	15q21	Lysosome-like organelles; melanosomes, cytolytic granules	Lytic granule release; melanosome transport (*ashen* mouse)
Rab27b	18q21.1		
Rab28	4p16.1		
Rab29	1q32		
Rab30	11q12–q14	Golgi	
Rab32	6		
Rab33a	X		
Rab33b	4q28	Golgi	Intra-Golgi transport
Rab34	17q11.2		
Rab35	12		
Rab36	22q11.22		
Rab37	17	Secretory granules	Regulated secretion
Rab38	11q14	Melanosomes	
Rab39a	11q22–23		
Rab39b	Xq28		
Rab40a	X		
Rab40b	17q24		
Rab40c			
Rab41			

Table 1. The human Rab GTPase family: nomenclature, chromosomal and subcellular localization and possible function. Reprinted from Seabra *et al. Trends in Mol Med* 8(1), Seabra *et al.*: 23-30, 2002 with permission from Trends Journals.

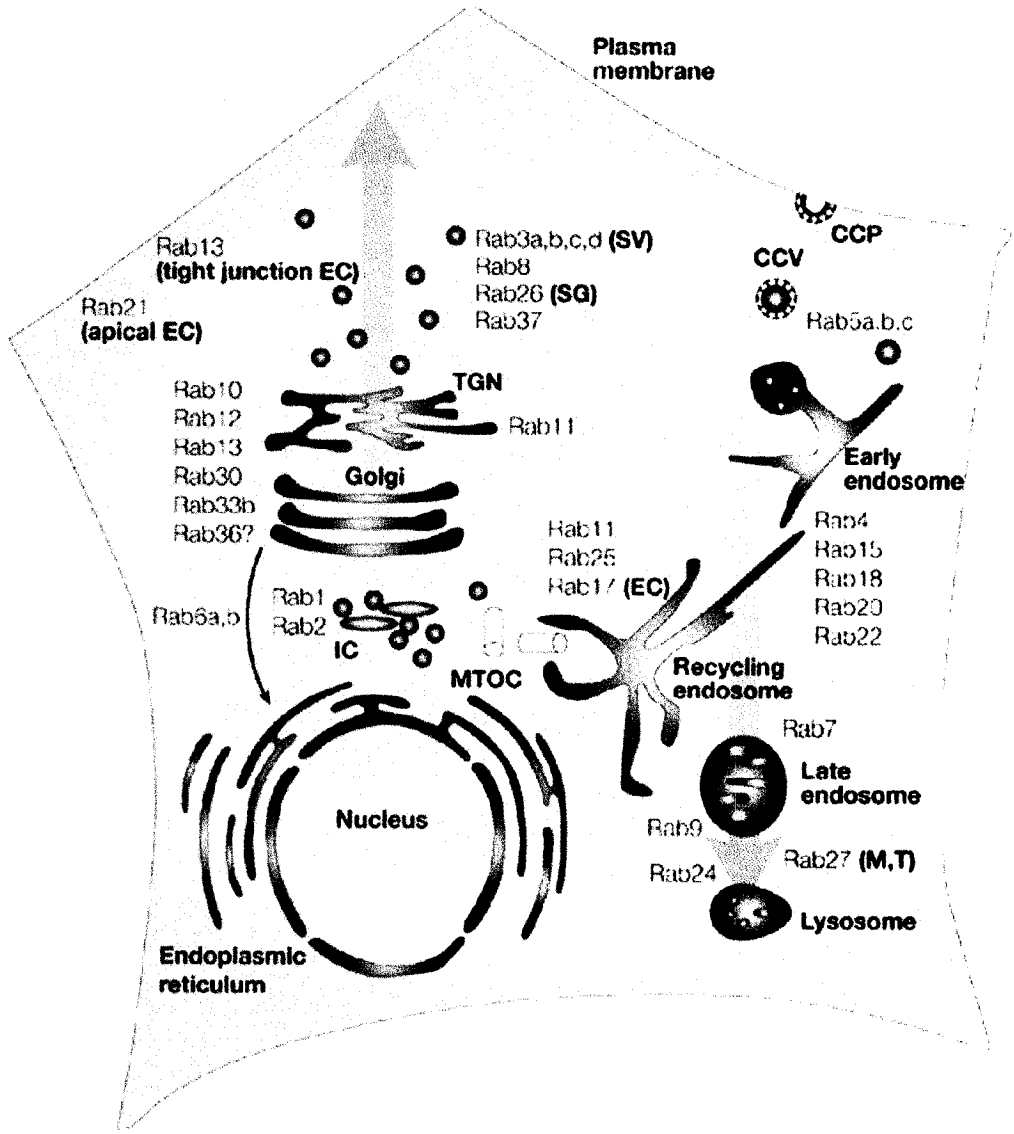

Figure 1. Summary of the intracellular localization of Rab proteins in mammalian cells. Some proteins are cell- (for example, Rab3a in neurons) or tissue-specific (for example, Rab17 in epithelia) or show cell-type-specific localization (for example, Rab13 in tight junctions). (CCV, clathrin-coated vesicle; CCP, clathrin-coated pit; EC, epithelial cells; IC, ER–Golgi intermediate compartment; M, melanosomes; MTOC, microtubule-organizing centre; SG, secretory granules; SV, synaptic vesicles; T, T-cell granules; TGN, *trans*-Golgi network.) Reprinted with permission from the author and *Nature Reviews Mol Cell Biol* 2, Marino Zerial and Heidi McBride, Rab proteins as membrane organizers: 107-119, 2001 (http://www.nature.com/).

of vesicles through membranous compartments of the eukaryotic exocytic and endocytic pathways (Lazar et al., 1997; Martinez and Goud, 1998; Novick and Zerial, 1997; Pereira-Leal and Seabra, 2000; Schimmoller et al., 1998; Segev, 2001a; Segev, 2001b; Zerial and McBride, 2001). The activated GTP-bound form is localized to the membrane whereas the inactive GDP-bound form is bound to the cytosolic carrier GDP dissociation inhibitor (GDI) (Figure 2). Proteins that regulate the cycling between the GDP- and GTP-bound forms are essential for Rab function. Translocation of the Rab GTPase between membrane and cytosol is dependent on GDI which extracts the Rab GTPase from the membrane following GTP hydrolysis as well as participates in the delivery of the GTPase to the correct membrane compartment (Dirac-Svejstrup et al., 1994; Sasaki et al., 1990; Takai et al., 1993) (Figure 2). The Rab GTPase is recruited to the membrane following dissociation from GDI, and GDP-GTP exchange catalyzed by a GDI dissociation factor (GDF) and a guanine nucleotide exchange factor (GEF) (Figure 2). A number of proteins are known to possess GEF activity including rabex-5 that acts specifically on Rab5 (Horiuchi et al., 1997), and a Rab3A-specific guanine nucleotide exchange protein (Wada et al., 1997). Mss4, a small cytosolic protein that interacts with a subset of Rab GTPases (Burton et al., 1994), appears to be involved in this process by transiently binding to the guanine nucleotide-free state (Nuoffer et al., 1997). By analogy to Ras, the GTP-bound form of Rab serves to recruit and activate effector proteins that eventually mediate the various aspects of vesicle trafficking from vesicle formation and cargo recruitment, transport, docking and eventual fusion. Proteins known to interact with the activated form of Rab GTPases include rabphilin-3A (Shirataki et al., 1993) and RIM 1 α /2 α (Wang et al., 1997), rabaptin-5 (Stenmark et al., 1995) and rabkinesin-6 (Echard et al., 1998) which recognize activated Rab3A, Rab5 and Rab6 respectively. Subsequent hydrolysis of the

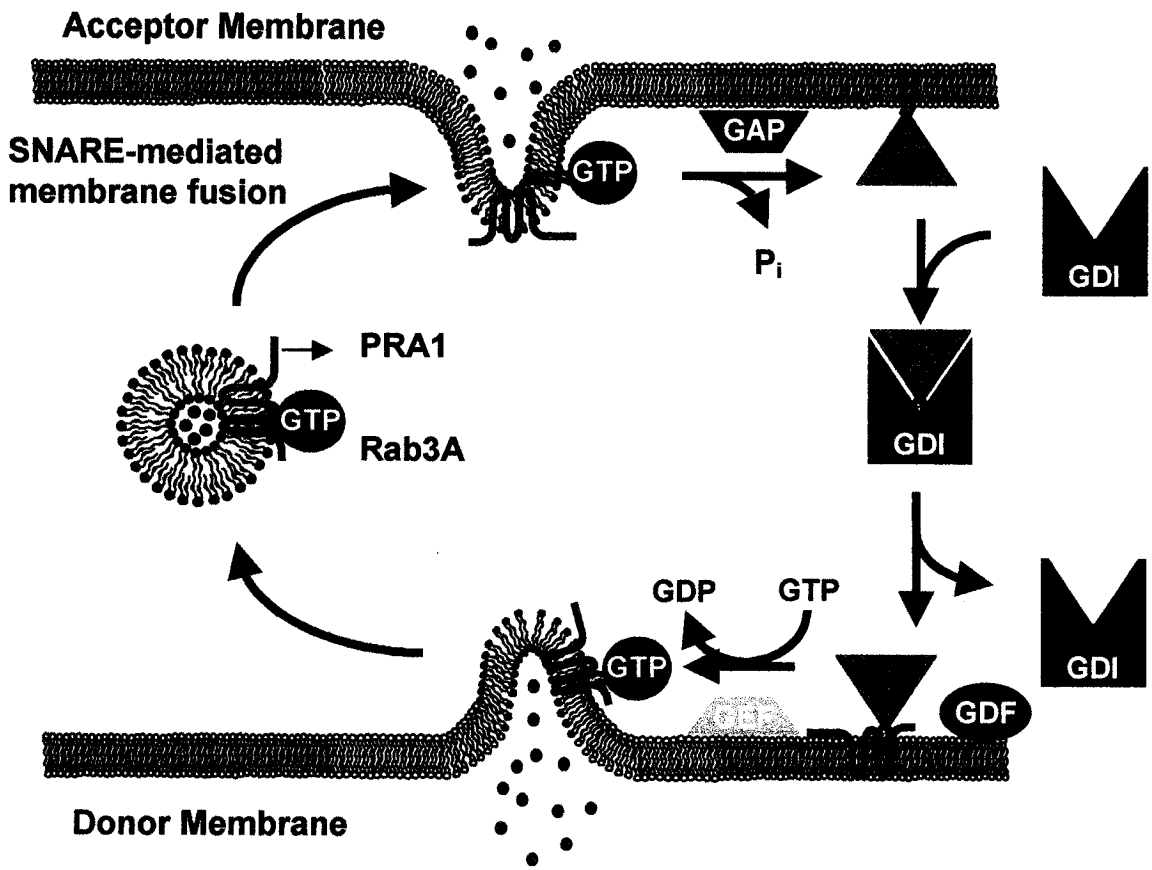

Figure 2. Rab GTPase cycle. The activated GTP-bound Rab3A is recruited to the budding membrane compartment and included in newly formed vesicles. Following vesicle fusion, the intrinsic GTPase activity of Rab3A is stimulated by a GTPase activating protein (GAP), which stimulates the hydrolysis of the GTP to GDP and the subsequent inactivation of Rab3A on the acceptor membrane compartment. This inactive GDP-bound Rab3A is extracted from the acceptor membrane by the GDP dissociation inhibitor 1 (GDI1), which mediates the delivery of the Rab3A to the donor compartment. The release of GDI1 is mediated by a GDI dissociation factor (GDF) and the re-activation of Rab3A is mediated by a guanine nucleotide exchange factor (GEF). PRA1 is shown in purple and is thought to act as a GDF for Rab5, 7 and 9 but not Rab1. No indication for such a function for Rab3A has been shown and therefore the GDF and PRA1 are shown as separate molecules.

bound GTP is thought to terminate the Rab signaling cycle. A GTPase activating protein (GAP), of which a Rab3A-specific (Fukui et al., 1997) and the yeast Ypt/Sec-specific (Albert et al., 1999) forms have been identified, stimulates the low intrinsic GTPase activity of Rab (Figure 2). The resulting GDP-bound Rab is subsequently extracted from the membrane by GDI, which maintains Rab in the cytosol to complete the cycle (Figure 2). Rab mutations altering GTP binding, hydrolysis or interactions with effector molecules are known to block exocytic or endocytic vesicle transport depending on the Rab isoforms targeted. (Gournier et al., 1998; Holz et al., 1995; Pind et al., 1994; Rybin et al., 1996; Turner et al., 1997).

Rab 1, 5, 27a and 3A as examples of different Rab activities

Different Rab isoforms are associated with different subcellular compartments but they appear to perform the similar function of mediating the trafficking and fusion of vesicles. Although the specific function of the Rab proteins remains elusive, some functions attributed to individual isoforms have been elucidated. *In vitro* reconstitution experiments in yeast indicate that the docking of ER-derived vesicles is sensitive to the GTPase, Ypt1p, which in turn regulates Uso1p-dependent tethering of donor vesicles to target membrane (Cao et al., 1998). This suggests that Ypt1p mediate tethering of ER-derived vesicles prior to membrane fusion. This observation is consistent with the proposed role of Rab1, the mammalian ortholog of Ypt1p, in mediating the docking of ER-derived vesicle with the cis-Golgi compartment. Rab1 has been shown to recruit the cytosolic tethering factors p115 to the vesicle (Allan et al., 2000) and to interact with the Golgi membrane proteins GM130 and GRASP (Moyer et al., 2001) to mediate the docking process.

Rabs have also been associated with the endocytic pathway where Rab5 appears to mediate the homotypic fusion of early endosomes (Bucci et al., 1992; Gorvel et al., 1991). Its function centers on the formation of protein scaffolds that include a number of effectors. Rab5 recruits a Rabaptin-5/Rabex5 complex which stimulates GDP/GTP exchange through the GEF activity of Rabex5 (Horiuchi et al., 1997; Stenmark et al., 1995). This causes the accumulation of active Rab5 on the endosome membrane which leads to the recruitment of the phosphatidylinositol-3-kinase (PI3K), hVPS34/p150 (Schu et al., 1993; Volinia et al., 1995), which in turn generates a local concentration of phosphatidylinositol-3-phosphate (PI3P). This accumulation of active Rab5 and PI3P on endosomal membranes allows for the recruitment of the tethering factor early endosome antigen 1 (EEA1) which requires both Rab5 and PI3P to associate with the endosome (Christoforidis et al., 1999) (Figure 3). In addition to binding the docking factor, EEA1, the combination of Rab5 and PI3P on the surface of early endosomes also serves to recruit another Rab5 effector, termed Rabenosyn. The latter, along with EEA1, are involved in recruiting the soluble N-ethyl maleimide sensitive factor (NSF) attachment protein receptors (SNARE) proteins involved in regulating homotypic fusion of early endosomes.

In addition to a role in vesicle docking of trafficking and endocytic vesicles, Rabs have been associated with exocytic pathways where mutations have been attributed to disease states directly related to the disruption of Rab function. Rab27a is involved in the specialized trafficking of melanocytes to the PM for the secretion of melanin, which is essential for proper hair and skin pigmentation. Mutations of Rab27a and Myosin Va are the causes of Type I and II Griscelli syndrome respectively (Menasche et al., 2000; Mercer et al., 1991; Pastural et al., 1997), a disease characterized by pigment dilution in the hair and reduced T-

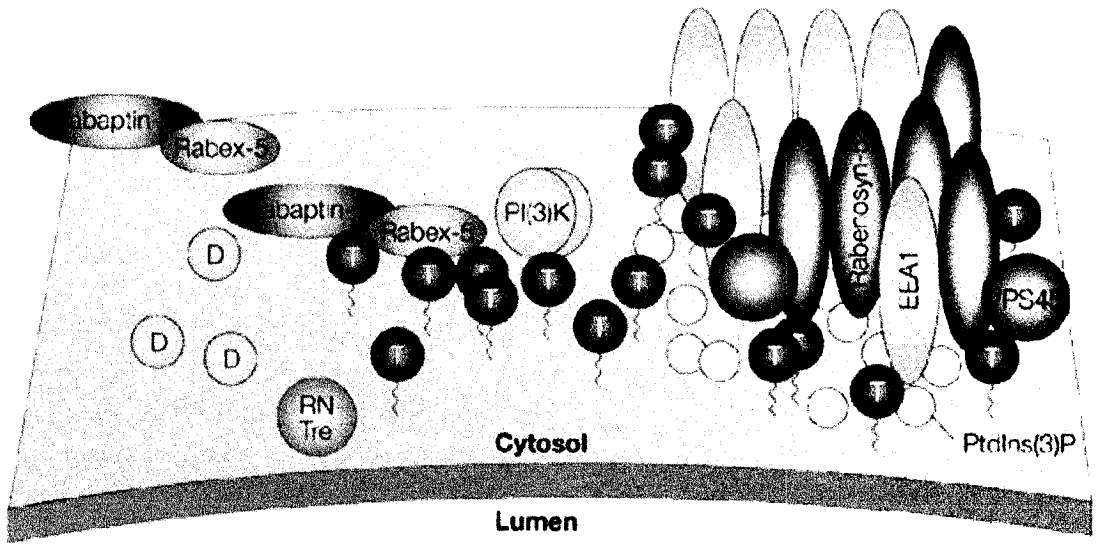

Figure 3. The Rab5 effector scaffold. The complex network of Rab5 regulators and effectors involves positive feedback loops and, according to the model presented in the figure, is designed to generate a local amplification of active Rab5 and the clustered recruitment of Rab5 effectors on the early endosome membrane. GDP- and GTP-bound Rab5 are shown as D and T respectively. Reprinted with permission from the author and *Nature Reviews Mol Cell Biol* 2, Marino Zerial and Heidi McBride, Rab proteins as membrane organizers: 107-119, 2001 (http://www.nature.com/).

cell cytolytic granule exocytosis (Griscelli and Prunieras, 1978; Klein et al., 1994). The mouse models of Griscelli syndrome, *ashen* and *dilute*, are also attributed to disruption of Rab27a and Myosin Va respectively (Mercer et al., 1991; Pastural et al., 1997; Wilson et al., 2000). The early hypothesis was that Rab27a, which associates with the melanocytes, recruited the myosin motor, Myosin Va to the granules to mediate transport of these melanocytes to the PM therefore mediating secretion of melanin. However, no direct interaction could be observed between these two proteins. A third mouse model, *leaden*, which exhibits the characteristic albinism of the *ashen* and *dilute* mice resolved this dilemma. This latter mouse model is attributed to deletion of the protein melanophilin, which is homologous to Rab effectors, Rabphilin and RIM. Melanophilin has been shown to be the linker between the melanocyte associated Rab27a and the cytosolic myosin motor myosin Va (Fukuda et al., 2002).

In addition to Rab27a, other Rab proteins, including Rab3, have been associated with the secretory pathway. Rab3 isoforms have been associated with synaptic vesicles and large dense core granules, which are part of the regulated secretory pathway in specialized neuronal and neuroendocrine cells. However, mutation and deletion of the synaptic vesicle (SV) specific Rab3A appears to affects a late step in exocytosis which follows docking since there is no change in the number of docked vesicles in the absence of Rab3A (Geppert et al., 1997). Knockout (KO) mice exhibit an increase in the number of exocytic events upon calcium-triggered release without a change in the release probability. Thus, the site of action of the Rab GTPases remains unclear and raises the possibility that there are differences in the mechanism of action of the various Rab GTPases. Although a number of Rab3 effectors, such as Rabphilin and Rim1 α /2 α have been identified, they do not fully account for the

regulation of Rab3 action. Rabphilin is a cytosolic protein which is recruited to the SV by the activated GTP-bound Rab3A (Chung et al., 1995; Mizoguchi et al., 1994; Shirataki et al., 1993). Despite the early evidence which suggested that the Rabphilin/Rab3A interaction was critical for the function of Rab3A(Burns et al., 1998; Chung et al., 1998; Chung et al., 1995; Komuro et al., 1996), Rabphilin KO mice exhibit none of the phenotype seen in Rab3A KO (Geppert et al., 1997; Schluter et al., 1999). Furthermore, over expression of Rab3A point mutants (R66 and R70) have no effect on Rabphilin or Rim binding but still result in secretory inhibition (Coppola et al., 1999). The interaction of Rab3A with the active zone associated protein Rim1 α, led to the hypothesis that this interaction mediates the tethering and/or docking of SV with the PM. However, both the Rim1 α and the Rab3A KO mice exhibit no decrease in the number of docked vesicles (Geppert et al., 1997; Schoch et al., 2002), putting into doubt the tethering function of this pairing. Therefore, the identification of other Rab3 effectors is required to gain insight in the precise role of the Rab3 subtype and shed light on the nature of possible effectors and function of other Rab GTPases.

PRA1 Project Objectives

To identify proteins regulating Rab function, a yeast two-hybrid screen using Rab3A as a bait, revealed a protein that interacts with both prenylated Rab GTPases and the v-SNARE VAMP2, and has been named prenylated Rab acceptor 1 (PRA1) (Figure 4) (Martincic et al., 1997). This dual Rab and VAMP2 binding property of PRA1 suggests that it may link the function of Rab GTPases and the SNAREs to mediate vesicle fusion. PRA1 is a 21 kDa protein that is conserved from yeast to human (Bucci et al., 1999; Yang et al., 1998). It contains two extensive hydrophobic domains (Figure 4 and 5) and is predicted to be a type

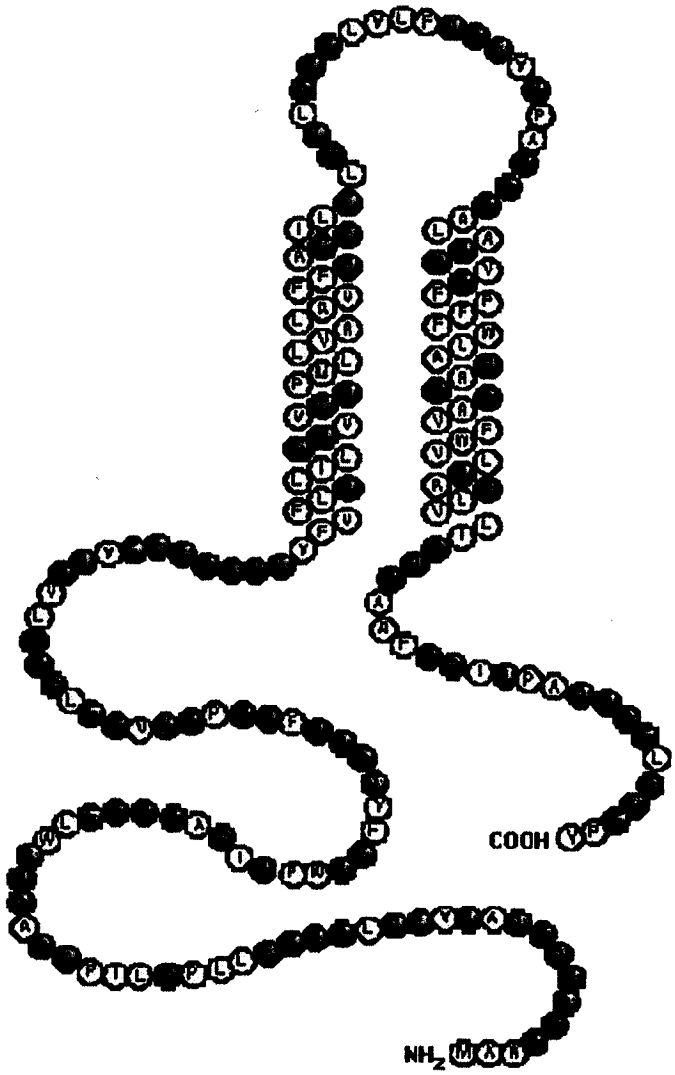

Figure 4. PRA1 structure and amino acid composition. The structure of PRA1 includes two extensive hydrophobic sequences and cytosolic amino and carboxy termini. The amino acid composition is depicted with acidic residues shown in red, basic residues shown in blue, non-polar residues in yellow and polar residues in green.

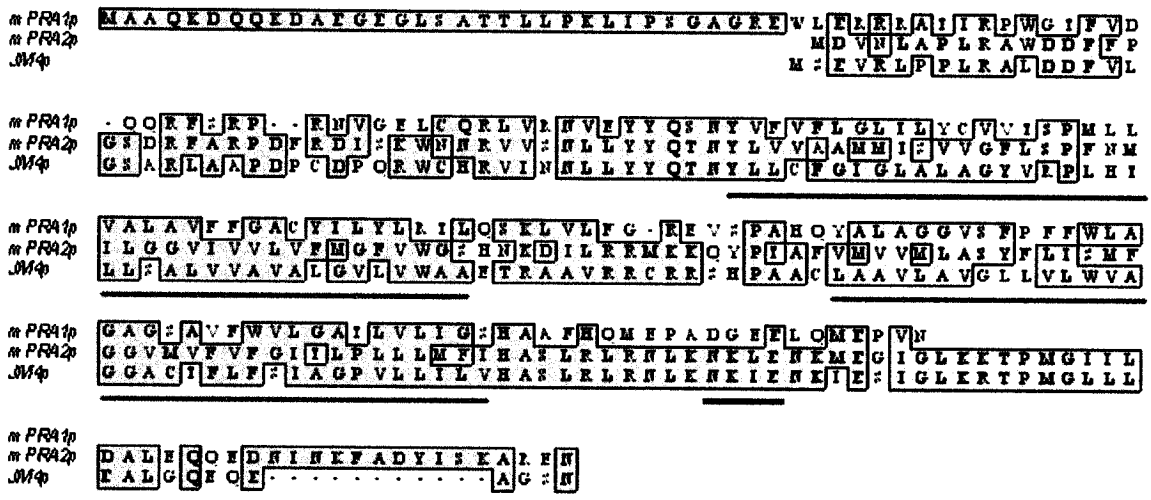

Figure 5. Sequence alignment of PRA1, PRA2 and JM4 (PRA3). The alignment depicts the sequence conservation among the 3 mammalian PRA isoforms (shaded). PRA1 has a longer amino-terminal region while PRA2 and JM4 are characterized by a longer carboxy-terminal tail. The hydrophobic domains (HD) are shown underlined in red and are thought to constitute 2 membrane-spanning regions each. The DXEE signal peptide for the Golgi localization of PRA1 and the KXRX signal peptide for the return of PRA1 to the ER are underlined in blue and green respectively.

III membrane protein. I have examined the subcellular localization and possible function of PRA1 in order to elucidate its possible role as a Rab3A effector. I report here that the full length PRA1 is associated with the Golgi complex and inhibits the extraction of GDP-bound Rab3A by GDI1. Truncation of the carboxy-terminus of PRA1 (1-164) results in mislocalization of the protein to the ER and results in a loss of inhibitory function in the GDI1-mediated extraction assay. Therefore, it appears that PRA1 is a novel effector of Rab3A, which localizes to the Golgi compartment where it could mediate the insertion of Rab3A GTPase following extraction from the PM.

As described above, the regulation of vesicle trafficking is critical to the proper function of cells and requires the concerted action of numerous protein families for the orderly progression of trafficking and secretory vesicles to their membranous compartment. In addition to this, the fusion of secretory vesicles in the regulated secretory pathway include an additional level of control, namely the calcium stimulation of secretion, which requires a sensing module in addition to the fusion proteins to ensure the proper regulation of the fusion reaction.

SNARE Proteins and Vesicle Fusion

The release of secretory proteins such as neurotransmitters and peptide hormones is regulated by the action of a superfamily of proteins commonly referred to as SNARE proteins (Terrian and White, 1997; Weimbs et al., 1997; Weimbs et al., 1998). The core SNARE complex is composed of two proteins on the plasma membrane—syntaxin (Stx) (Bennett et al., 1992) and SNAP-25 (Oyler et al., 1989), collectively termed target SNARES (t-

SNARES), and the SNARE protein on the vesicle (v-SNARE), called vesicle-associated membrane protein (VAMP) or synaptobrevin. Formation of the SNARE complex is essential for membrane fusion and it is thought to function by bringing the fusing membranes into close apposition. A number of isoforms of each SNARE protein have been identified, including 18 Stxs (Teng et al., 2001), 3 members of the SNAP-23/25/29 family (Oyler et al., 1989; Ravichandran et al., 1996; Steegmaier et al., 1998), and 8 VAMP isoforms in mammals (Advani et al., 1998; Bock et al., 2001; Elferink et al., 1989; McMahon et al., 1993).

The vesicle membrane SNARE (v-SNARE) VAMP

The v-SNARE family is composed of 8 VAMP isoforms in mammals and 5 yeast VAMP orthologs (Gerst et al., 1992; Protopopov et al., 1993). They are small type II integral membrane proteins of approximately 120 amino acids. Their structural features include a cytosolic domain composed of a single extended or 2 short α -helical domains termed H1 and H2 (named from the amino-terminal) (Gerst, 1997; Grote et al., 1995; Regazzi et al., 1996), which are predicted to form a coiled-coil region, followed by a carboxy terminal transmembrane domain (figure 6). The targeting of VAMP to the vesicle membrane is mediated by the H1 α -helix (Grote et al., 1995) while binding to t-SNAREs requires both helical domains, which is better known as the highly conserved SNARE domain (Chapman and Jahn, 1994; Grote et al., 1995; Hao et al., 1997; Hayashi et al., 1994; Regazzi et al., 1996). A functional role for VAMP in vesicle fusion was established when it was shown that the tetanus (TeNT) and the botulinum neurotoxins (BoNT) serotypes B, D, F and G, which impair vesicle fusion, specifically cleaved VAMP isoforms with varying specificities (Cornille et al., 1997; Foran et al., 1994; McMahon et al., 1993; Schiavo et al., 1992a;

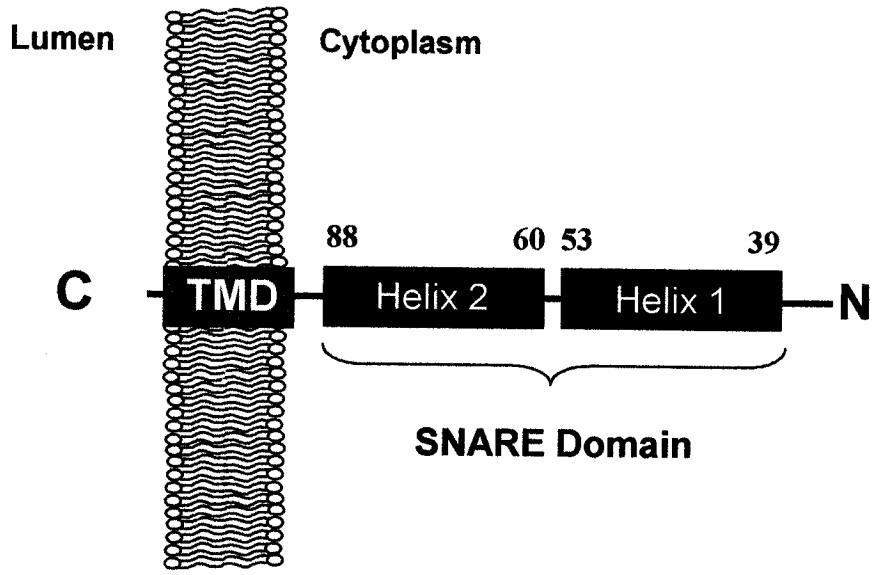

Figure 6. Schematic diagram of the domain arrangement of VAMP. Domain arrangement of vesicle associated membrane protein (VAMP). VAMP is a Type II integral membrane protein with a carboxy-terminal transmembrane domain (TMD). The amino-terminus is exposed to the cytoplasm is primarily composed of a single or 2 α -helical domains, identified as H1 and H2 which together constitute the SNARE domain. This region is directly involved in binding to the Q-SNARE proteins syntaxin and SNAP-25 to form the core SNARE complex that mediates membrane fusion.

Schiavo et al., 1993a; Schiavo et al., 1993b; Shone and Roberts, 1994; Yamasaki et al., 1994a; Yamasaki et al., 1994b). In addition, deletion of VAMP2 in mice or the yeast snc1 or 2 resulted in impaired fusion of secretory vesicles (Protopopov et al., 1993; Schoch et al., 2001), thus supporting a critical for the VAMP proteins in mediating the fusion of trafficking vesicles.

Target membrane SNAREs (t-SNAREs) Syntaxin and SNAP-25

The t-SNAREs include both the Stx and the SNAP-25 protein families. The Stx family includes 16 mammalian (Table 2) and 7 yeast isoforms (Table 3), which localize to different subcellular compartments. All of the Stxs, except Stx 11, are type II integral membrane proteins. The cytoplasmic region of Stx contains several hydrophobic regions predicted to form coiled coil domains (Figure 7). The membrane proximal coiled coil is the 60 amino acid long SNARE domain (Weimbs et al., 1997), which is conserved among all Stxs, and is involved in the formation of the SNARE core complex with VAMP and SNAP-25. In addition to the SNARE domain, several Stx isoforms, including Stx1, contain an autonomously folded amino-terminal region that contains 3 additional coiled-coil domains termed Ha, Hb and Hc (named from amino to carboxy terminus) (Lerman et al., 2000) (Figure 7A & B). This amino-terminal region is believed to bind to the Stx SNARE domain to generate a "closed" conformation (Figure 7B) and mediate the availability of the SNARE domain for core complex formation (Dulubova et al., 1999). This "closed" conformation of Stx is critical for binding to the Stx effector nSec1/Munc18-1 (Dulubova et al., 1999) which holds Stx in this conformation until a structural change is induced in Munc18-1 which results in release of Stx which then unfolds into its "open" conformation (Figure 7A) exposing the SNARE domain. This mechanism is believed to ensure proper timing of core complex

Syntaxins	Chromosomal localization*	Cellular localization	Tissue distribution	Known function
Syntaxin 1A (A and C)	7q11.23	Presynaptic plasma membrane	Neuronal and secretory cells	Neuronal exocytosis; regulated secretion
Syntaxin 1B	16p11.2	Presynaptic plasma membrane	Neuronal and secretory cells	Neuronal exocytosis; regulated secretion
Syntaxin 2 (A, B, C and D)	7	Plasma membrane	Ubiquitous	Exocytosis; morphoregulator during development
Syntaxin 3 (A, B, C and D)	11cen-11q12.3	Plasma membrane	Ubiquitous	Exocytosis
Syntaxin 4	16p13.13-16p12.3	Plasma membrane	Ubiquitous	Glut4 translocation
Syntaxin 5 (long and short form)	11cen-11q12.1	ER-Golgi boundary	Ubiquitous	ER-Golgi transport
Syntaxin 6	1	TGN	Ubiquitous	TGN-endosome transport; endosome-TGN transport; fusion of immature secretory granules
Syntaxin 7	6	Endosome	Ubiquitous	Late endosome fusion; late endosome-lysosome fusion
Syntaxin 8	17p12	Endosome	Ubiquitous	Late endosome fusion
Syntaxin 10	19p13.2	TGN	Ubiquitous	?
Syntaxin 11	6q23.1-6q25.3	TGN/late endosome	Ubiquitous	?
Syntaxin 12/13	1	Endosome	Ubiquitous	Recycling of surface protein; early endosome fusion
Syntaxin 16 (A, B and C)	20p11.23-20p11.21	Golgi/TGN	Ubiquitous	Early endosome-TGN transport
Syntaxin 17	?	Smooth ER	Steroidogenic tissues	Trafficking to smooth ER
Syntaxin 18	4	ER	?	ER-Golgi transport; ER homotypic fusion

Table 2. Function, subcellular localization and tissue distribution of mammalian syntaxin isoforms. Reprinted with permission from Genome Biology 2(11) Teng *et al.*: 3012.1-3012.7 (2001)

Syntaxins	Cellular localization	Null phenotype	Known function
Sso1p (YPL232W)	Plasma membrane	Viable	Transport to cell surface
Sso2p (YMR183C)	Plasma membrane	Viable	Transport to cell surface
Ufe1p (YOR075W)	ER	Lethal	ER homotypic fusion
Sed5p (YLR026C)	Golgi	Lethal	ER-Golgi transport; retrograde transport to Golgi
Tlg2p (YOL018C)	Golgi	Viable	Endosome biogenesis; cytoplasm to vacuole transport, endosomal recycling
Pep12p (YOR036W)	Golgi/vacuole/endosome	Viable	Vacuolar targeting
Vam3p (YOR106W)	Vacuole	Viable	Vacuolar targeting; phagosome fusion to vacuole

Table 3. Function and cellular distribution of yeast orthologs of the syntaxin family. Reprinted with permission from Genome Biology 2(11) Teng *et al.*: 3012.1-3012.7 (2001)

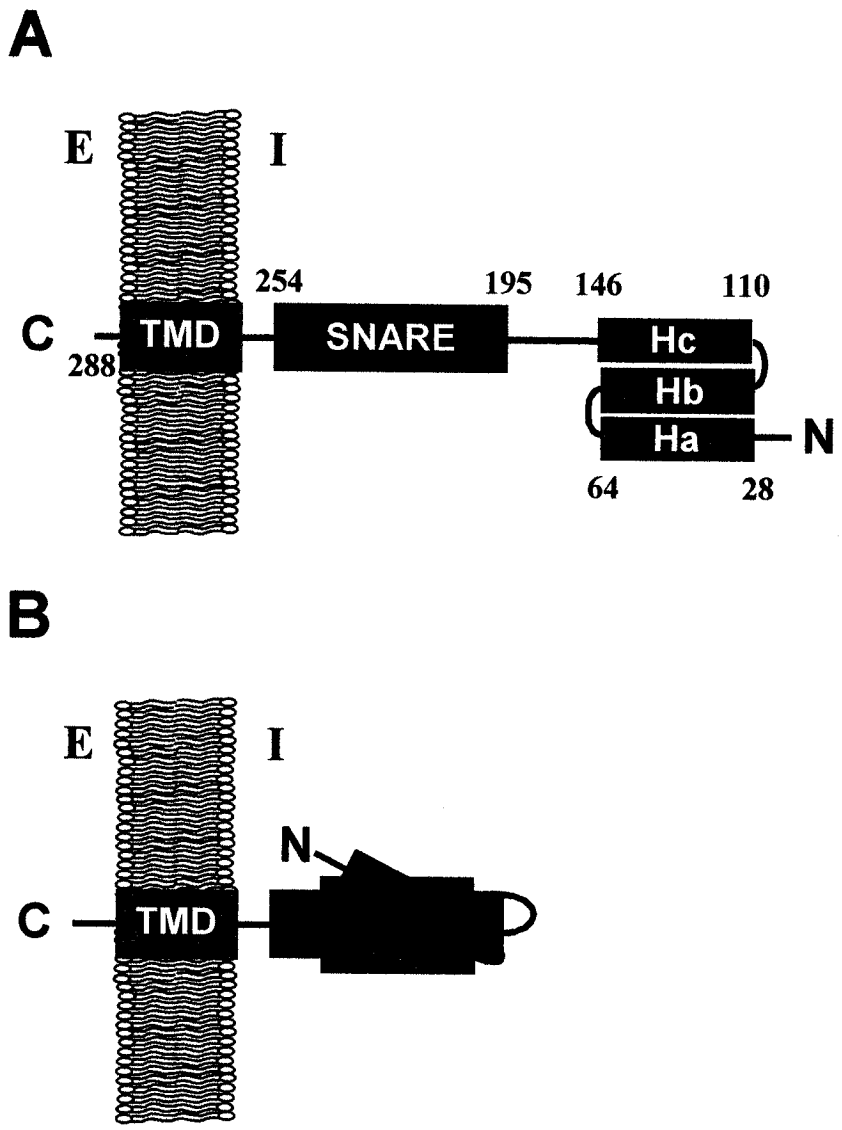

Figure 7. Schematic diagram of the domain arrangement of Syntaxin. A. The syntaxin family of proteins are type II integral membrane proteins characterized by a series of α -helical domains found in the cytoplasmic portion of the protein. The membrane proximal domain is the 60 amino acid SNARE motif (residues 195-254), shown in blue, which is involved in the formation of the core SNARE complex by binding to VAMP and SNAP-25 isoforms. The amino-terminal region of certain syntaxin isoforms, such as Stx1a, contains an autonomously folded domain composed of 3 α -helices named Ha (residues 28-64), Hb (residues 68-105) and Hc (residues 110-146) from the amino-terminal end. **B.** The N-Stx domain folds over and a groove between Hb and Hc interacts with the SNARE domain to generate a closed conformation of syntaxin. This conformation allows syntaxin to interact with Munc-18 and mediates the availability of the SNARE domain for core complex formation. E = extracellular and I = intracellular

formation and membrane fusion. As seen for VAMP, a functional role for Stx in mediating membrane fusion was proposed when it was shown that it is the target of BoNT serotype C (Blasi et al., 1993b; Hansen et al., 1999; Marsal et al., 1997; O'Connor et al., 1997; Schiavo et al., 1995).

The SNAP-25 family is composed of 3 mammalian isoforms, termed SNAP-23, -25 and -29 (Oyler et al., 1989; Ravichandran et al., 1996; Steegmaier et al., 1998) and 1 yeast ortholog, termed Sec9 (Brennwald et al., 1994). Unlike its t-SNARE partner Stx, SNAP-25 is not a membrane protein, rather it is peripherally associated with the acceptor membrane compartment via palmitoylation of cysteine residues (Lane and Liu, 1997; Oyler et al., 1989; Veit et al., 1996). The structural features of SNAP-25 also differ from that Stx and VAMP in that it contains 2 SNARE domains joined by a palmitoylated linker sequence (Figure 8). As with VAMP and Stx, a functional role for SNAP-25 in SV fusion originates from the discovery that it is the target for BoNT serotypes A, C and E (Binz et al., 1994; Blasi et al., 1993a; Bruns et al., 1997; Foran et al., 1996; Schiavo et al., 1993a; Vaidyanathan et al., 1999; Washbourne et al., 1997; Williamson et al., 1996).

SNARE complex

The characteristic feature of SNARE proteins is the presence of the 60 amino acid SNARE motif (Terrian and White, 1997; Weimbs et al., 1997; Weimbs et al., 1998). As previously mentioned, the SNARE complex is composed of the plasma membrane proteins syntaxin (Bennett et al., 1992) and SNAP-25 (Oyler et al., 1989) with the vesicle-associated membrane protein (VAMP) or synaptobrevin (Baumert et al., 1989; Trimble et al., 1990) in a *trans* conformation with a 1:1:1 stoichiometry (Figure 9). The resulting protein complex is

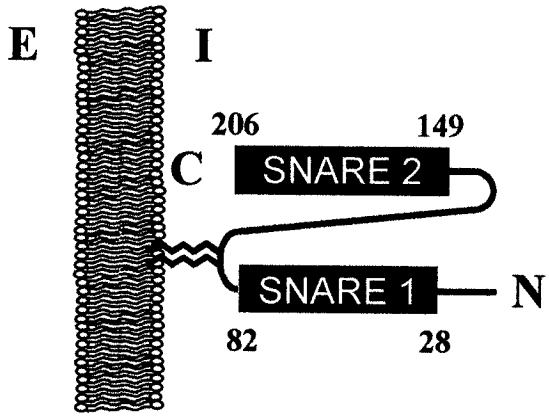

Figure 8. Schematic diagram of the SNARE helices of SNAP25. The domain structure of SNAP-25B, showing the two helices that participate in the core SNARE complex.

extremely stable as it is resistant to heat (Fasshauer et al., 1997), SDS and to proteolysis by botulinum and tetanus neurotoxins (Hayashi et al., 1994). The SNARE core complex consists of a parallel 4-helix bundle (Sutton et al., 1998) which results from the association of a single helical SNARE motif from syntaxin and VAMP and 2 SNARE motifs from SNAP-25 (Figure 9). In certain fusion reactions the 2 SNARE motifs from SNAP-25 can be replaced by 2 Stx SNARE motifs to maintain the 4-helix bundle configuration. The center of the core complex consists of an ionic layer composed of 3 glutamine and 1 arginine residues (Sutton et al., 1998) which originate from the PM and vesicular SNARE proteins respectively (Figure 10). Hence the SNARE proteins have been re-classified as Q- or R-SNAREs in addition to the previous target- (t-) or vesicular- (v-) SNARE nomenclature.

Assembly of the SNARE complex

The assembly of the core complex takes place in a multi-step manner. Firstly, the syntaxin-munc-18 interaction is dispersed causing syntaxin to adopt its "open" conformation and subsequently bind to SNAP-25 (Figure 11) forming an R-SNARE hetero-dimer on the acceptor membrane compartment. This transient complex now is able to interact with VAMP and assemble in a zipper-like manner from N- to C-terminus to initiate the formation of the stable coiled-coil structure of the core complex (Figure 11). The formation of this stable complex generates enough energy to overcome the repulsive energy barrier preventing membrane fusion and thus bringing the 2 membranes into close apposition and ready for fusion.

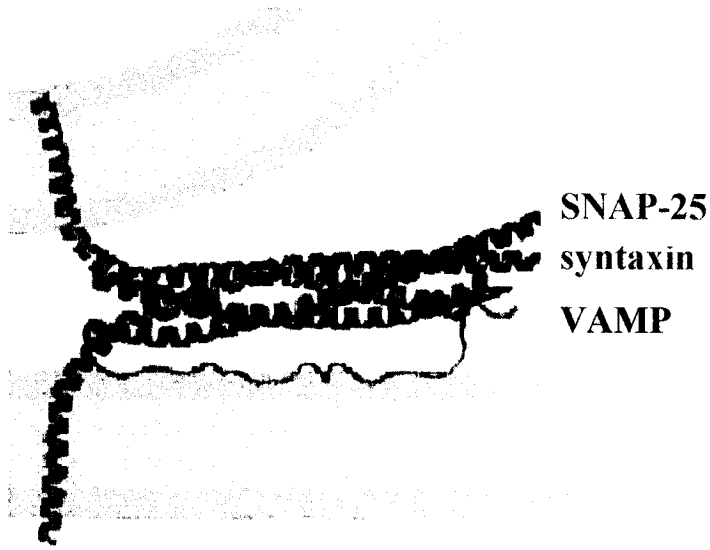

Figure 9. Ribbon diagram of the SNARE 4 helix bundle. The SNARE domains of syntaxin, SNAP-25 and VAMP associate in a parallel 4-helix bundle. This stable complex brings the membranes into close apposition to allow vesicle fusion with its target membrane. The transmembrane domain of VAMP and syntaxin are shown in a darker shade of green than that of SNAP-25 and the palmitoylated linker of SNAP-25 is shown in brown. Reprinted with permission from the author and *Nature 395*, Sutton *et al.*, Crystal Structure of a SNARE complex involved in synaptic exocytosis at 2.4 A resolution: 107-119, 2001 (http://www.nature.com/).

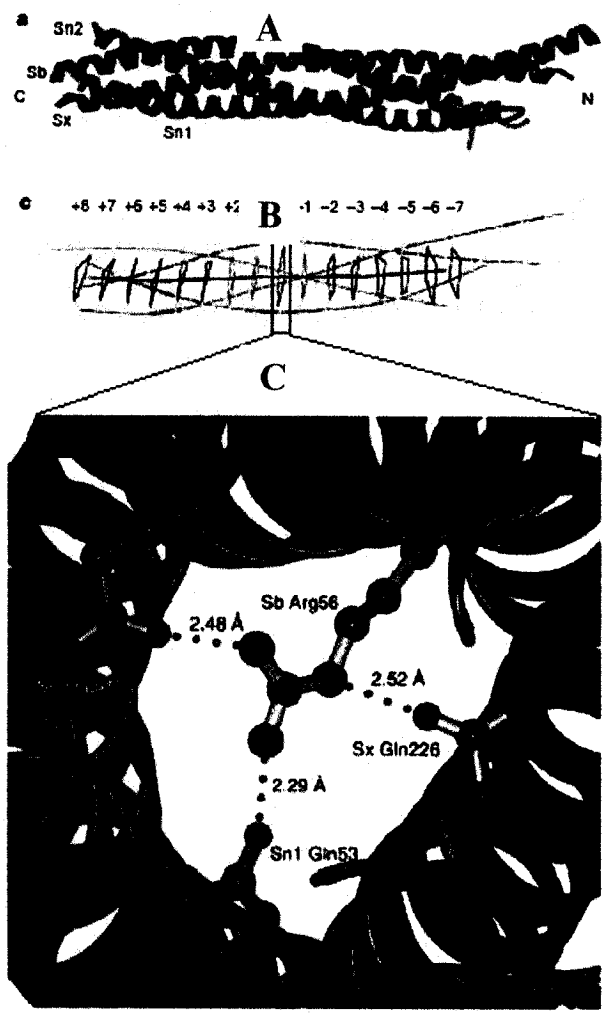

Figure 10. The ionic layer of superhelical SNARE core complex. A. Ribbon diagram of the synaptic SNARE complex. The SNARE helices from Syntaxin (Sx), VAMP (Sb) and SNAP-25 (Sn1 and Sn2) are shown in red, blue and green respectively. **B.** Ionic layers comprising the core complex superhelical structure. The "0" layer is highlighted by a red diamond and magnified in C. **C.** Magnification of the ionic "0" layer. The arginine 56 (Arg 56) from VAMP, the glutamine 226 (Gln 226) from syntaxin and the Gln 53 and and Gln 174 from the 1st and 2nd SNARE helices of SNAP-25 are shown as a ball and stick diagram while the remainder of the SNARE helices are shown as ribbon diagrams. The colors are as described in A. Reprinted with permission from the author and *Nature 395*, Sutton *et al.*, Crystal Structure of a SNARE complex involved in synaptic exocytosis at 2.4 A resolution: 107-119, 2001 (http://www.nature.com/).

A.

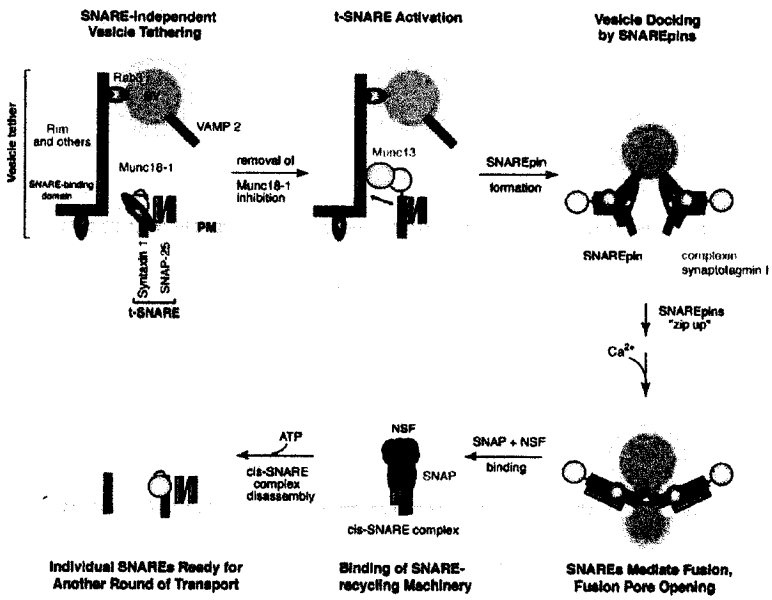

B.

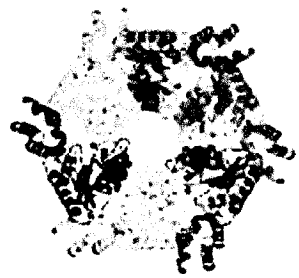

Figure 11. SNARE complex assembly. **A.** Prior to the assembly of the core complex, syntaxin is bound to Munc18/nSec1 (shown in red), which keeps it in the closed conformation. Upon release of Munc18/nSec1, syntaxin is able to assemble into a transient Q-SNARE dimer with SNAP-25. The dimer rapidly associates with the R-SNARE motif of VAMP and the 4-helix bundle adopts an unstable loose confirmation. The complex then associates with complexin, which maintains the assembly of the complex, and synaptotagmin, which serves to transduce the increase in cytoplasmic Ca^{2+} to the core complex. These interactions mediate the full zippering of the core complex and membrane fusion. Following fusion, the cis-SNARE complex recruits the cytosolic protein α -SNAP which is bound to hexameric NSF protein. The ATPase activity of NSF activates the uncoiling of the SNARE domains and generates the monomeric SNARE proteins for recycling or another round of fusion. Reprinted from Molecular Membrane Biology, 20, Sollner TH., 209-220, 2000, with permission http://www.tandf.co.uk **B.** Ribbon diagram of the NSF hexamer. Reprinted with the permission of Annual Review of Biophysics and Biomolecular Structure, Volume 30 © 2001 by Annual Review www.annualreviews.org

SNARE complex disassembly by SNAP and NSF

Due to the stability of the core complex, cells have adopted a chaperone to ensure disassembly of the complex following vesicle fusion. The ATPase NSF in conjunction with the soluble NSF attachment protein (SNAP), bind to the assembled core complex and unravel the coiled-coil structure when they are present in *cis* on the surface of a membrane compartment. One of 3 members of the SNAP family (Clary et al., 1990; Whiteheart et al., 1993), which has no relation to the R-SNARE SNAP-25, binds to the SNARE complex and recruits the cytosolic NSF hexamer. Binding of NSF to its adaptor protein activates ATPase activity, which induces a separation of SNARE proteins allowing them to be recycled in the case of VAMP isoforms or readily accessible for another round of docking/fusion in the case of Syntaxin and SNAP-25 isoforms (Figure 11).

The essential role of the SNARE proteins in fusion is supported by the observation that they were the targets of botulinum and tetanus neurotoxins (Binz et al., 1994; Blasi et al., 1993a; Blasi et al., 1993b; Link et al., 1992; Montecucco and Schiavo, 1995; Schiavo et al., 1994; Schiavo et al., 1992b; Sudhof et al., 1993). Cleavage of SNARE proteins by these toxins prevents assembly of the core complex and inhibits neurosecretion (Hayashi et al., 1994). The role of SNAREs in vesicle fusion is also supported by the observation that Q- and R-SNAREs reconstituted onto separate liposomes are sufficient to mediate fusion (Weber et al., 1998) however, the fusion reaction occurs with a half-time on the order of minutes (Parlati et al., 1999) whereas *in vivo* SV fusion occurs on the order of milliseconds and this system is unable to account for the regulation imposed by calcium in the regulated secretion of SV and large dense core vesicles (LDCV).

Synaptotagmin as a Calcium Sensor for SNARE-mediated Fusion

Despite the critical role that the core SNARE proteins are proposed to play in triggering vesicle fusion, Ca^{2+}-mediated secretion requires an additional regulatory mechanism that can transduce the increase in cytoplasmic Ca^{2+} to the SNARE fusion machinery. The established candidates for this calcium sensor are members of the synaptotagmin (Syt) family. There are at least 15 distinct mammalian Syt isoforms expressed in both neuronal and non-neuronal cells (Babity et al., 1997; Fukuda, 2003a; Fukuda, 2003b; Geppert et al., 1991; Hilbush and Morgan, 1994; Li et al., 1995; Mizuta et al., 1994; Perin et al., 1990; Thompson, 1996; von Poser and Sudhof, 2001). All Syt isoforms are transmembrane proteins with a hypervariable intravesicular N-terminus. The functional portion of the protein consists of a large cytoplasmic carboxy-terminal domain which contains two Ca^{2+} binding motifs with homology to the C2 domains of a number of other Ca^{2+}-sensitive proteins, and are designated C2A and C2B (Ponting and Parker, 1996) (Figure 12). Each C2 domain is composed of an eight-stranded β -sandwich with 3 flexible loops protruding from the top of the structure (Figure 12). Loops 1 and 3 of each C2 domain contain aspartic acid residues which are involved in the coordination of 3 Ca^{2+} ions for C2A (Ubach et al., 1998) and 2 Ca^{2+} ions for C2B (Fernandez et al., 2001). In addition to these critical calcium-coordinating residues, additional amino acids are required for individual effector interactions.

Synaptotagmin is essential for Ca^{2+}-mediated release

Functional studies have provided direct evidence that Syts are involved in triggering exocytosis in response to increases in intracellular Ca^{2+} (Ca^{2+}_i) (Bommert et al., 1993; Elferink et al., 1993; Fukuda et al., 1995; Mikoshiba et al., 1995). In addition, animal models

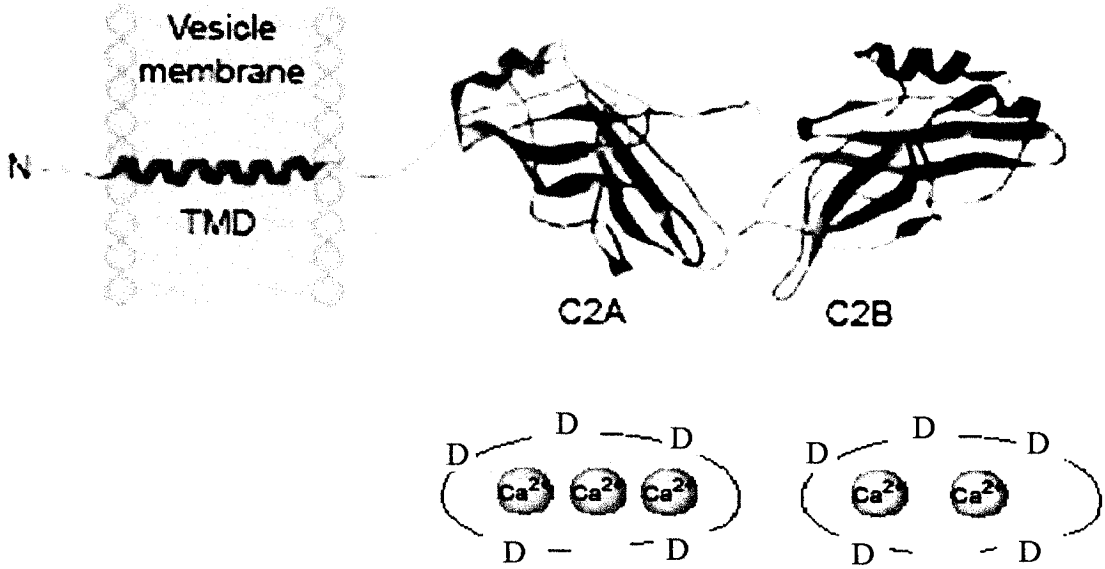

Figure 12. Ribbon diagram of Synaptotagmin I with the top view of the Ca^{2+}-coordination sites. The structure of the synaptotagmin family is conserved and consists of an intravesicular amino-terminal hypervariable domain, a single transmembrane domain (TMD) and a cytoplasmic region containing 2 Ca^{2+}-binding C2 domains named C2A and C2B for the membrane proximal and distal domains respectively. The C2 domains for autonomously folded 8-stranded β sandwich, which contain a series of aspartic acid residues on loops 1 and 3 at the top of each domain, which serve as coordination sites for 3 and 2 Ca^{2+} ions for the C2A and C2B domain respectively. Reprinted from Trends in Biochem Sci 29(3), Bai and Chapman: 143-151 (2004) with permission from Trends Journals.

where the Syt gene has been disrupted exhibit a loss of regulated secretion (Broadie et al., 1994; DiAntonio et al., 1993; Geppert et al., 1994; Littleton et al., 1993; Nonet et al., 1993). In Syt 1 knockout mice, only the rapid component of synaptic transmission was lost (Geppert et al., 1994) while the total number of vesicles released by hypertonic sucrose, which releases only docked and primed vesicles in a Ca^{2+}-independent manner (Aravamudan et al., 1999), remains unchanged in both wt and mutant animals (Geppert et al., 1994). This observation indicates that the number of docked vesicles is unchanged in the absence of Syt and that this protein must function after the vesicles have docked with the plasma membrane. What this role for Syt might be is unclear, but a number of effector molecules have been identified and further understanding of the nature of these interactions might shed light on its role in mediating vesicle fusion in response to Ca^{2+}.

Properties of Synaptotagmin

The best characterized Ca^{2+}-mediated interaction for Syts is their ability to bind to anionic phospholipids (PL), such as phosphatidylserine (PS) and phosphatidylinositol-3,4-bisphosphate ($PI3,4P_2$), which exhibits an EC_{50} of 5-20 μM Ca^{2+} (Davis et al., 1999; Nalefski et al., 2001). This preference for negatively charged PL is due to the presence of an incomplete Ca^{2+}-coordination sphere generated by the Asp residues in both C2 domains of Syt, which is completed by its proximity to negatively charged PL. Syt-lipid binding could bring the vesicle into close apposition to the PM in order to overcome the energy barrier that prevents bilayer fusion. However, this interaction does not display a preference for *cis* or *trans* membranes. Therefore, there must be additional factors directing the C2 domains of Syt to the *trans* membrane. In addition to lipid binding, Syts exhibit Ca^{2+}-dependent binding to

both R-SNAREs, Stx (Bennett et al., 1992; Sollner et al., 1993) and SNAP-25 (Gerona et al., 2000; Schiavo et al., 1997) with an EC_{50} of 100-200 μM Ca^{2+} (Chapman et al., 1995; Gerona et al., 2000; Littleton et al., 2001). This binding to R-SNAREs links the calcium sensor to the core SNARE fusion machinery, which allows for direct signaling to the core complex subsequent to an increase in intracellular Ca^{2+}. Syts also possess the ability to form hetero- and homo-oligomers (Brose et al., 1992; Perin et al., 1991) with varying Ca^{2+} requirements. The latter property of Syt has gained recent interest since Syt 3, 6 and 7 have been shown to localize to the PM rather then to secretory granules as has been shown for other isoforms (Butz et al., 1999; Gao et al., 2000). This raises the possibility that Syts could associate with one another in *trans* to mediate vesicle docking or fusion in response to Ca^{2+} signaling. In addition to the afore mentioned properties, Syt also binds to calcium channels (Leveque et al., 1994; Sheng et al., 1996; Wiser et al., 1997) and are therefore ideally situated to quickly sense increases in $Ca^{2+}{}_i$ mediated by influx through activated calcium channels.

Extensive analysis of the residues involved in the Ca^{2+}-dependent properties of Syt I has been performed and it is has been revealed that in addition to the Ca^{2+}-coordinating Asp residues, other amino acids located at the top of the loops 1-3 contribute to effector interactions. All of the Ca^{2+}-dependent effector binding properties of Syt requires the presence of the 5 Asp residues of C2A (D172, D178, D230, D232 and D238) and C2B (D303, D309, D363, D365 and D371) (Figure 12 & 14), since mutations of these residues results in elimination of all Ca^{2+}-mediated interactions (numbered according to Syt I nomenclature). This observation led to the identification of other residues which specifically mediate individual properties in order to weigh the contribution of each effector interaction to the overall function of Syt isoforms The Ca^{2+}-dependent PL binding exhibited by Syt I is

A.

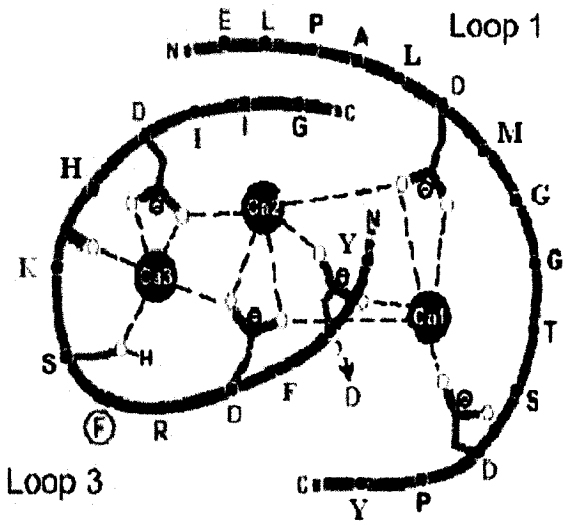

B.

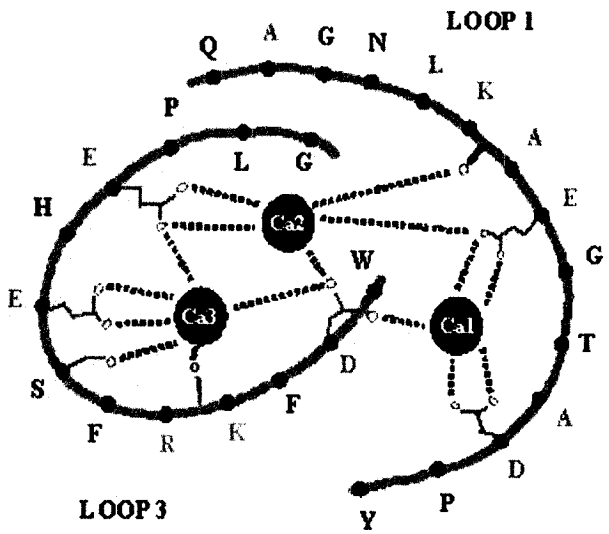

Figure 13. Schematic diagram of the calcium coordination in the C2A of Syt I and VIII. **A.** The theoretical coordination scheme for the C2A of Syt I mediated by the 5 aspartic acid (D) residues and the accessory lysine (K) and serine (S). **B.** The possible coordination of 3 Ca^{2+} ions by loops 1 and 3 of the C2A of Syt VIII. The cartoon is based on the theoretical coordination scheme proposed for Syt I.

mediated by the incomplete coordination sphere generated by the 5 Asp residues in loops1 and 3 which is completed by the proximity to negatively charged PL such as PS and $PI3,4P_2$. In addition to these residues, a critical arginine (R233) contributes to PL binding (Fernandez-Chacon et al., 2001) (Figure 13). Mutation of this residue (R233Q) results in a 2-fold reduction in PL binding *in vitro*, while mice expressing this mutant form of Syt I also exhibit a 2-fold reduction in secretion. One of the key effector interactions for Syt I function is binding to the R-SNARE protein Stx1. The interaction is mapped to the C2A domain (Shao et al., 1997), but the presence of the tandem C2A and C2B (C2AB) increases the affinity of Syt I for Stx1 (Chapman et al., 1996). The mechanism governing this interaction is thought to be electrostatic. The residues, which neighbor the Asp residues at the top of the C2A domain, include 4 positively charged amino acids. When the C2A domain is not bound to Ca^{2+}, the electrostatic potential of the domain is zwitterionic. However, when the C2A domain binds to its 3 Ca^{2+} ions, it generates a positive electrostatic region, which interacts with the acidic residues that are though to constitute the Syt recognition sequence of Stx1. Mutations of a number of these key positively charged residues in Syt I (R199Q, R233Q, and K236Q) and two double mutants (R199Q-R233Q and R199Q-K236Q) (Figure 13) results in a decrease or loss of Stx1-Syt I interaction (Shao et al., 1997). Another Ca^{2+}-dependent property, which is believed to contribute to the functional role of Syt in fusion of secretory vesicles, is the Ca^{2+}-dependent homo- and hetero-oligomerization. This property is mediated by the C2B domain of Syt isoforms (Fukuda and Mikoshiba, 2000; Littleton et al., 2001; Ubach et al., 2001). Once again additional residues, outside the Ca^{2+}-coordinating Asp residues, appear to contribute to the oligomerization property of Syts (Figure 13). Fukuda *et al.* have established that mutation of Y312N in the C2B domain of Syt II disrupts Ca^{2+}-dependent and independent

C2A

```
Syt I      168 LPALDMGGTSDPYVKVFLLPDKKKKFETKVHRKTLNPVFN 207

Syt VIII   137 AGNLKAEGTADPYAWVSVSTQSGRRHETKVHRGTLSPMFE 176

Syt I      208 EQFTFKVPYSELGGKTLVMAVYDFDRFSKHDIIG 241

Syt VIII   177 ETCCFLVPPAELPKATLKVQLWDFKRFSEHEPLG 210
```

C2B

```
Syt I      299 LKKMDVGGLSDPYVKIHLMQNGKRLKKKKTTIKKNTLNPY 338

Syt VIII   265 EARGLRPGLAEPYVKVQLMLNQRKWKKRKTATKKGTAAPY 303

Syt I      339 YNESFSFEVPFEQIQKVQVVVTVLDYDKIGKNDAIG 374

Syt VIII   304 FNEAFTFLVPFSQVQNVDLVLAVWDRSLPLRTEPVG 239
```

Figure 14. Sequence alignment of the C2 domains of Syt I and VIII. The sequence alignment of Syt I and VIII reveals a number of conserved residues. The C2A domain of Syt I contains 5 aspartatic acid residues (D) (shown in red), which are believed to constitute the Ca^{2+}coordination residues. The C2A of Syt VIII has conserved 2 of these aspartic acids (position 2 and 3) and substituted position 5 with a glutamic acid (E). Two other possible glutamic acids are found in Syt VIII at a shifted position (shown in blue). Two accessory residues that have been shown to participate in the coordination of Ca^{2+} ions are also conserved (shown in purple). Secondary residues critical for both phospholipids and R-SNARE binding are shown in green and are conserved between Syt I and VIII. The C2B of Syt I also contains 5 aspartic acid residues (red) that mediate the coordination of 2 Ca^{2+} ions. The 4 position is not conserved in Syt VIII but positions 2, 3 and 5 are conserved where positions 2 and 4 have glutamic acid (E) instead of aspartic acid (D) (red). The glutamic acid in the C2B of Syt VIII that could constitute the 1st position is shifted (blue). In addition the tyrosine (Y) residue, which is critical for Syt oligomerization, is conserved from Syt I to Syt VIII (green).

oligomerization (Fukuda et al., 2000). It is of note that the extensive sequence conservation of Syt isoforms within the C2A domain includes both conservation of the Ca^{2+}-coordinating Asp residues and the accessory residues, which mediate the various binding properties (Figure 13). Therefore, the various Syt family members that exhibit the individual properties described above also exhibit a conservation of all the residues, which mediate the said property.

Sperm as a Model System to Study Secretion

Upon stimulation either by direct contact with the zona pellucida (ZP), the glycoprotein coat that surrounds the egg, or stimulation by progesterone signaling via an unidentified pathway, the sperm undergoes the regulated exocytosis of its single secretory granule, the acrosome. This acrosome reaction (AR) must occur before the sperm can penetrate the ZP, since the acrosome contains hydrolytic enzymes necessary for degradation of the surrounding zona (Figure 15). In addition, the newly exposed membrane surface, the inner acrosomal membrane (IAM) (Figure 15), contains secondary binding sites that mediate continued binding to the ZP during penetration and could be involved in the sperm-egg fusion which leads to insertion of the male pronucleus and completion of fertilization. Therefore, the AR is a prerequisite for sperm-egg plasma membrane binding and fusion (Wassarman et al., 2001). It has been established that a rise in intracellular calcium ($Ca^{2+}{}_i$) subsequent to ZP3 or progesterone binding triggers the AR (Arnoult et al., 1996; Bailey and Storey, 1994; Florman, 1994; Green, 1978; Kobori et al., 2000; Meizel et al., 1997; Murase and Roldan, 1996; Roldan et al., 1994; Shi and Roldan, 1995), a mechanism reminiscent of regulated fusion of SV or LDCV seen in somatic cells.

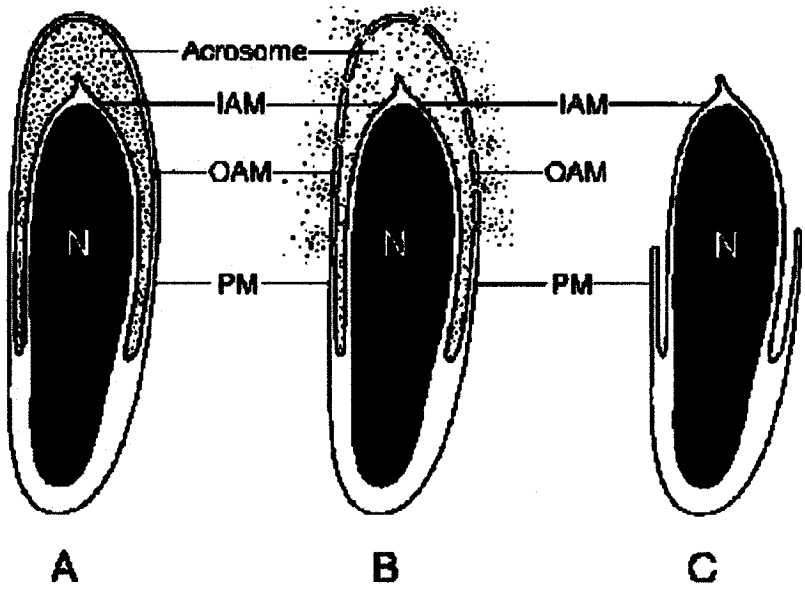

Figure 15. Membrane regions of the sperm head. Schematic diagram illustrating the various membrane compartments of the mammalian sperm head. **A.** The intact sperm contains the acrosome, a secretory vesicle like structure, which contains digestive enzymes required for digestion and penetration of the zona pellucida. It is bounded by the outer acrosomal membrane (OAM) and the inner acrosomal membrane (IAM). **B.** Upon stimulation by binding to ZP3 or progesterone, the OAM and the plasma membrane (PM) fuse at multiple sites in a process known as the acrosome reaction (AR), which results in vesiculation of the OAM-PM layer overlaying the sperm. This fusion reaction results in the secretion of the acrosomal contents, which mediate the zona penetration. **C.** Upon completion of the AR, the sperm IAM is exposed and is thought to mediate fusion of the sperm with the egg PM to allow for the introduction of the male pronucleus into the egg. Taken from Abou-Haila *et al.* Arch of biophys and biochem 379 (2) (2000). Reprinted from Arch of biophys and biochem, 379 (2), Abou-Haila *et al.*, Mammalian sperm acrosome: formation, contents, and function, 175-182, 2000, with permission from Elsevier

The Acrosome as a Secretory Vesicle

The hypothesis that the acrosome behaves as a large secretory vesicle in sperm is supported by the establishment of its origin in spermatogenesis and the identification of SNARE proteins and synaptotagmin isoforms which could mediate the regulated secretory process in response to the Ca^{2+} stimulus.

The acrosome originates from the Golgi complex during early spermiogenesis. Acrosomal biogenesis resembles formation of the lysosomal compartment. The vesicles that contribute to the developing Golgi originate from the TGN (Thorne-Tjomsland et al., 1988), both compartments have an acidic pH, as shown by the orange staining seen with acridine orange, and they contain common enzymatic components such as acid glycohydrolases, proteases, acid phosphatases and aryl sulfatases (Tulsiani et al., 1998; Zaneveld, 1991). Despite its similarity to the lysosomal compartment, the secretory property of the acrosome has led to its classification as a secretory vesicle. This classification may not be accurate since recent evidence has suggested that lysosomal vesicles are able to fuse with the PM in response to membrane damage in a Ca^{2+}-dependent manner (Andrews, 2000; Martinez et al., 2000; Rao et al., 2004; Reddy et al., 2001; Rodriguez et al., 1999; Rodriguez et al., 1997), suggesting that the acrosome could be more closely related to the lysosome than to a secretory vesicle. This difference in classification is not critical to the study of the acrosomal exocytosis since both the fusion of secretory vesicles and lysosomal vesicles appear to be mediated by isoforms of the SNARE and synaptotagmin family of proteins. However the nature of the isoforms identified suggests that the acrosome may exhibit unique secretory properties.

SNARE Proteins in Sperm

There is growing evidence that isoforms of SNARE proteins are involved in the fusion of the outer acrosomal membrane and the plasma membrane in the sperm AR, consistent with the AR being a form of Ca^{2+}-mediated exocytosis. All three SNARE proteins—Stx, VAMP and SNAP-25—were first shown to be present in sperm in the sea urchin, where they remained tightly associated with the shed acrosomal vesicles following the acrosome reaction, indicating co-localization with the fusion machinery (Schulz et al., 1998; Schulz et al., 1997). In mammalian sperm, VAMP and SNAP-25 proteins were also found to be present, and disruption of VAMP with Botulinum neurotoxin inhibited AR (De Blas et al., 2002). The expression and functional importance of Stx isoforms in sperm has been controversial. Stx1A, 1B, 4 and 6 have all been reported in human sperm, based upon their detection with antisera (Ramalho-Santos et al., 2000; Tomes et al., 2002). However, BoNT C, which selectively cleaves Stx1 and 2 inhibited the AR, suggesting that Stx4 and 6 in human sperm are not able to compensate for the inactivation of these isoforms (Tomes et al., 2002). In addition, the identification of Stx isoforms may also suffer from non-specificity of the antisera used, since the Stx1 antiserum appears to detect a protein in sperm lysate that is smaller than predicted for Stx1 (Ramalho-Santos et al., 2000). In the mouse, mRNA for Stx2 and 4, but not 1 or 3, are expressed in the testis, and Stx2 protein, but not Stx4 protein (Katafuchi et al., 2000) is present in the sperm, suggesting that it is Stx2 that plays an active role in the AR in sperm.

Synaptotagmins in Sperm

In accordance with the hypothesis that sperm undergo regulated secretion in a manner analogous to that seen in somatic cells, the presence and role of Syt isoforms has also been

examined. There is supporting evidence for the expression of Syt VI and VIII in rat testis (Li et al., 1995) and the latter proteins have clearly been shown to be localized to the human and mouse acrosome, respectively, and thus could potentially function as Ca^{2+} sensors to trigger the AR (Hutt et al., 2002; Michaut et al., 2001). A difficulty with this scenario, however, is that the binding of both of these Syt isoforms to the individual SNARE proteins and the assembled SNARE complex had been reported to be Ca^{2+}-insensitive (Li et al., 1995; von Poser et al., 1997), as had phospholipid binding by Syt VIII (Fukuda et al., 1996; Li et al., 1995; Rickman et al., 2004). In addition, at least in nerve terminals, Syt VI is apparently not localized to exocytotic vesicles (Butz et al., 1999). On the other hand, no other Syt isoforms had been conclusively identified in sperm and therefore no other candidates for the calcium sensor exist. While Syt I was previously reported to be present in sperm (Ramalho-Santos et al., 2000), the antiserum used has since been shown to cross-react with almost all other Syt isoforms (Hutt et al., 2002), invalidating this identification. In addition, mRNA for Syt I is not expressed in the testis, unlike Syt VI and VIII (Li et al., 1995), and similarly, Syt I mRNA is absent from spermatogenic cells while Syt VIII is present (Hutt et al., 2002).

Synaptotagmin VIII

An initial examination of the sequence of the ubiquitously expressed Syt VIII reveals that it lacks some of the critical Asp residues that are involved in the coordination of Ca^{2+} ions of Syt I in both the C2A and C2B domain (Figure 13 & 14). The 2nd and 4th Asp residues (position D2 and D4) in loop 1 and 3 respectively, are conserved in the C2A of Syt VIII while the D5 position, located in loop 3, is substituted for a Glu. This later amino acid differs from an Asp by the addition of a single carbon in the side chain but still contains the carboxyl

group involved in the interaction with Ca^{2+} ions, and therefore could substitute for the missing Asp. The D1 position is absent in the C2A of Syt VIII but could be replaced with a C-terminally located Glu (Figure 13 & 14). The longer side chain of the Glu could allow the carboxyl group to project further into the folded loop structure at the tip of the C2A and participate in the coordination of the Ca^{2+} ions. The D3 position, D232 of Syt I, is also absent in Syt VIII. This position in Syt VIII is occupied by a lysine residue (K201 of Syt VIII), while the K236 of Syt I, which was described above as critical for Stx1 binding is replaced by a Glu in loop 3 of Syt VIII (Figure 14). This suggests that the critical Asp and Lys residues are inverted but more importantly suggests that Syt VIII does contain 5 potential Ca^{2+}-coordinating residues (Figure 13). In addition to this conservation, the C2A of Syt VIII also contains all the critical residues for Ca^{2+}-dependent PL (R202) and Stx (R168, K201 and R202) binding (Figure 14). The C2B of Syt VIII is less conserved than its C2A and does lack one of the 5 Asp residues involved in Ca^{2+} binding, namely the D4 position (Figure 14). The D2, D3 and D5 positions of the C2B are all conserved, while the D1 position is once again potentially shifted with the appearance of a Glu 5 residue amino-terminally to the D303 of Syt I (Figure 13). In addition, the tyrosine residue, which Fukuda *et al.* have shown to be critical for oligomerization, is also conserved in Syt VIII (Y276) (Figure 14), however the latter isoforms only exhibits strong Ca^{2+}-independent homo-oligomerization. There is weak Ca^{2+}-dependent hetero-oligomerization with Syt VII and IX as well as weak Ca^{2+}-independent hetero-oligomerization with III, IV, V, VI and X.

The hypothesis that Syt VIII could behave as a Ca^{2+}-responsive isoform contradicts the empirical data of Li *et al.*, which suggest that Syt VIII does not exhibit Ca^{2+}-dependent Stx1 binding. However, these experiments were performed with only the C2A domain of Syt

VIII rather than the complete C2AB, which, as mentioned above, increases the affinity of Syt1 for Stx1 (Chapman et al., 1996). The question of Syt VIII calcium dependence therefore requires re-examination.

Synaptotagmin VIII Project Objectives

I have examined the expression and localization of Syt VIII in the mouse sperm and assessed its function in the murine acrosome reaction. I have also determined that Syt VIII is expressed in spermatogenic cells while Syt I is expressed in the brain and not in the spermatogenic cells, which confirms the observation of Li *et al.* which showed that Syt VIII was expressed in rat testis while Syt I expression was limited to brain tissue. In addition, I have used an isoform specific Syt VIII antibody to establish that the protein is expressed in mouse sperm and that it localizes to the acrosome. Similar to what is seen with the SNARE proteins in sea urchin sperm, Syt VIII is lost following induction of the AR, suggesting that it is may be a component of the fusion machinery where it could function as the calcium sensor. In order to confirm this hypothesis, I have re-examined the Ca^{2+}-dependent binding of Syt VIII to sperm isoforms of the Stx family, namely Stx1 and 2. Indeed, I report here that, despite the interaction of Syt VIII with Stx1 being previously identified as Ca^{2+}-insensitive (Li et al., 1995), Syt VIII actually exhibits isoform-specific, Ca^{2+}-regulated binding to both Stx isoforms. I then used the streptolysin O (SLO)-permeabilized sperm preparation to establish that these Syt and Stx isoforms are critical in acrosomal exocytosis in the mouse.

MATERIALS AND METHODS

Reagents. The pGEX-KG Syt constructs were obtained from Dr. T. Sudhof and the pGEX-2T Stx constructs were obtained from Dr L. Elferink. SLO was purchased from Sigma and recombinant SLO was purchased from Dr S. Bhakdi from the Institute of Medical Microbiology (Mainz University, Germany).

Cloning and purification of recombinant PRA1, GDI1 and Rab3A. The influenza hemagglutinin (HA) tag was added to the amino terminus of the PRA1 clone by subcloning the PCR amplified product into a HA tag containing Bluescript plasmid. The following primer pairs were used to PCR amplify the full-length PRA1 (1–185): 5'-CAT GCC ATG GCG GCC CAG AAG G-3' and 5'-AGG TCC ATG GAG GAC ACT TTA CAC-3'. For the truncated PRA1 (1–164), the latter primer was replaced with 5'-TGA CTC GAG CTA GCC TAT AAG TAC CA-3'. The PCR fragments were blunt-end subcloned into the *Eco*RV site of a HA tag containing Bluescript plasmid. The *Xho*I to *Xba*I fragment was then excised and blunt-end subcloned into the *Sal*I site of the 6xHis tag pQE11 (Qiagen). Both recombinant full length and truncated PRA1 (1-164) contained a 6xHis followed by a HA tag at the amino terminus. Expression and purification on Ni-NTA resin (Qiagen) were as described by the manufacturer. Briefly, bacteria from 1 litre of culture were disrupted by homogenization with glass beads (0.5mm) in lysis buffer (50 mM phosphate buffer, pH 8.0, 300 mM NaCl) at 2ml/g of pellet. The lysate was supplemented with Triton X-100 to a final concentration of 1% and incubated for 1hr at 4°C. The lysate was subsequently cleared of debris and glass beads by centrifugation at 10,000xg for 20 minutes. The cleared lysate was bound to Ni-NTA resin and washed with 20–40 volumes of 50 mM phosphate, pH 6.0, 300 mM NaCl, 10%

glycerol, 1% Triton X-100. The fusion proteins were eluted from the resin with 0.25 or 0.3 M imidazole in 50 mM phosphate, pH 6.0, 300 mM NaCl, 10% glycerol containing 0.05% Triton. The 6xHis-HA-tagged fusion proteins were detected by Western immunoblot analysis using anti-HA monoclonal antibodies (Roche).

The rat GDI1 was subcloned into Bluescript (Stratagene) vector containing the hemagglutinin (HA) tag by blunt-end ligation onto the EcoRV site. GDI1 was PCR amplified using the following oligonucleotides: 5'-CAT GCC ATG GAT GAG GAA TAC G-3' and 5'-GGG AAG CTT CAC TGA TCG GCT TCT CC-3'. The HA-tagged GDI1 was then isolated as a XhoI/BamHI fragment and subcloned into the EcoRI site of pGEX-2T (Novagen) vector by blunt-end ligation. The purification of GDI1 was as described by the manufacturer for GST-fusion proteins. Briefly, the cells were homogenized in 25 mM Tris-HCl pH 7.5, 150 mM NaCl, 1 mM DTT, and 2 mM PMSF. After centrifugation at 10,000 x g for 20 min, the supernatant was loaded onto a glutathione-agarose column. The column was washed with Wash Buffer 1 (25 mM Tris-HCl pH 7.5, 500 mM NaCl, 10% glycerol, 1 mM DTT) followed by Wash Buffer 2 (25 mM Tris-HCl pH 7.5, 150 mM NaCl, 10% glycerol, 1 mM DTT). The fusion protein was then eluted with 10 mM glutathione in Wash Buffer 2.

The rat Rab3A was subcloned as a BamHI/HindIII fragment into pRSET-A (Invitrogen). The NdeI to HindIII fragment was then isolated and blunt-end ligated into the EcoRI site of pAAR6, between the constitutive yeast ADH1 promoter and terminator. The BamHI fragment was then transferred to pRS424 plasmid and transformed into yeast Y190 strain by the LiCl method (Gietz et al., 1995). To purify the 6xHis tagged Rab3A, the transformed yeast was grown to saturation in 200 ml of tryptophane (Trp) drop-out medium. The cells were harvested at 3,000 x g for 5 min, transferred to 1 L of YPD and grown at 30°C

for 8 h. The cells were then collected by centrifugation at 3,000 x g for 5 min, and homogenized with acid-washed glass beads (0.5 mm diameter) in lysis buffer (10 mM Tris-HCl pH 7.5, 1 mM ß-mercaptoethanol, 2 mM PMSF) at 1 ml/g cell pellet. The cell debris and glass beads were removed by centrifugation at 3,000 x g for 5 min. Triton X-100 was added to the supernatant at 1% final concentration and incubated at 4°C for 1 h. The insoluble material was then removed by centrifugation at 100,000 x g for 1 h. The supernatant was loaded onto 1 ml of Ni-NTA beads (Qiagen) and washed with 40 volumes of wash buffer (10 mM Tris-HCl pH 7.5, 150 mM NaCl, 1 mM ß-mercaptoethanol, 0.05% Triton X-100, 10% glycerol). The 6xHis-tagged Rab3A was eluted with 300 mM imidazole in the above wash buffer.

Cloning of syntaxin to pQE9. The cytoplasmic region of Stx1 and 2 were PCR-amplified from pGEX-Stx1 or 2 using the following oligonucleotides: Stx1 (forw) 5'-TCC CTG CAG ACA TGA AGG ACC GAA CCC AGG-3' and Stx1 (rev) 5'-GTA AGC TTC TAC TTC TTC CTG CGT GCC-3', Stx2 (forw) 5'-ATT AGA TCT ATG CGG GAC CGG CTG CCG GAC-3' and Stx2 (rev) 5'-AGA AAG CTT TCA CCA CTT TTT CCG TCT GGC C-3'. The fragments were cut with PstI/HindIII and BglII/HindIII respectively and cloned into pQE9 vector (Qiagen), which has been modified to contain a hemagglutinin (HA) tag between the 6xHis tag and the multiple cloning site.

Cloning of synaptotagmin to pQE9. The cytoplasmic region of Syt I, VI and VIII, referred to as C2AB, were PCR amplified from pGEX-KG Syt I, VI and VIII using the following oligonucleotides: Syt I (forw) 5'-CGA GAT CTG AGA AAC TGG GAA AGC TCC AAT

ATT CA-3'and Syt I (rev) 5'-CAG AAG CTT ACT TCT TGA CAG CCA GCA TGG CAT C-3', Syt VI (forw) 5'-CGA GAT CTG CCA AGA GCT GTG GGA AGA TCA-3' and Syt VI (rev) 5'-CTG AAG CTT CAC AAC CGG CGG GTT CCC TCT-3', Syt VIII (forw) 5'-TAG GAT CCG TTC AAC CAG ATG TGG ACT GC-3' and Syt VIII (rev) 5'-TTG AAT TCA GGA GCG AGG CCT AAG CAG-3'. The Syt I and VI C2AB were digested with BglII and HindIII and cloned into the modified pQE9 (above). The Syt VIII C2AB was digested with BamHI and EcoRI, which was blunt ended and the fragment was cloned into modified pQE9 (above) cut with BglII and SmaI.

Expression and transfection of PRA1 in mammalian cells. HA-tagged PRA1 and PRA1 (1-164) were subcloned into the bicistronic pIRESpuro (Clontech). The PRA1 sequences from the pQE constructs previously described (Martincic et al., 1997) were PCR amplified using the oligonucleotides 5'-CCA TCG ATA TGT ACC CAT ACG ATG TTC CA-3' and 5'-CGG AAT TCT GAG GTC ATT ACT GGA TCT ATC-3'. The resulting PCR fragments were restriction digested and subcloned into the ClaI and EcoRI sites of pIRESpuro. BHK cells were transfected with the bicistronic pIRESpuro constructs of wild-type PRA1 and truncated PRA1 (1-164) using Lipofectamine (Life Technologies). Briefly, 1 x 10^5 BHK cells were seeded on cover slips overnight. Plasmid DNA (0.5 μg) was mixed with 1 μl of Lipofectamine in 100 μl final volume of Opti-MEM (Life Technologies). The lipid-DNA mixture was added to the PBS-washed cells containing 200 μl of Opti-MEM and incubated at 37°C for 3-5 h. The medium was replaced with MEM α supplemented with 5% FBS and antibiotics. The cells were processed for immunocytochemistry after 36-48 h. Briefly, the cells were fixed in 4% paraformaldehyde (EM Sciences) in PBS for 30-60 min and washed

with PBS supplemented with 100 mM glycine. The cells were incubated with Blocking Buffer (1% BSA, 2% normal goat serum, 10 mM NaN_3, and 0.4% saponin in PBS) for 30-60 min. Rabbit anti-calnexin (Stressgen), or anti-mannosidase II (generously provided by Dr. M. Farquhar) were used in conjunction with monoclonal anti-HA in double immunofluorescent labeling reaction. The primary antibodies were diluted in Blocking Buffer and incubated with the cells at room temperature for 1-2 h. The cells were then washed with PBS and fluorescein- or rhodamine-labeled secondary antibodies (Chemicon) were used to detect the bound primary antibodies. The cover slips were mounted with SlowFade anti-quench solution (Molecular Probes). Images were captured with a Bio-Rad MRC-1024MP laser confocal microscope.

In vitro binding of PRA1 and GDI α. The binding of GDI1 to full-length and truncated PRA1 (1-164) was done using bacterially expressed proteins in an *in vitro* pull down assay. GDI1 was purified on glutathione-Sepharose as described above. To demonstrate binding of PRA1 to GDI1, 40 pmoles of recombinant PRA1 was added to either GST or GST-HA-GDI1 fusion protein in 200 µl of TBS (25 mM Tris-HCl pH 7.5 and 125 mM NaCl). After incubation at 37°C for 10 min, the GST fusion proteins were recovered with glutathione-Sepharose and washed 4 times with TBS. Both recombinant GDI1 and PRA1 were detected with anti-HA antibodies (Roche). To demonstrate the reciprocal binding, GST-HA-GDI1 was thrombin cleaved to remove the GST tag since this gave more efficient binding. The GST-HA-GDI1 fusion protein was cleaved with 3 mU of thrombin/pmol of protein at 37°C for 2 hours in 50 mM Tris-HCl pH 7.5, 150 mM NaCl, 2.5 mM $CaCl_2$ and 288 µM β -mercaptoethanol, and stopped by the addition of 2 mM PMSF. The HA-GDI1 was subsequently incubated with 40

pmoles of Ni-NTA purified wild-type PRA1 or truncated PRA1 (1-164) at 37°C for 30 min in 25 mM Tris-HCl pH 7.5 and 125 mM NaCl. The resulting protein complex was pulled down using Ni-NTA agarose beads and washed four times with 25 mM Tris-HCl pH 7.5, 125 mM NaCl, 1 mM $MgCl_2$ and 0.03% CHAPS. Denaturing loading buffer was added to the beads and proteins subject to Western immunoblot analysis. The GDI1 and PRA1 were detected with anti-GDI1 and anti-HA antibodies, respectively.

In vitro binding of syntaxin and synaptotagmin. Determinations of binding of Stx1 and 2 to Syt I, VI and VIII were performed using bacterially expressed proteins in a pull-down assay. GST-tagged cytoplasmic region of Syt were purified by glutathione-Sepharose as described above and incubated with equal amount of 6xHis/HA-tagged Stx1 or 2 for 4 hrs at 4°C in binding buffer (10 mM Tris-HCl pH 7.4, 150 mM NaCl and 0.05% Triton X-100) with the indicated free Ca^{2+} concentration added from 10X stock solutions. Following the incubation, the beads were washed 3 times with the appropriate ice-cold binding buffer and bound proteins were subjected to Western immunoblot analysis using anti-HA (Roche) antibody and Alexa-488 goat anti-mouse secondary antibody (Invitrogen) to detect bound Stx. Densitometric analysis was performed using a typhoon 8600 imager (Amersham Biosciences). The results are an average of at least 3 separate experiments.

Preparation of PC12 Microsomal Membranes and Cytosol PC12 cells from two 100 mm dishes were harvested with 5 ml of 5 mM EDTA in PBS. The cells were homogenized by sonication in 1 ml of TBS (10 mM Tris-HCl pH 7.5, 150 mM NaCl) with 1 mM PMSF. The cell debris was removed by centrifugation at 10,000 x g for 10 min. The resulting supernatant

was spun at 150,000 x g for 60 min. The supernatant was discarded and the membrane pellet was resuspended by brief sonication in 0.2 ml of 20 mM HEPES-KOH pH 7.5, 300 mM sucrose, 1 mM PMSF. Protein concentration was determined by Bradford assay (Bio-Rad).

Cytosolic Proteins that Interact with PRA1. To determine cytosolic proteins that might bind to recombinant PRA1, the supernatant from the 150,000 x g centrifugation from two 100 mm dishes of PC12 described above was added to 30 pmoles of recombinant His-tagged PRA1 in 1 ml final volume. A buffer blank was used as a control. The samples were supplemented with $MgCl_2$ and GDP at 1 mM and 0.2 mM, respectively. After incubation at 30°C for 30 min, 40 µl of 50% slurry of Ni-NTA was added and incubated with gentle agitation at 4 °C for 30-60 min. The Ni-NTA beads were then washed 3 times with ice-cold HBS (10 mM HEPES-KOH pH 7.4, 150 mM NaCl). The proteins were eluted from the beads with SDS sample buffer and separated on SDS polyacrylamide gel. After transfer to nitrocellulose membrane, the blot was processed with anti-GDI (Zymed) followed by the appropriate secondary antibodies and ECL (Amersham Pharmacia).

Extraction of Rab3A by GDI1. PC12 cells were homogenized as described above. After the 10,000 x g centrifugation step, the membranes were isolated from the resulting supernatant by centrifugation at 200,000 x g for 30 min. The resulting pellet was suspended in 0.2 ml of TS (10 mM Tris-HCl pH 7.5, 300 mM sucrose). A typical assay contained 25 µg of PC12 membranes, recombinant GDI1 and PRA1 in 10 mM Tris-HCl pH 7.5, 1.5 mM $MgCl_2$, 250 µM GDP in a 200 µl final volume. After incubation at 37°C for 20 min, the samples were

chilled on ice and subjected to centrifugation at 250,000 x g for 30 min. The supernatant and pellet were then subjected to Western immunoblot analysis using anti-Rab3A (Santa Cruz).

PCR and southern blotting. PCR amplification of synaptotagmin I (Syt I) and synaptotagmin VIII (Syt VIII) was performed from 1 μg of mouse brain cDNA as well as from pachytene spermatocyte and round spermatid phage cDNA libraries at 2 x 10^8 pfu each (generously provided by Dr. J. McCarrey by Southwest Foundation for Biomedical Research, Texas). Mouse brain cDNA was prepared from 2 μg of freshly isolated total RNA (Qiagen total RNA isolation kit) using a RETROscript first strand synthesis kit (Ambion Inc.). The PCR amplification was performed using isoform-specific primers for Syt I (5'-GCG GAT CCC TAC TGC CGG CAA GCT GAC T-3' and 5'-CTT CTA GAC AGC CAG CAT GGC ATC AAC C-3') and Syt VIII (5'-CTG GAT CCC TGA AGG CTG AGG GCA CA-3' and 5'-CGG AAT TCT AAC GGG AAC CAG GAA GAC G-3'). Samples were resolved on a 1% agarose gel and transferred to nitrocellulose membrane for Southern blot analysis. The blot was pre-hybridized for 1 h at 60°C in 6x SSC, 5x Denhardt's, 100 μg/ml of sheared and denatured salmon sperm DNA, and 0.5% SDS. ^{32}P-labelled probes were prepared from purified DNA constructs of the cytoplasmic regions of Syt I and Syt VIII using a random hexamer labeling kit (Life Technologies) and unincorporated nucleotides were removed using NuncTrap columns (Stratagene). The blots were hybridized overnight at 60°C with 2 x 10^6 cpm/ml of pre-hybridization buffer and washed twice with 2 x SSC, 0.1% SDS for 10 minutes at room temperature and twice with 0.2 x SSC, 0.1% SDS for 10 minutes at 60°C.

Anti-synaptotagmin VIII antiserum. New Zealand white rabbits were immunized at 2-week intervals with 0.2 mg of the Syt VIII specific peptide, TVDLQHVLESWYQ, mixed with Freund's adjuvant. The antigen was injected intramuscularly in the hind limbs and antiserum was collected biweekly.

Small scale purification of GST-synaptotagmin. *E. coli* transformed with GST-synaptotagmin isoforms (generously provided by Dr. T. C. Sudhof) were induced to express the GST-synaptotagmin fusion proteins by a 4 h incubation with 1 mM IPTG at 37°C. The bacteria were harvested at 5,000 x g for 10 minutes and the pellets were resuspended in lysis buffer containing 25 mM Tris-HCl pH 7.5, 1 mM EDTA, 2 mM PMSF, 2 mM DTT and 1 mg/ml lysozyme. The bacteria were lysed with 0.1% Nonidet P40 (NP40), the DNA sheared by sonication at 35% power for 1 minute using a Fisher Sonic Dismembrator model 300, and the debris was pelleted at 10,000 x g for 10 minutes. The fusion proteins were purified from the homogenate by incubation with glutathione agarose beads (Sigma) for 1 h with shaking. The beads were then pelleted and washed extensively with wash buffer containing 25 mM Tris-HCl pH 7.5, 100 mM KCl, 1 mM EDTA, 2 mM DTT and 0.1% NP40 prior to elution of the protein with SDS loading buffer. GST-synaptotagmin fusion proteins were resolved by SDS-PAGE and blotted to nitrocellulose. The blot was then probed with anti-Syt VIII, anti-Syt (Transduction Laboratories) or with anti-GST. HRP-labeled secondary antibodies (Chemicon) and ECL (Amersham) were used to visualize the bound antibodies.

Large scale purification of GST-synaptotagmin. The purification of GST-tagged Syts was performed as described by the manufacturer for GST fusion proteins. Briefly, the bacterial

cells were homogenized in 25 mM Tris-HCl pH 8, 150 mM NaCl and 2 mM PMSF. After centrifugation at 10,000 x g for 20 minutes to clear the homogenate, the supernatant was incubated with glutathione-Sepharose beads (Amersham Pharmacia) overnight at 4°C. The beads were washed with wash buffer 1 (25 mM Tris-HCl pH 7.5, 500 mM NaCl and 0.5% Triton X-100) followed by wash buffer 2 (25 mM Tris-HCl pH 7.5, 150 mM NaCl and 0.05% Triton X-100). The amount of bound GST fusion protein was quantified by Coomassie blue staining of a polyacrylamide gel using BSA as a standard.

Large scale purification of 6xHis/HA tagged syntaxin and synaptotagmin. The purification of 6xHis/HA-tagged Stx for *in vitro* binding assay was performed as described by the manufacturer. Briefly, the cells were homogenized in 50 mM sodium phosphate pH 8, 300 mM sucrose and 2 mM PMSF. The homogenate was supplemented with Triton X-100 to a final concentration of 1%. Following centrifugation at 10,000 x g for 20 minutes, the supernatant was added to Ni-NTA beads pre-equilibrated in lysis buffer and incubated overnight at 4°C. The beads were successively washed with wash buffer 1 (50 mM sodium phosphate pH 7, 500 mM NaCl and 1% Triton X-100) and wash buffer 2 (50 mM sodium phosphate pH 7, 150 mM NaCl and 0.01% Triton X-100). The fusion protein was eluted in wash buffer 2 containing 250 mM imidazole and quantified by Coomassie brilliant blue staining of polyacrylamide gel using BSA as a standard. The purification of 6xHis/HA fusion proteins for inhibition of acrosome reaction was performed as described by the manufacturer for 6xHis-tagged fusion proteins. Briefly, the cells were resuspended in 50 mM Tris-HCl pH 8, 150 mM NaCl, 1 mM DTT and protease inhibitor cocktail (Sigma) and disrupted by French Press. Following centrifugation at 35,000 x g for 25min at 4°C, the supernatant was added to

Ni-NTA beads and incubated overnight at 4°C. The column was washed extensively with wash buffer (50 mM Tris-HCl, 500 mM NaCl and 25 mM imidazole) until the OD_{280} is below 0.05 followed by Krebs Ringer buffer (KRB) pH 7.4 without $CaCl_2$. The 6xHis-tagged fusion proteins were eluted in KRB containing 250 mM imidazole and quantified by Coomassie brilliant blue staining of polyacrylamide gel using BSA as a standard.

Acrosome reaction of murine sperm. Sperm were collected from cauda epididymides of 12-15 week old mice and allowed to "swim-up" for 15 minutes in Krebs Ringer Bicarbonate Buffer (KRB) media containing 1.7 mM $CaCl_2$, pH 7.4 (37°C / 5% CO_2). An aliquot of the sperm was then added to an equal volume of KRB, which contained either 0.4% DMSO or 20 μM of A23187 in 0.4% DMSO and incubated at 37°C / 5% CO_2 for 30 minutes. Sperm intended for immunohistochemistry were fixed by addition of paraformaldehyde to a final concentration of 4% and incubated at 4°C overnight. Sperm intended for Western blotting were counted, resuspended in SDS loading buffer at a concentration of 1 x 10^5 sperm/μl and sonicated for 15 seconds at 30% power in order to reduce viscosity. The proteins were resolved on a 10% SDS-PAGE gel and blotted on nitrocellulose. The resulting blots were probed with Anti-Syt VIII at 1:200. Densitometric analysis was performed using a BioRad Molecular Analyst program.

Immunohistochemistry of Mouse Sperm. Sperm aliquots were air-dried onto glass slides and washed with PBS containing 0.1 M glycine prior to staining. Fixed sperm were permeabilized with blocking buffer containing 1% BSA, 2% normal goat serum and 0.4% saponin in PBS for 30 minutes at room temperature. Labeling was performed with anti-Syt VIII diluted 1:20

with blocking buffer for 1-2 h. Samples were extensively washed with PBS containing 0.1 M glycine prior to labeling with Alexa 594-conjugated goat anti-rabbit secondary antibody (Molecular Probes) for 1h. The slides were mounted with Slow Fade (Molecular Probes). The sperm were imaged using a BioRad MRC1024 confocal microscope and BioRad Laser Sharp imaging software.

Membrane fractionation. This experiment was performed by the laboratory of Dr Richard Cardullo and the Western blot was provided to me for analysis with anti-synaptotagmin VIII anti-serum. All buffers contained a protease inhibitor cocktail of leupeptin (20 μg/ml), aprotinin (20 μg/ml), PMSF (1 mM), benzamidine (200 μg/ml). Sonicated sperm membranes were prepared with a probe sonicator (VirTis, Gardiner, NY) for 15 sec, on ice, repeated 3 times at intervals of 1 min. Cell debris was pelleted (500 x g for 15 min) and the membrane supernatant was collected, diluted to 5 ml with 1/10 TN (130mM NaCl, 20mM Tris-HCl pH 7,0), and crude membranes (CMs) pelleted by ultracentrifugation (SW 50.1 swinging bucket rotor at 108,000 x g for 1 hr, 4°C). CMs were fractionated on a sucrose step gradient (0.5 ml membranes, 1.5 ml 30% sucrose, 1.5 ml 40% sucrose, and 1.0 ml 45% sucrose) for 2 hrs at 125,000 x g at 4°C. Membrane fractions were collected from the interfaces: Band 1 = 0/30% interface, Band 2 = 30/40% interface, Band 3 = 40/45% interface, Band 4 = pellet.

Calcium Buffers. 10X stock calcium buffers were prepared by mixing the appropriate amount of 1 M $CaCl_2$ and 0.5 M EGTA to obtain the predicted 10X final free calcium concentration. The precise free calcium concentration of the 1X buffer for each concentration

used was determined by a calcium selective electrode (Corning) calibrated with calcium standards.

Titration of Streptolysin O in Non-Capacitated and Capacitated Sperm. Sperm were collected from cauda epididymides of 12-15 week old CD-1 mice and allowed to "swim-up" for 15 minutes at 37°C / 5% CO_2 in Krebs Ringer Bicarbonate Buffer (KRB) pH 7.4 media (5.6 mM glucose, 0.55 mM sodium pyruvate, 25 mM sodium bicarbonate, 53 μM sodium lactate, 99.6 mM sodium chloride, 4.8 mM potassium chloride, 1.2 mM potassium dihydrogen phosphate and 1.2 mM magnesium sulphate and 1.7mM $CaCl_2$). Live sperm were collected from the debris and dead sperm and processed for capacitation and AR. The extent of capacitation was assessed by examining the sperm hyper-motility. Samples with greater that 70% hypermotility were deemed capacitated and used. Samples with lower levels of hyeprmotility were not tested. Capacitated sperm were collected in KRB containing 3 mg/ml BSA and incubated at 37°C / 5% CO_2 for 1hr following "swim up". Sperm were pelleted at 300 x g for 5 minutes and resuspended in Ca^{2+}-free KRB pH 7.4 and diluted to a concentration of 5.0 x 10^6 sperm/ml with Ca^{2+}-free KRB pH 7.4. Sperm were permeabilized with the indicated concentration of recombinant SLO for 5 min at 37°C / 5% CO_2 and subsequently supplemented with $CaCl_2$ solutions to a final concentration of 1mM Ca^{2+}. Sperm were incubated for an additional 20 minutes at 37°C / 5% CO_2 and fixed with 4% paraformaldehyde. The extent of acrosome reaction was determined by Coomassie brilliant blue staining as indicated below.

Ca^{2+}-titration of the acrosome reaction in Streptolysin O permeabilized mouse sperm. Sperm were collected from cauda epididymides of 12-15 week old CD-1 mice and allowed to "swim-up" for 15 minutes at 37°C / 5% CO_2 in Krebs Ringer Bicarbonate Buffer (KRB) pH 7.4 media containing 3 mg/ml BSA. Live sperm were collected from the debris and dead sperm and capacitation was allowed to continue for 1hr at 37°C / 5% CO_2. Sperm were pelleted at 300 x g for 5 minutes and resuspended in Ca^{2+}-free KRB pH 7.4 and diluted to a concentration of 5.0 x 10^6 sperm/ml with Ca^{2+}-free KRB pH 7.4. Sperm were permeabilized with SLO (Sigma) at a final concentration of 0.6 U/ml (Johnson et al., 1999) for 5 min at 37°C / 5% CO_2 and subsequently supplemented with 10X $CaCl_2$ solutions to the indicated final concentration. Sperm were incubated for an additional 20 minutes at 37°C/5% CO_2 and fixed with 4% paraformaldehyde. The extent of acrosome reaction was determined by Coomassie brilliant blue staining as indicated below.

Introduction of recombinant proteins and antisera into Streptolysin O permeabilized mouse sperm. Sperm were collected and capacitated in KRB media pH 7.4 containing BSA at 3mg/ml as described above. Sperm were pelleted at 300 x g for 5 minutes and resuspended in Ca^{2+}-free KRB pH 7.4 and diluted to a concentration of 5.0 x 10^6 sperm/ml with Ca^{2+}-free KRB pH 7.4. Sperm were permeabilized with 0.6 units/ml (Sigma) for the antibody treatment of capacitated sperm or 5 μg/ml recombinant SLO for the antibody treatment of non-capacitated sperm and the recombinant protein treatment of capacitated sperm for 5 min at 37°C / 5% CO_2 in the presence of the indicated blocking agent. The samples were subsequently supplemented with $CaCl_2$ to a final concentration of 1 mM and incubated for an additional 20 minutes at 37°C / 5% CO_2 and subsequently fixed with 4% paraformaldehyde.

Recombinant proteins or antibodies were added at the permeabilization step from a concentrated stock in KRB to the indicated final concentrations and maintained throughout the subsequent incubation.

Assessment of acrosomal status. Fixed sperm were harvested by centrifugation at 800 x g for 5 minutes and washed 2 times with 0.5 ml of 0.1 M ammonium acetate pH 9.0. The sperm were subsequently resuspended in 0.1 M ammonium acetate pH 9.0 and air-dried on glass slides. The slides were then washed with water, methanol, and water for 5 minutes each. The sperm were stained with 0.625% Coomassie brilliant blue G-250 in 50% methanol and 10% acetic acid for 10 min at room temperature (Larson and Miller, 1999). The coomassie brilliant blue dye will stain all the protein in the sperm, but owing to the density of enzymes condensed within the small acrosome compartment, the latter appears dark blue following this staining procedure. The slides were subsequently washed 4 times with distilled H_2O and mounted with 30% glycerol in PBS. Sperm were imaged by bright-field microscopy using a Zeiss AxioPhot microscope and scored for acrosomal staining.

Data Processing. Data for the SLO-treated sperm were corrected for spontaneous AR by subtracting the percentage of AR in non-permeabilized sperm from that of SLO-permeabilized sperm and the maximal value was subsequently normalized to 100%. Two models were compared for fit to the data obtained from the Ca^{2+} titration of the AR in SLO-permeabilized sperm. These included a model that assumed a single binding site for Ca^{2+} of the form:

$$y = \max/(1+10^{(\log EC50-x)*\text{Hill slope}}),$$

where max = the maximum AR at saturating Ca^{2+}, EC50 = the Ca^{2+} at half-maximal binding, and Hill slope is the Hill coefficient that reflects cooperativity. The data were fit by nonlinear least squares regression (SigmaPlot) with max and EC50 as parameters of the fit. In addition, the fit to the data was compared assuming either a fixed Hill slope of 1 (no cooperativity) or a variable Hill slope fit to the data. The other model that was tested assumed 2 binding sites with different Ca^{2+} affinities ($EC50_1$ and $EC50_2$), which had the form:

$$y = max*(F1/(1+10^{(logEC50_1-x)Hill\ Slope_1})+(1-F1)/(1+10^{(logEC50_2-x)*Hill\ slope_2})),$$

where F1 is the fraction of the sperm with $EC50_1$.

In order to determine whether a model with fixed or variable Hill slope was appropriate, the Hill coefficient from the regression analysis was compared to that extrapolated from the Hill plot of the log(AR/nAR) as a function of $log[Ca^{2+}]$ where AR is the fraction of acrosome reacted sperm and nAR is the fraction of acrosome intact sperm. The fit comparison between the 1- and 2-site models was done by an F-test of the residuals. The *in vitro* Syt-Stx binding were fitted to a 1-site model with a fixed slope using the equation described above with a Hill slope of 1.

RESULTS

PRA1 Localizes Primarily to the Golgi Complex. To determine the subcellular localization of PRA1, the mammalian expression vector pIRESpuro containing the cDNA for the full-length protein was transfected with Lipofectamine into BHK cells and processed for immunocytochemical analysis after 48hrs. The full length PRA1 exhibited a perinuclear staining pattern with various punctuate loci dispersed throughout the cytoplasm (Figure 16A & 16C). This subcellular distribution is reminiscent of a Golgi and endosomal localization. Truncation of the carboxy-terminal tail of PRA1 resulted in a reticular staining pattern throughout the cell (Figure 16E & 16G), which is reminiscent of an ER distribution. In order to confirm the intracellular organelle with which each of these constructs is associated, the transfected cells were co-stained with mannosidase II and calnexin, a known Golgi complex (Velasco et al., 1993) and ER (Wada et al., 1991) marker, respectively. The full length PRA1 was found to co-localize with the Golgi marker mannosidase II (Figures 16A and 16B) and not with the ER marker calnexin (Figures 16C and 16D). In contrast, the reticular pattern of the truncated PRA1 (1-164) showed extensive co-localization with calnexin (Figures 16G and 16H) with little or no co-localization with mannosidase II (Figures 16E and 16F). These results clearly indicate that the wild-type PRA1 is preferentially associated with the Golgi whereas most of the truncated PRA1 (1-164) remains tightly associated with the ER structures.

GDI1 Co-precipitates with PRA1. In order to explore cytosolic factors that might interact with PRA1 by affinity chromatography, cytosol from PC12 cells was mixed with recombinant 6xHis-tagged PRA1, which was subsequently recovered by Ni-NTA beads. Protein

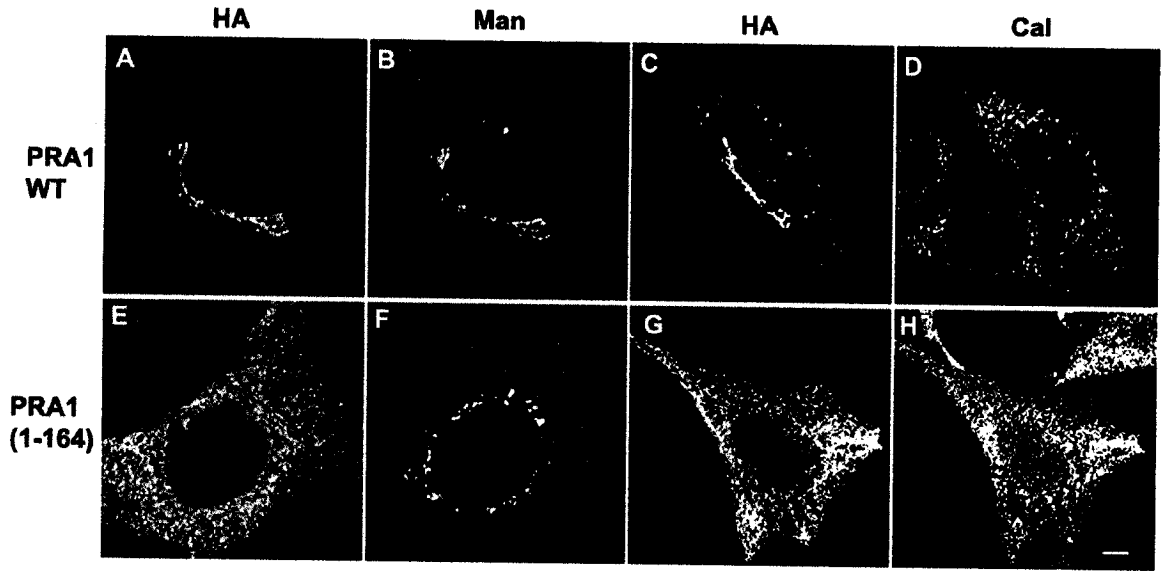

Figure 16: Immunocytochemical analysis of PRA1. Double immunofluorescent micrographs showing co-localization of HA-tagged PRA1 with mannosidase II (Man) and calnexin (Cal). BHK cells were transfected with HA-tagged wild-type (panels A, B, C and D) or truncated PRA1(1-164) (panels E, F, G and H). The cells were stained with monoclonal anti-HA (panels A, C, E and G) together with rabbit polyclonal anti-mannosidase II (panels B and F) or anti-calnexin (panels D and H). The membrane-bound wild-type PRA1 co-localized with the Golgi marker mannosidase II (panels A and B) but not with the ER marker calnexin (panels C and D). In contrast, the truncated PRA1(1-164) extensively co-localized with calnexin (panels G and H) and showed little or no co-localization with mannosidase II (panels E and F).

complexes eluted from the beads were analyzed by Western immunoblot with anti-GDI antibodies. The results revealed the presence of GDI1 co-precipitating with the recombinant PRA1 (Figure 17A). Only a small fraction of the total cellular GDI1 was associated with the recombinant PRA1 but none was found to co-precipitate with the Ni-NTA beads in its absence. This may reflect a low avidity in the interaction between the two proteins under my binding and washing conditions. Alternatively, since most of the cytosolic GDI1 exists as a complex with a Rab GTPase, it is possible that the interaction is limited to free or unbound GDI1. This appears to be the case as I was unable to detect the presence of a stable PRA1-Rab3A-GDI1 trimeric complex. To verify this interaction between PRA1 and GDI1, I examined the binding of these two proteins *in vitro*. Recombinant 6xHis/HA-tagged PRA1 was added to bacterially expressed GST or GST-HA-GDI1 in a pull down assay. The GST-tagged proteins were then recovered with glutathione-Sepharose. PRA1 was readily detected with the GST-HA-GDI1 fusion protein but not with the GST control, indicating that PRA1 can form a complex with GDI1 (Figure 17B). Conversely, I examined whether GDI1 can be recovered with recombinant PRA1. The GST-HA-GDI1 fusion protein was cleaved with thrombin to remove the GST moiety, which I have subsequently discovered to be more efficient in binding to PRA1 (data not shown). This was added to either the full length or truncated 6xHis/HA-tagged PRA1, and Ni-NTA beads were then used to recover the recombinant PRA1. As shown in Figure 17C, recombinant GDI1 was recovered along with the full length PRA1 in the Ni-NTA beads. No GDI1 was recovered with the Ni-NTA beads in the absence of PRA1. Truncation of the carboxy-terminal 21 amino acids of PRA1 eliminated the binding to GDI (Figure 17C). This suggests that the GDI1 shares a common binding region on PRA1 with Rab3A, which could explain why a trimeric complex composed

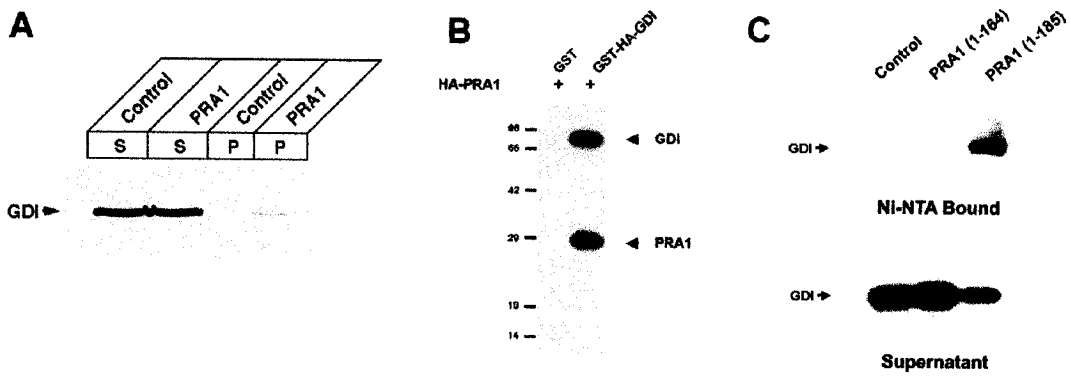

Figure 17: *In vitro* binding assay of PRA1 to GDI1. A, recombinant 6xHis-, HA-tagged PRA1 was added to PC12 cytosol and recovered with Ni-NTA beads. The proteins were analyzed with anti-GDI1 antibodies. No recombinant protein was used in the control sample. B, confirmation of the interaction using GST-fusion of HA-tagged GDI1. Recombinant 6xHis-, HA-tagged PRA1 was incubated with either GST or GST-HA-GDI1. Glutathione-Sepharose was used to recover the GST-tagged protein and analyzed with anti-HA antibodies, which detect both recombinant PRA1 and GDI1. C, Thrombin-cleaved HA-tagged GDI1 was incubated with 6xHis, HA-tagged PRA1 with the 6xHis-tagged proteins subsequently recovered with Ni-NTA beads. Proteins recovered with the Ni-NTA beads (top panel) and remaining in the supernatant (bottom panel) were analyzed with anti-GDI antibodies. GDI1 was recovered in the Ni-NTA beads only with the wild-type PRA1(1-185), and not in its absence (Control) or in the presence of the truncated PRA1(1-164).

of these 3 proteins could not be isolated. Thus, it would appear that PRA1 could interact directly with GDI1 in the absence of Rab, and that deletion of the carboxy-terminal domain also abolished this activity.

PRA1 Inhibits the GDI1-Mediated Extraction of Rab3A from the Membrane. Removal of GDP-bound Rab from the membrane is dependent on GDI, which is also involved in inhibiting the dissociation of GDP from the Rab GTPases, and in delivering Rab to the correct membrane compartment (Dirac-Svejstrup et al., 1994; Peter et al., 1994; Ullrich et al., 1993). Since PRA1 binds to Rab GTPases and weakly to GDI1, I sought to examine whether PRA1 can influence the cycling of Rab GTPases. I first confirmed that the recombinant GST-HA-GDI1 fusion protein could indeed extract membrane bound Rab GTPases in an *in vitro* extraction assay. Purified recombinant GDI1 was added to PC12 microsomal membranes in the presence of GDP and Mg^{2+}, conditions known to facilitate extraction of Rab GTPases by GDI1 by favoring the GDP-bound form of the Rab GTPase. After incubation at 37°C for 20 min, the membranes were chilled on ice and recovered by high-speed centrifugation. Both supernatant and pellet fractions were analyzed by Western immunoblot for the presence of Rab3A. Extraction of Rab3A from the PC12 membranes would result in its appearance as a soluble Rab3A-GDI1 complex in the supernatant fraction. I first determined the amount of recombinant GDI1 required to effectively extract the membrane-bound Rab3A. As shown in Figure 18A, addition of recombinant GDI1 resulted in the extraction of membrane-bound Rab3A in a concentration dependent manner. Approximately 10 nM of GDI1 was required to extract 50% of the total Rab3A in 25 μg of PC12 microsomal membranes (Figure 19A). Increasing the amount of recombinant GDI1 to 25 nM extracted nearly all the membrane-

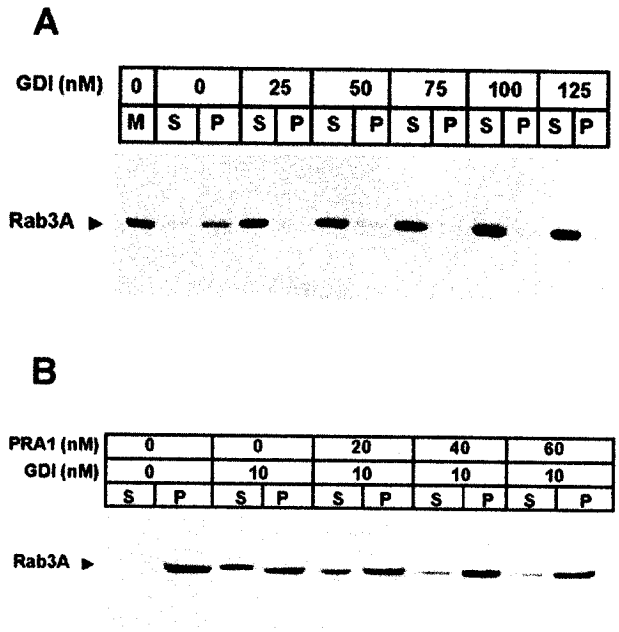

Figure 18: PRA1 inhibits the extraction of membrane-bound Rab by GDI1. A, representative immunoblot of GDI1 titer assay. Recombinant GST-HA-GDI1 in the concentration indicated (nM) was added to 25 μg of PC12 membranes in the presence of $MgCl_2$ and GDP. After incubation at 37°C for 20 min, the membranes were recovered by high-speed centrifugation and the fractions analyzed with anti-Rab3A antibodies. There was little loss of Rab3A from the membranes in the absence of GDI1. B, addition of recombinant PRA1 to PC12 membranes inhibited the removal of membrane-bound Rab3A. Addition of 10 nM of recombinant GDI1 removed approximately 50% of the Rab3A in 25 μg of PC12 membranes. This activity was blocked by the addition of recombinant PRA1 in the concentrations indicated.

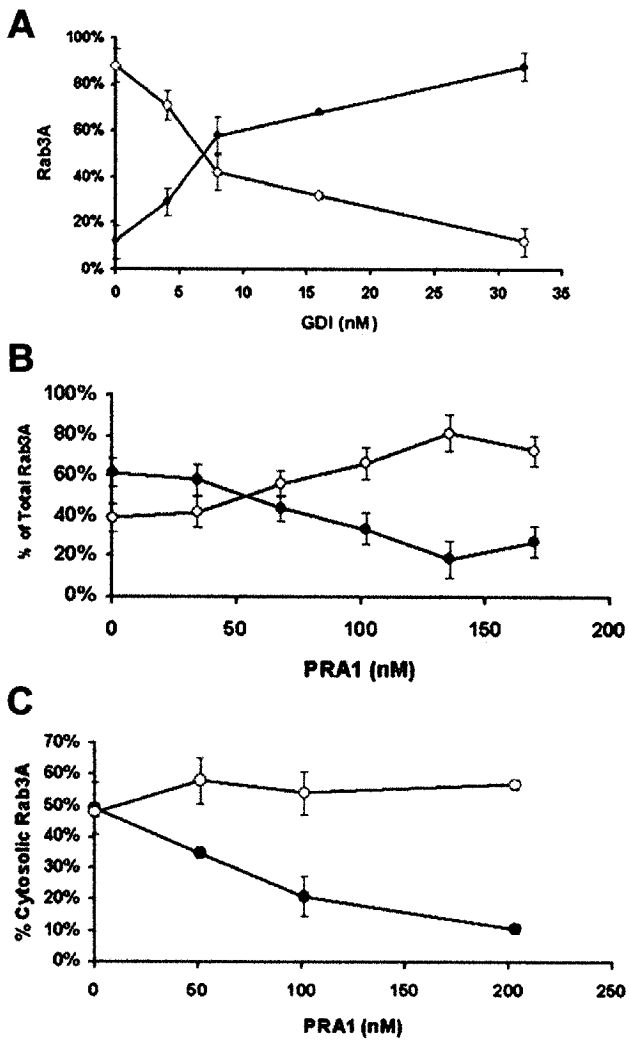

Figure 19: Inhibition of GDI1-mediated removal of Rab3A by PRA1. The Western immunoblots as described in the Materials and Methods were scanned, and the relative distribution of Rab3A in the supernatant and membrane fractions was expressed as a percentage of the total in the sample. A, removal of membrane-bound Rab3A by recombinant GDI1. (•), cytosolic Rab3A; (○), membrane-bound Rab3A. Each point represents the mean ± SEM (n=3). B, addition of recombinant PRA1 to the reaction with 10 nM of GDI1 inhibited the removal of Rab3A from the membrane. Each sample contains 25 μg of PC12 membranes and 10 nM of GDI1. Increasing amount of recombinant PRA1 was added to the samples and the distribution of Rab3A in the cytosol (•) and membrane (○) was determined by Western immunoblot. Each point represents the mean ± SEM (n=6). C, effect of full length (•) and truncated PRA1(1-164) (○) on GDI1-mediated removal of Rab3A from PC12 membranes. The assay conditions were as described in panel B except only the cytosolic Rab3A expressed as a percentage of the total was plotted. Each point represents the mean ± SEM (n=4).

bound Rab3A (Figure 18A & 19A). A higher amount of GDI1 was required to extract Rab1A, which may reflect either a difference in efficacy or a greater amount of Rab1A in the membrane (data not shown). To test whether recombinant PRA1 can influence the extraction of Rab3A by GDI1, enough recombinant GDI1 was added to effectively remove approximately 50% of the membrane-bound Rab3A. Under these conditions, addition of increasing amounts of recombinant PRA1 resulted in inhibition of GDI1 extraction of membrane-bound Rab3A (Figure 18B & 19B). There was a concomitant increase in Rab3A remaining in the membrane pellet with increasing amount of recombinant PRA1. In contrast, addition of recombinant truncated PRA1 (1-164), which was unable to bind to either Rab GTPases or GDI1, failed to inhibit the extraction of Rab3A by GDI1 (Figure 19C). Thus, the presence of excess amount of PRA1 exerted an inhibitory effect on the extraction of Rab3A by GDI1 resulting in membrane retention of the Rab GTPase.

It appears that PRA1 plays a critical role in the cycling of Rab3A, which suggests that it is critical for the proper trafficking of secretory vesicles in the regulated pathway. However, in addition to understanding the regulation of trafficking of vesicles to the site of fusion, it is important to understand the regulation of the fusion reaction itself. The fusion of vesicles in the regulated pathway requires a calcium sensing module to transmit the increase in intracellular Ca^{2+} to the SNARE core complex. This role has been attributed to the synaptotagmin family of proteins. However, the exact manner in which this protein family performs this task is not known, since they are also believed to participate in the endocytic pathway in addition its role in the exocytic pathway. In order to address the possible function

of synaptotagmin in the secretory pathway, I have examined the fusion of the sperm acrosome with the PM, an exocytic event which does not contain an endocytic component.

Synaptotagmin VIII is expressed in the testis. In order to ascertain which Syt isoforms may function as a Ca^{2+} sensor for the AR, I decided to confirm the observation by Li *et al.*, which showed that Syt VI and VIII are expressed in rat testis. I performed PCR amplification of Syt I, VI and VIII from pachytene spermatocyte and round spermatid λ phage libraries as well as from a mouse brain cDNA. The Syt VI PCR results were inclusive while Syt VIII amplification from both the spermatogenic libraries and the brain indicated that it is expressed in germ cells. Southern blot analysis revealed that the 531 bp product of Syt VIII was amplified in all three samples while the 411 bp amplification product of Syt I was detected only in the mouse brain (Figure 20).

Having confirmed that Syt VIII mRNA is expressed in germ cells, I next sought to establish if Syt VIII was present at the protein level in murine sperm. In order to distinguish Syt VIII from other Syt isoforms, I generated a Syt VIII-specific antiserum since no commercial source was available. All Syt isoforms contain two C2 domains (Figure 12) and the region between these two calcium-binding regions shows the greatest divergence. Hence, a 13-mer peptide in this region (amino acids 218-230) was chosen as the antigen to ensure antibody specificity. The specificity of the antiserum was verified using bacterially expressed GST fusion proteins of the cytoplasmic domains (C2AB) of Syt I to VIII. A single band was detected for Syt VIII fusion protein while no bands were detected for any other isoforms tested (Figure 21A). Expression and loading of each Syt isoform was confirmed by detection with anti-GST antibodies (Figure 21A). A commercially available Syt antibody from

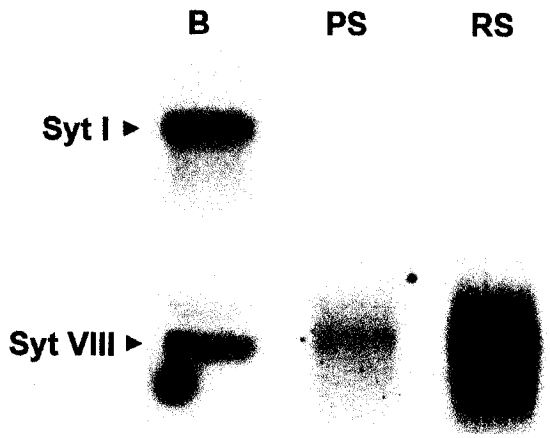

Figure 20: Southern blot analysis of PCR amplified Syt I and Syt VIII products from spermatogenic libraries. The PCR amplified products were separated on agarose gel, transferred to nitrocellulose membranes, and hybridized with Syt I- or Syt VIII-specific probes. Syt I was detected in brain cDNA but absent from the two spermatogenic libraries whereas Syt VIII was detected in both spermatogenic cDNA libraries and in brain. B, brain; PS, pachytene spermatocyte; RS, round spermatid.

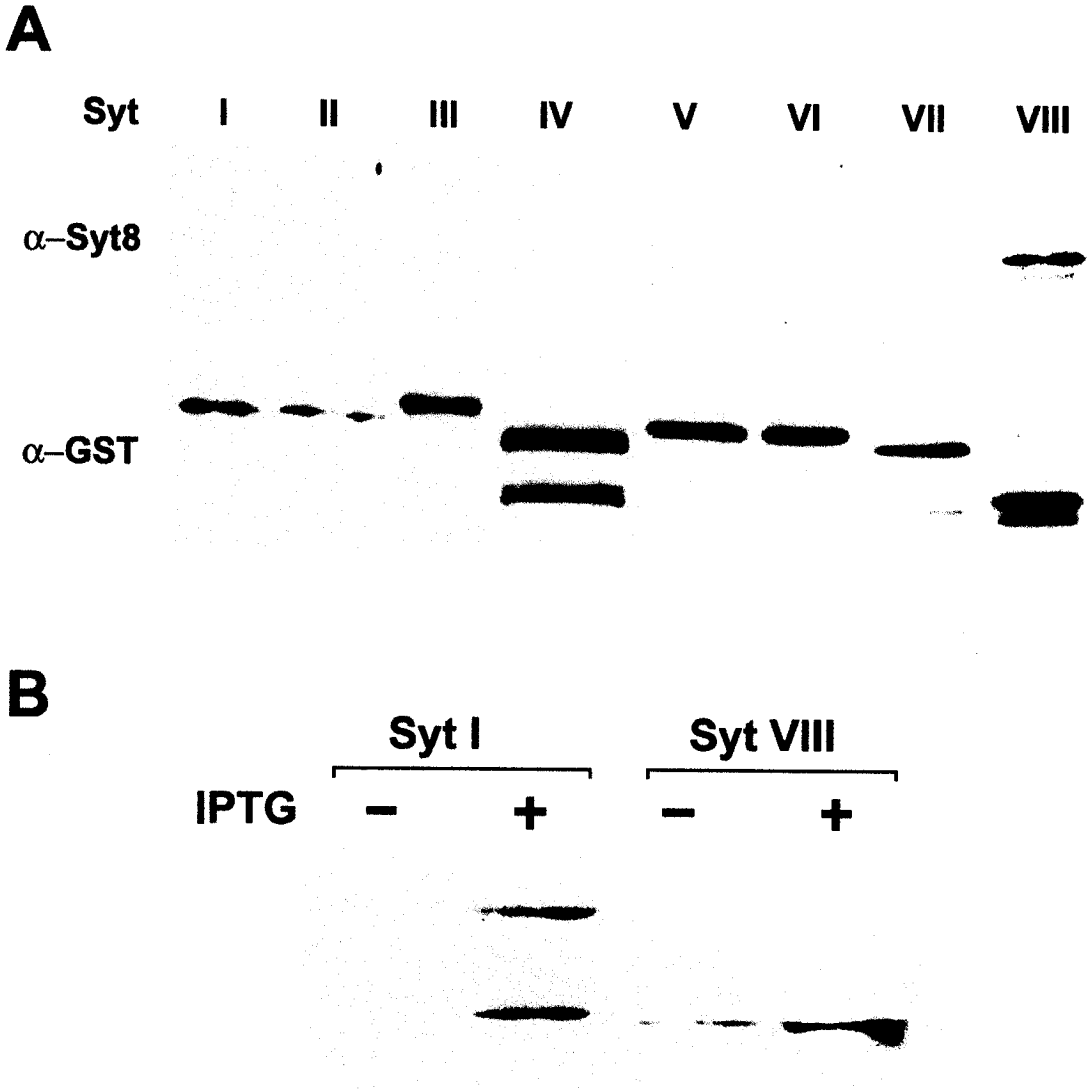

Figure 21: Specificity of Syt VIII antiserum. A. Western immunoblot of GST fusion protein probed with anti-Syt VIII (upper panel) or anti-GST (lower panel). **B.** Western immunoblot of GST fusion protein of Syt I and Syt VIII from bacteria grown in the absence of (-) or induced with (+) IPTG. The immunoblot was probed with anti-Syt from Transduction Laboratories.

Transduction Laboratories detected both recombinant Syt I and VIII upon induction with IPTG (Figure 21B). Hence, these results confirmed that the antiserum is specific to Syt VIII among the isoforms tested in contrast to the commercial antiserum, which cross-reacts with several Syt isoforms.

Synaptotagmin VIII is present in sperm and localizes to the acrosomal region. In order to determine whether the Syt VIII protein is present in mature spermatozoa, whole sperm homogenate was probed with Syt VIII antiserum as well as the anti-Syt from Transduction Laboratories and compared to brain homogenate. Both antibodies detected a single clear prominent band at ~65 kDa in sperm homogenates (Figure 22), which corresponds to the expected size of the synaptotagmin family of proteins (Perin et al., 1990). Both antibodies also detected a faint band of the same size in the brain homogenate with a major additional faster-migrating band detected in brain only by the cross-reactive Syt antibody from Transduction Laboratories (Figure 22). This result confirms that Syt VIII is present in mature spermatozoa and indicates that the faster-migrating isoforms(s) prominent in the brain homogenate is or are not present in sperm.

I next determined the subcellular localization of Syt VIII in sperm. Western immunoblot analysis of sperm subcellular membrane fractions using our anti-Syt VIII antiserum (Figure 23) revealed that Syt VIII is found almost entirely within membrane fraction band 2. This fraction contains membranes derived from the sperm head, as indicated by the presence of several proteins known to be localized to the sperm head, including the sperm-specific β -1,4 galactosyltransferase and PH20/hyaluronidase (Baker et al., 2002). This suggested that Syt VIII partitioned with membranes derived from the sperm head. In order to

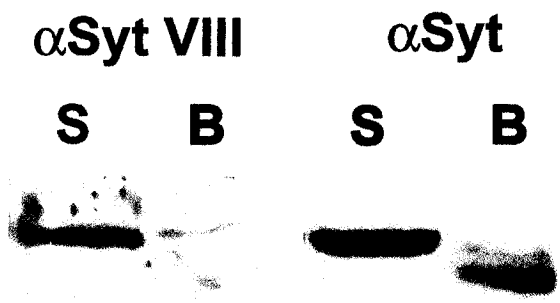

Figure 22: Western immunoblot of sperm and brain homogenates. Each lane contained 50 μg of protein and the blot was reacted with either anti-Syt VIII or anti-Syt from Transduction Laboratories. A single band was detected using anti-Syt VIII in both mouse sperm and brain homogenates. The commercial anti-Syt detected a single band in the sperm homogenate and multiple bands in the brain homogenate.

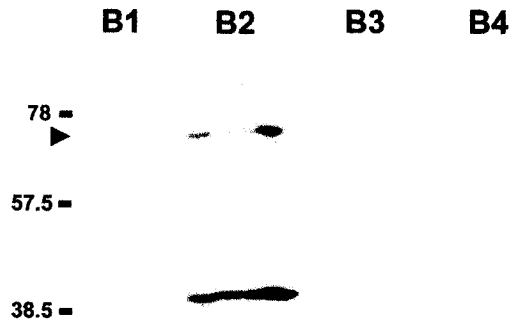

Figure 23: Western immunoblot of sperm membrane fractions. Crude membranes were isolated from sonicated sperm and separated on a 3-step (30-45%) sucrose density gradient. Three fractions representing membranes at the sucrose gradient interfaces (B1 to B3) and the resulting pellet at the bottom (B4) were analyzed by Western immunoblot using anti-Syt VIII.

further define the cellular localization of the protein, an immunocytochemical analysis was performed on fixed sperm using the anti-Syt VIII antiserum. Syt VIII was localized to the head of murine sperm in a crescent shaped pattern that is characteristic of the acrosome (Figure 24). These results taken as a whole confirmed that Syt VIII is indeed present in the acrosomal region of murine sperm and would be properly localized to participate in the membrane fusion event known as the AR.

Synaptotagmin VIII is shed upon acrosome reaction. Following the AR, components of the fusion machinery would be lost with the shed vesicles and would therefore become undetectable in acrosome-reacted sperm (Schulz et al., 1998; Schulz et al., 1997). In order to determine whether Syt VIII is shed upon acrosome reaction, I used the calcium ionophore A23187 to induce acrosomal exocytosis, and compared the immunoreactivity of Syt VIII in mock-treated and A23187-treated sperm. I assessed an aliquot of each sample to determine the fraction of acrosome reacted sperm using the Coomassie Blue staining method (Larson and Miller, 1999) and assessed a parallel sample for Syt VIII immunoreactivity. A representative sample of triplicate experiments is shown in Figure 25 (Panel A & B). The acrosome, which appears as a darker crescent structure when stained with Coomassie Blue, was lost following the AR (Figure 25A). Likewise, Syt VIII immunoreactivity was lost upon acrosomal exocytosis (Figure 25B). The fluorescent signal observed in the tail of the sperm is due to non-specific immunoreactivity since it was present in sperm stained with pre-immune serum (data not shown). As shown in Figure 25 (panel C), A23187 caused approximately 52% of the sperm to undergo acrosome reaction as assessed by Coomassie Blue staining. This correlated well with the 47% loss in Syt VIII-immunoreactive sperm upon A23187 treatment.

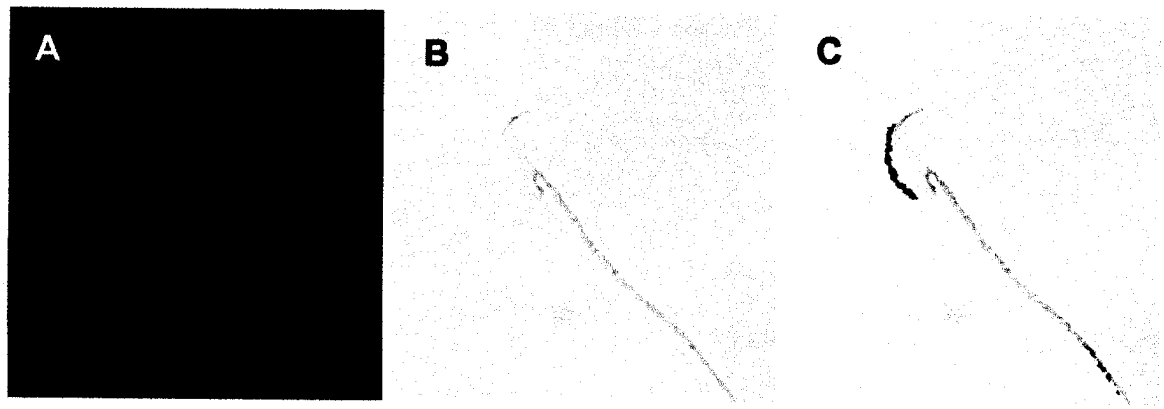

Figure 24: Immunocytochemical localization of Syt VIII in murine sperm. A, Mouse sperm were fixed and reacted with anti-Syt VIII. The bound antibodies were visualized with Alexa 594-conjugated secondary antibodies. Syt VIII showed a crescent shaped staining pattern on the convex side of the sperm head characteristic of the acrosome. B, DIC image of the same sperm shown in panel A. C, Merged image of panels A and B confirming that Syt VIII is localized to the acrosomal region of murine sperm.

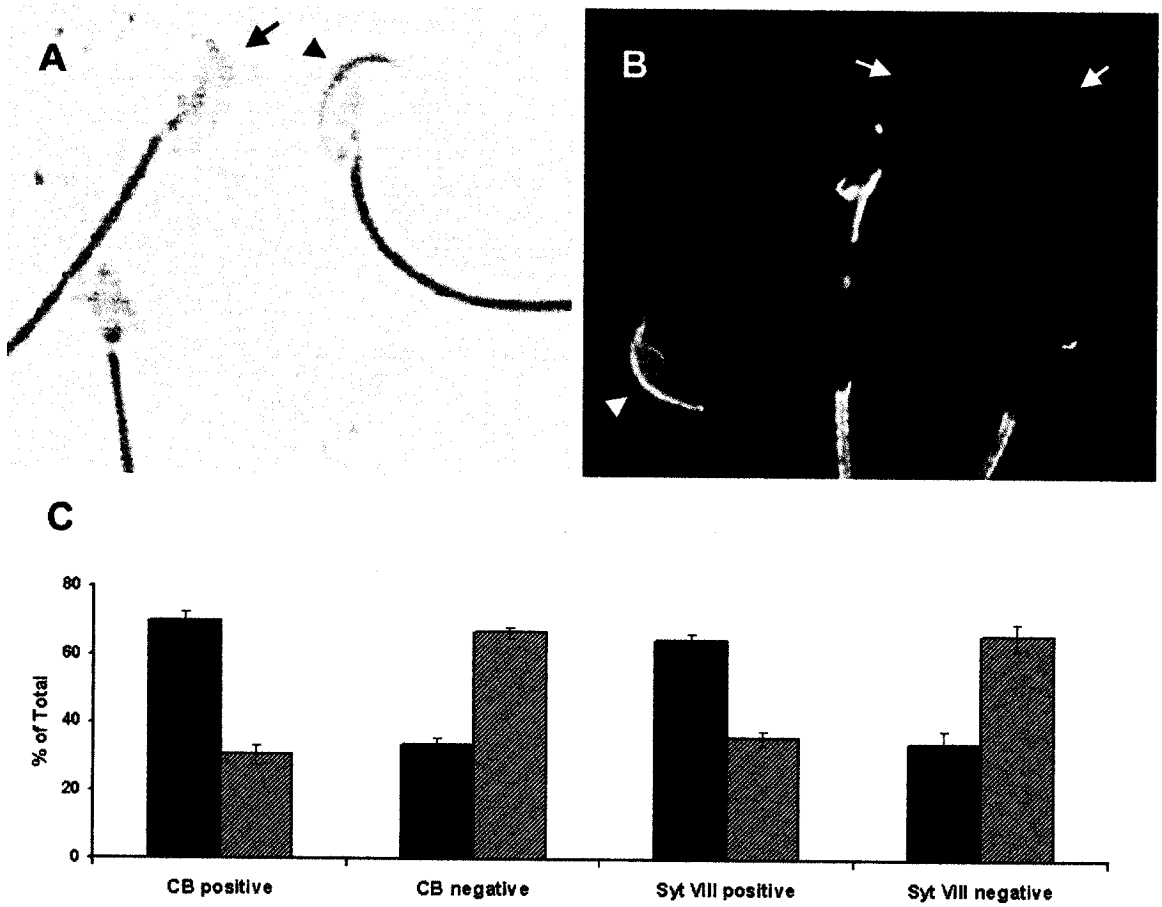

Figure 25. Acrosome reaction induced with the Ca^{2+} ionophore A23187. Representative images of A23187-treated sperm stained with either Coomassie Blue (A) or anti-Syt VIII (B). Each panel contained acrosome intact (arrowhead) and acrosome reacted (arrow) sperm. **C.** Quantitative analysis averaged from three experiments of acrosome reaction by counting the number of Coomassie Blue (CB) or Syt VIII positive and negative sperm. The sperm were either mock-treated with DMSO (solid bars) or induced to acrosome react with A23187 (hatched bars). The results are expressed as the percentage of acrosome reaction ± SEM (n = 3)

To further confirm this observation, I quantified the loss of Syt VIII immunoreactivity by densitometric analysis of Western immunoblots of mouse sperm homogenates following induction of AR with A23187 (Figure 26). The mock- and A23187-treated samples were adjusted to a concentration of 10^5 sperm/µl, and 0.5, 1.0 and 2.0 x 10^6 sperm were solubilized and processed for Western immunoblot. Densitometric analysis of the Syt VIII signal intensity showed a 54% decrease in Syt VIII immunoreactivity in the A23187-treated sperm relative to mock-treated samples (Figure 26A). This decrease in Syt VIII immunoreactivity correlated well with the extent of sperm that undergo acrosome reaction as assessed by Coomassie Blue staining or by Syt VIII immunocytochemistry (Figure 26C). Thus, taken together, the immunohistochemical and densitometric analyses indicate that Syt VIII is lost upon acrosome reaction. The observations above suggest that Syt VIII may act as a Ca^{2+}-sensor in the regulation of fusion between the OAM and the PM in mouse sperm. In order to confirm this hypothesis, I sought to investigate the functional role of Syt VIII in the murine AR.

Calcium Dependence of the Acrosome Reaction. One of the difficulties with assessing the role of a given protein in vesicle fusion is its possible involvement in the endocytic or retrograde pathway. Therefore, deciphering if a protein is involved in either fusion or endocytosis or both is difficult to interpret. One system which allows for analysis of membrane fusion in the absence of endocytosis is the sperm AR in which the OAM fuses with the overlying PM resulting in vesiculation and shedding of the vesicles with no possibility for endocytic retrieval (Figure 15). I have chosen this system in order to determine the possible role of Syt VIII as a Ca^{2+} sensor in membrane fusion. To estimate the calcium dependence of

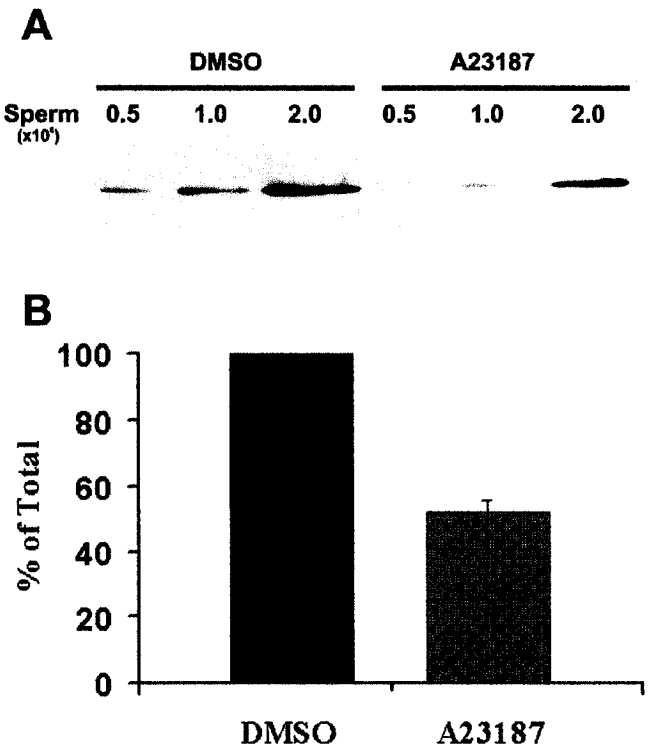

Figure 26. Quantitative analysis of Syt VIII in acrosome reacted sperm. A. Varying amounts of acrosome intact (DMSO-treated) and reacted (A23187-treated) sperm were analyzed by Western immunoblot using anti-Syt VIII. The band was determined by densitometry. **B.** Histogram of densitometric analysis of the Western immunoblot representing three independent experiments. The intensities of the A23187-treated samples (shaded bar) were expressed as a percentage of the mock (DMSO)-treated samples (solid bar) (n = 3).

the membrane fusion event in the AR of murine sperm, the free calcium concentrations in the sperm incubation media were varied from 0 to 2 mM, and the extent of AR assessed in sperm whose plasma membranes had been selectively permeabilized with SLO (Figure 27) to allow equilibration of calcium at the site of fusion with external calcium. As predicted, increasing the extracellular calcium concentration resulted in a dose-dependent increase in AR in SLO-permeabilized sperm (Figure 28A), which appeared to reach saturation as calcium concentrations approached the millimolar range. The analysis of the data was performed using a 1-site sigmoidal-dose response model as described in the methods, which yielded an EC_{50} of 87 μM Ca^{2+}. Regression analysis of the curve revealed a Hill slope of 0.67, which suggests that the AR does not exhibit cooperativity. This conclusion is supported by analysis of the Hill plot, which yielded a linear regression with a similar Hill slope of 0.73 (Fig 28A, inset). Analysis of the data using a unitary Hill slope did not yield a significantly different fit to the data since both curves can be overlayed and the EC50 value of 98 μM is near the value obtained for the variable slope model. The distribution of the data suggested that a 2-site sigmoidal dose-response model could possibly provide a better fit (Figure 28B), however a comparison of the fit with the 1-site model by an F-test of the residuals revealed an F value of 0.45 ($p = 0.72$). This result shows that the more complicated 2-site model does not provide a significantly better fit and therefore I have chosen to use the 1-site model for further comparison. In addition, regression analysis of the 2-site model revealed EC_{50} values of 1 mM and 36 μM for the 1st and 2nd sites, respectively (Figure 28B). While the EC_{50} value of 36 μM is close to that obtained for the 1-site model, the value for the 1st site is not physiologically relevant, further arguing against this model.

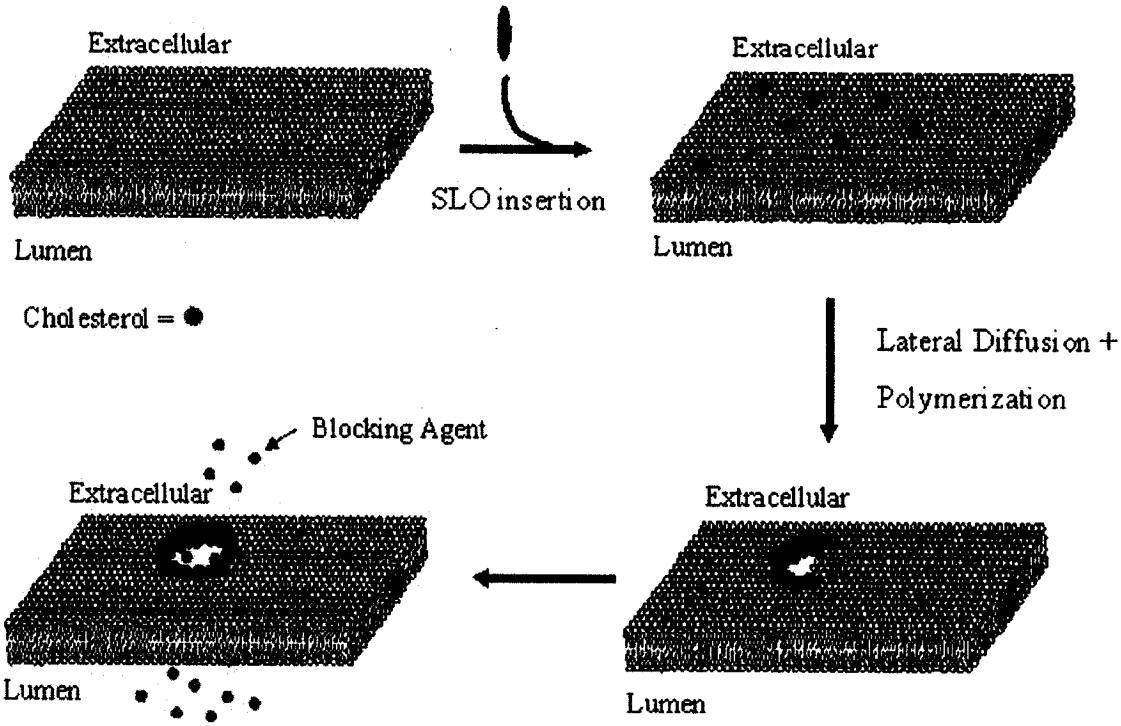

Figure 27. Cartoon depicting the membrane permeabilization by Streptolysin O. Streptolysin O (blue) is a bacterial pore toxin that inserts into the membrane as monomers by interacting with membrane cholesterol (red). Once inserted into the membrane the SLO monomers are capable of lateral diffusion and they polymerize in the membrane to generate a large non-selective pore by which large polypeptides (green) can be introduced into the permeabilized cell.

A

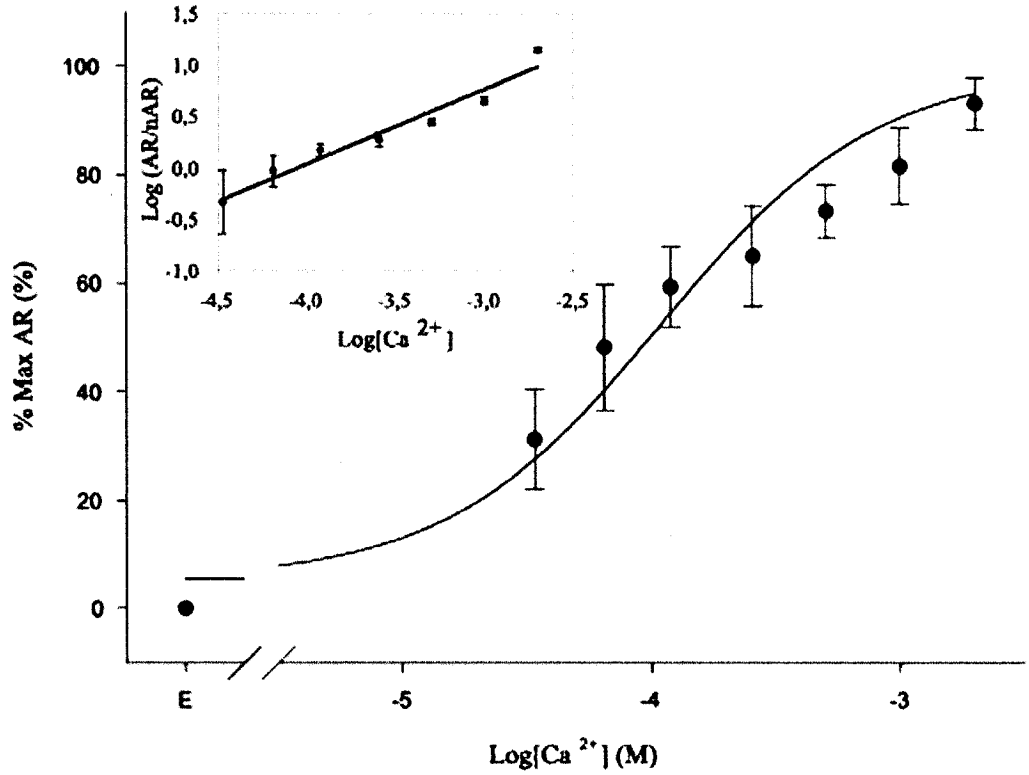
% Max AR (%)
100
80
60
40
20
0
E
-5
-4
-3
Log[Ca 2+] (M)
Log (AR/nAR)
1,5
1,0
0,5
0,0
-0,5
-1,0
-4,5
-4,0
-3,5
-3,0
-2,5
Log[Ca 2+]

B

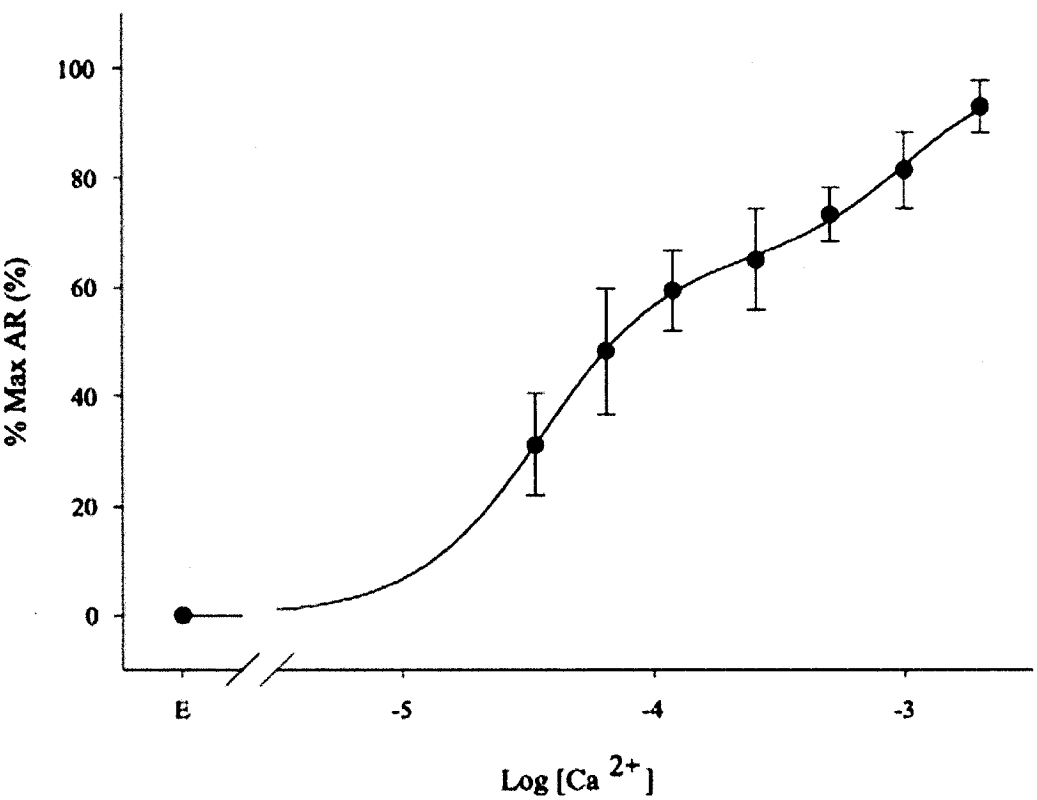
% Max AR (%)
100
80
60
40
20
0
E
-5
-4
-3
Log [Ca 2+]

Figure 28: Calcium titration of the mouse sperm acrosome reaction. SLO-permeabilized sperm were incubated in KRB containing various concentrations of free calcium from 34 μM to 2 mM for 20 minutes at 37°C / 5% CO_2. The sperm were fixed and stained with Coomassie brilliant blue and the extent of AR was assessed by counting at least 200 sperm per slide. The data is expressed as a percentage of maximal AR, which is obtained after subtracting the extent of AR in non-permeabilized sperm from that seen in SLO-permeabilized samples at each calcium concentration and subsequently expressing each as a percentage of the maximal AR. The values represent the average of 5 independent experiments. **A.** AR data plotted using a 1-site model with variable slope. The EC_{50} value for the calcium titration of the AR is 87 μM. Inset. A Hill plot for the Ca^{2+} titration of the AR is shown. The linear regression reveals a Hill coefficient of 0.73. **B.** AR data plotted using a 2-site model with variable slope. The EC_{50} values for the calcium titration of the AR are 34 μM and 1 mM. The actual extent of AR seen in the mock treated samples at all concentrations of Ca^{2+} was 25.8 ± 0.5%, while the true extent of AR seen in SLO-permeabilized sperm ranged from 24.8 ± 1.5% at 0 mM Ca^{2+} to 41.8 ± 1.5% at the highest concentration of 2 mM Ca^{2+}.

Calcium Dependence of Binding between Synaptotagmin and Syntaxin Isoforms in Sperm. Results from Li *et al.* have reported that the isoforms of Syt which have been shown to be present in sperm, namely Syt VI and VIII (Hutt et al., 2002; Li et al., 1995; Michaut et al., 2001), do not exhibit Ca^{2+}-dependent binding to the SNARE protein Stx or to PL, properties which are believed to mediate the activity of Syt as a Ca^{2+} sensor (Li et al., 1995). These conclusions were based on experiments performed with only the 1st C2 domain (C2A) of Syt VI and VIII. In order to fully assess the Ca^{2+} dependence of binding between the isoforms of Syt and Stx reported to be present at the protein level in sperm, namely Syt VI and VIII and Stx2 (Hutt et al., 2002; Katafuchi et al., 2000; Michaut et al., 2001), I performed *in vitro* pull down assays using the entire cytoplasmic region of these proteins. Although the binding has been mapped to the C2A domain (Shao et al., 1997), the presence of the tandem C2A and C2B (C2AB) has been shown to increases the affinity of Syt I for Stx1 (Chapman et al., 1996). Recombinant 6xHis/HA tagged Stx1 or 2 was added to GST-C2AB of Syt I, VI or VIII bound to glutathione-Sepharose in the presence of varying Ca^{2+} concentrations. The amount of Stx that bound to Syt was measured by Western immunoblot using anti-HA (Figure 29) and the extent of binding quantified by densitometric analysis. I utilized the binding of Syt I to Stx1 as a positive control since this interaction has been extensively characterized and shown to exhibit an EC_{50} value in the order of 100-180 μM Ca^{2+} (Chapman et al., 1995; Littleton et al., 1993). The EC_{50} value of 117 μM Ca^{2+}, which I obtained for this same pairing (Figure 30A) is within the previously determined range. In addition, I have shown here that Syt I binds to Stx2, and determined the EC_{50} for this interaction to be somewhat higher than that for Stx1, at 175 μM (Figure 30B).

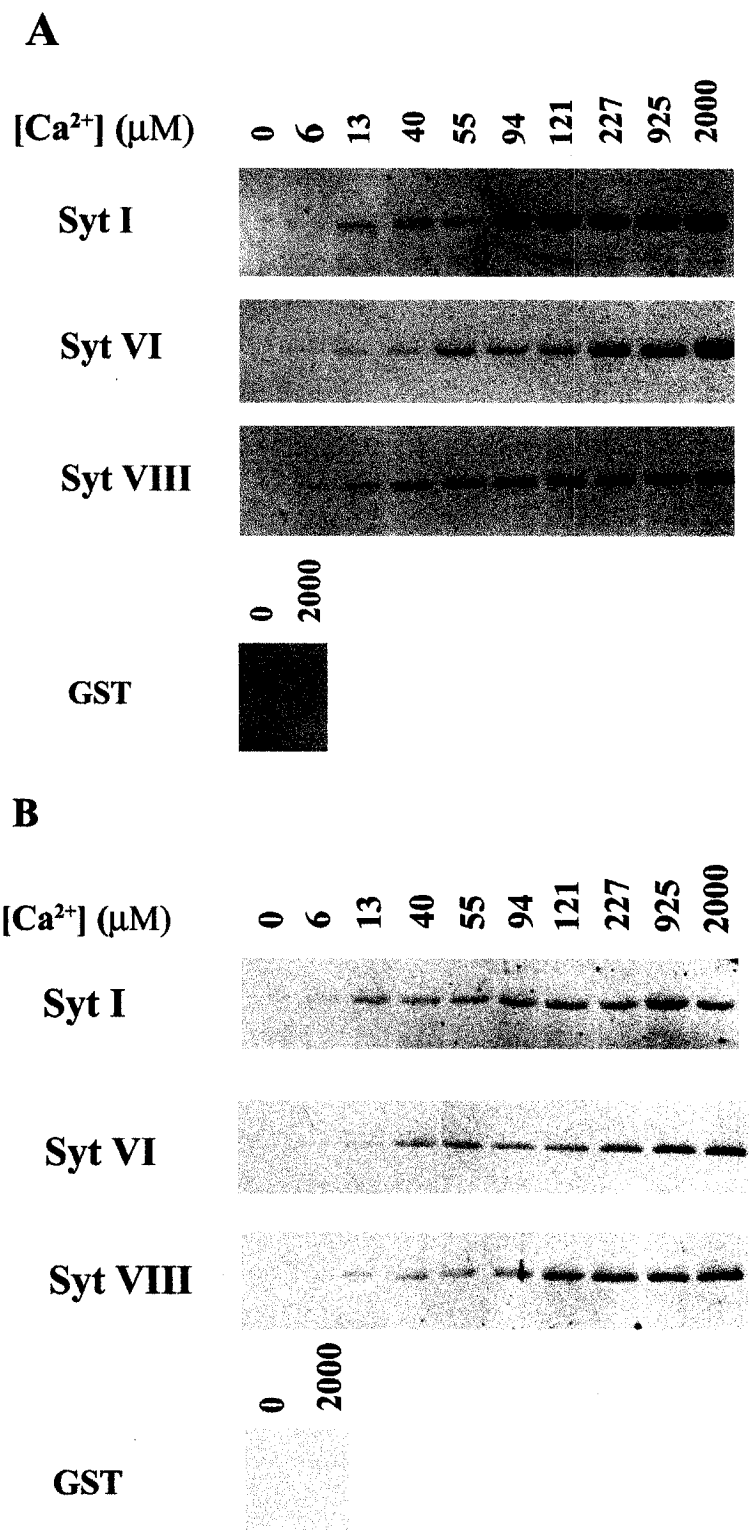
A
[Ca2+] (μM)
0 6 13 40 55 94 121 227 925 2000
Syt I
Syt VI
Syt VIII
0 2000
GST
B
[Ca2+] (μM)
0 6 13 40 55 94 121 227 925 2000
Syt I
Syt VI
Syt VIII
0 2000
GST

Figure 29. Western blot of the in vitro binding assay between syntaxin and synaptotagmin isoforms. Recombinant His/HA-tagged Stx was added to recombinant GST-tagged Syt C2AB bound to glutathione agarose beads and incubated in binding buffer with the indicated Ca^{2+} concentration. The beads were washed extensively with binding buffer. The bound protein were eluted with SDS buffer and separated on SDS-PAGE. Western immunoblot analysis with anti-HA antibody was performed to detect the bound Stx. **A.** A representative blot of Stx1 binding to Syt I, VI and VIII at varying Ca^{2+} concentrations and to GST at 0 and 2000μM free-Ca^{2+}. **B.** A representative blot of Stx2 binding to Syt I, VI and VIII at varying Ca^{2+} concentrations and to GST at 0 and 2000μM free-Ca^{2+}.

A

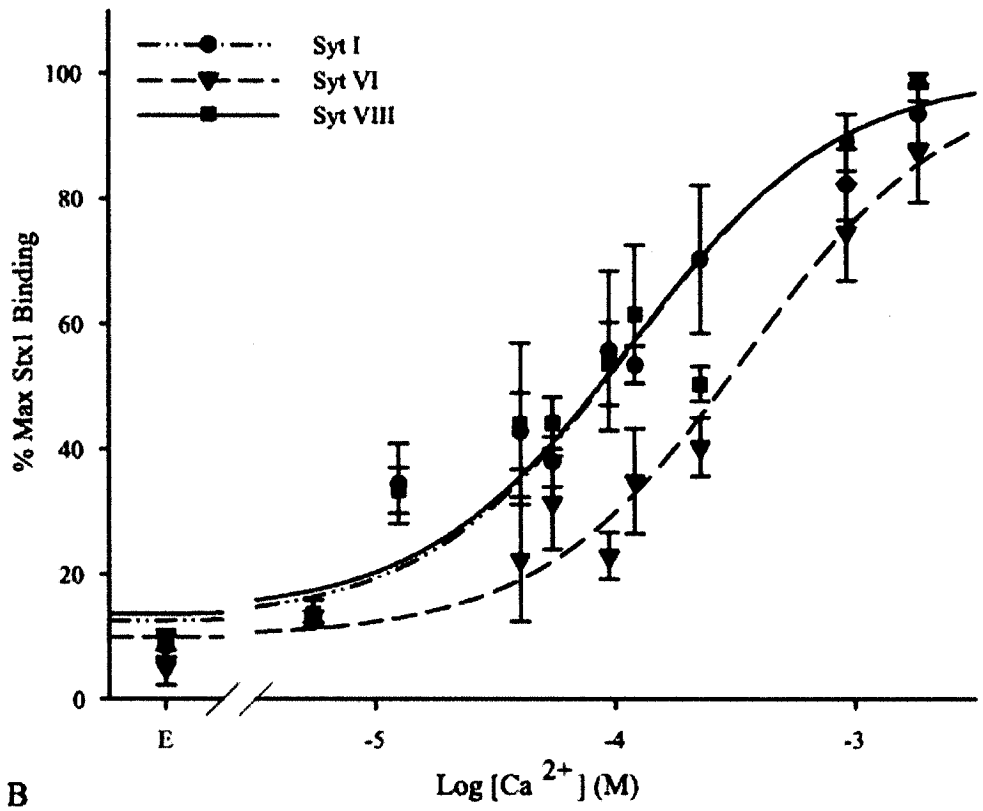
Syt I
Syt VI
Syt VIII
% Max Stx1 Binding
100
80
60
40
20
0
E
-5
-4
-3
Log [Ca 2+] (M)

B

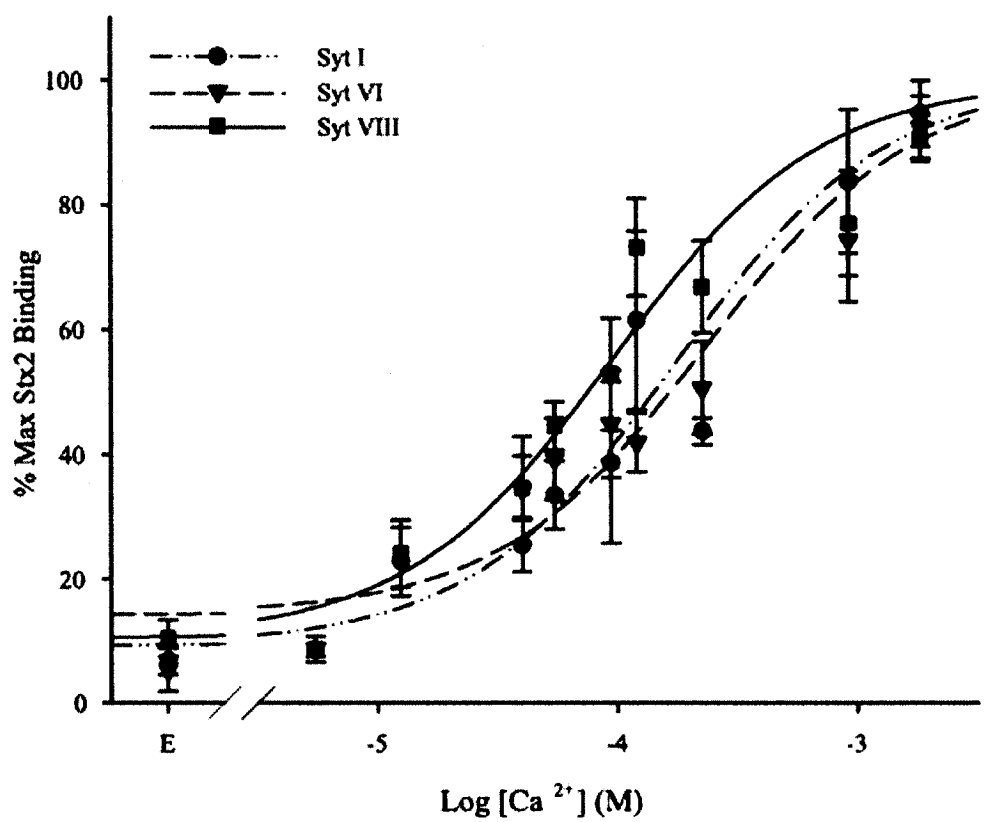
Syt I
Syt VI
Syt VIII
% Max Stx2 Binding
100
80
60
40
20
0
E
-5
-4
-3
Log [Ca 2+] (M)

Figure 30. Calcium dependence of synaptotagmin binding to syntaxin. GST-tagged Syt I, VI or VIII were incubated with 6xHis/HA-tagged Stx1 or 2 in TBS with 0.05% Triton X-100 containing the indicated concentration of free calcium for 4 hrs at 4°C. The bound Stx were analyzed by Western blot using anti-HA antibody. The values are expressed as a percentage of maximal binding ± SEM ($n \geq 3$). **A.** Stx1 binding to Syt I (● / double hatched line), VI (▼/ hatched line) and VIII (■ / solid line) show that Syt I and VIII have a similar affinity for Stx1 with EC_{50} values of 117 and 118 μM Ca^{2+}, respectively, while Syt VI has a lower affinity for Stx1 with an EC_{50} of 352 μM. **B.** Stx2 binding to Syt I (● / double hatched line), VI (▼/ hatched line) and VIII (■ / solid line) show that Syt VIII has the highest affinity for Stx2 amongst the isoforms tested with an EC_{50} value of 96 μM Ca^{2+}. Syt I exhibits a lower affinity for Stx2 than for Stx1 with an EC_{50} of 175 μM Ca^{2+}. Conversely, Syt VI exhibits a higher affinity for Stx2 than for Stx1 with an EC_{50} of 233 μM Ca^{2+}.

I next found that the C2AB of Syt VIII bound to Stx2, and that this binding was Ca^{2+}-dependent (Figure 30B) with an EC_{50} of 96 μM. I also observed that Syt VIII binding to Stx1 is also Ca^{2+}-dependent (Figure 30A), with a similar EC_{50} of 118 μM. Thus, in contrast to a previous report (Li et al., 1995), I have found here that Syt VIII interacted in a Ca^{2+}-dependent fashion with both Stx isoforms tested, with similar affinity for Ca^{2+}.

I also found that the Syt VI C2AB bound to both Stx isoforms, and that the binding was similarly Ca^{2+} dependent. However, binding occurred only at much higher Ca^{2+} concentrations, with an EC_{50} for binding to Stx2 of 233 μM (Figure 30B) and for Stx1 of 352 μM (Figure 30A). Taken together, these observations suggest that Syt VIII is able to bind to Stx in a Ca^{2+}-dependent manner and could therefore behave similarly to the brain Syt I and act as a Ca^{2+} sensor for the AR.

The data for the binding curves were plotted using a 1-site model as described in the methods section. Regression analysis of both the Stx1 and Stx2 binding curves reveals that the interactions do not exhibit cooperativity since all of the Hill coefficients were below the unitary value. The Stx1 binding to Syt I, VI and VIII yielded Hill coefficients of 0.75, 0.92 and 0.76 respectively, while binding of these Syt isoforms to Stx2 yielded Hill coefficients of 0.89, 0.68 and 0.71. In order to confirm this observation I generated Hill plots for the binding data (Figure 31). The slope of these linear regressions is the Hill coefficient. The resulting Hill coefficients for Stx1 binding to Syt I, VI and VIII were 0.69, 0.82 and 0.88 respectively and those for Stx 2 binding were 0.78, 0.56 and 0.69 respectively. These values are not significantly different than the Hill coefficients obtained from the regression analysis of the sigmoidal curve. This observation confirms that the binding of Stx isoforms to various synaptotagmins does not exhibit cooperativity.

A

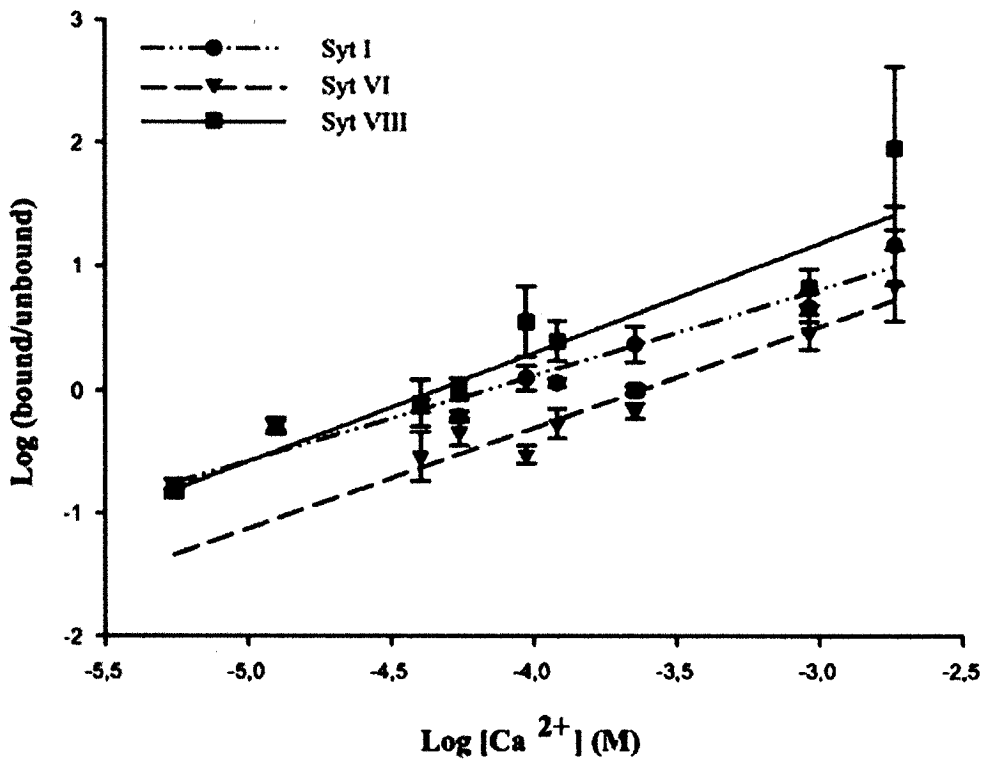
Syt I
Syt VI
Syt VIII
Log (bound/unbound)
Log [Ca 2+] (M)
3
2
1
0
-1
-2
-5,5
-5,0
-4,5
-4,0
-3,5
-3,0
-2,5

B

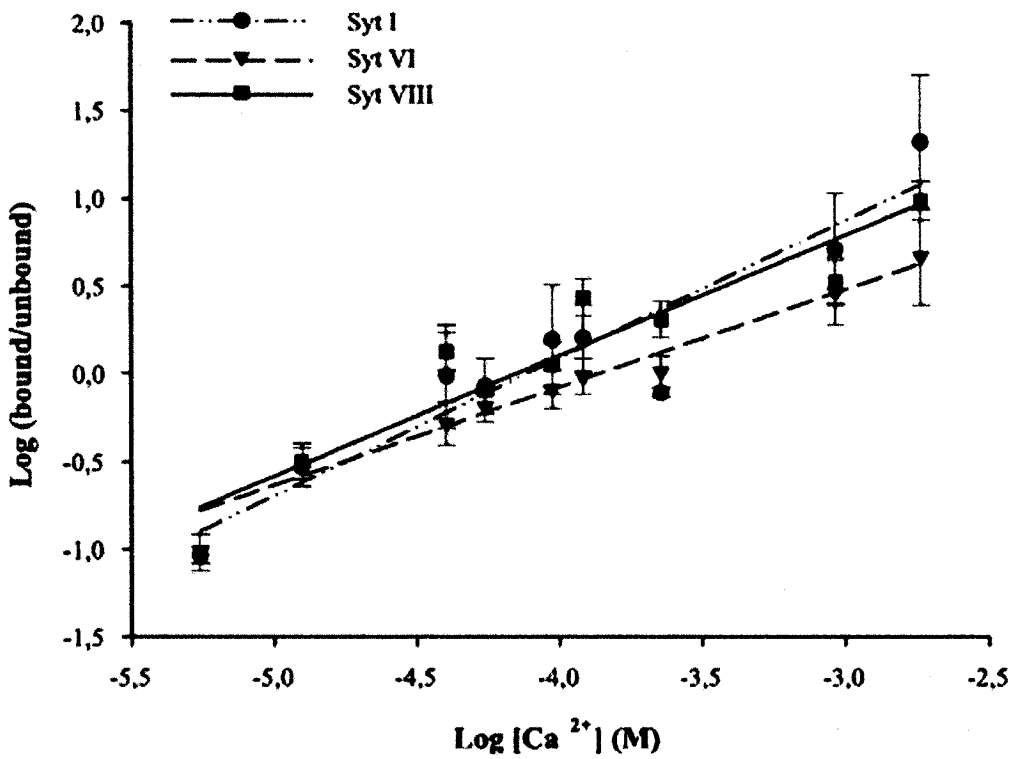
Syt I
Syt VI
Syt VIII
Log (bound/unbound)
Log [Ca 2+] (M)
2,0
1,5
1,0
0,5
0,0
-0,5
-1,0
-1,5
-5,5
-5,0
-4,5
-4,0
-3,5
-3,0
-2,5

Figure 31. Hill plots for the syntaxin in vitro binding assay. The data for the in vitro binding assay was expressed as a log bound Stx / unbound Stx and plotted against the log of the Ca^{2+} concentration. The slope of the linear regression is the Hill coefficient. **A.** The Hill coefficients for syntaxin 1 binding to synaptotagmin I, VI and VIII are 0.69, 0.82 and 0.88 respectively. **B.** The Hill coefficients for syntaxin 2 binding to synaptotagmin I, VI and VIII are 0.78, 0.56 and 0.69 respectively.

Inhibition of the Acrosome Reaction by Anti-Synaptotagmin VIII Antisera. The data reported in Figure 29 and 30 indicated that, between the isoforms known to be present in mouse sperm, the interaction between Syt VIII and Stx would occur first as Ca^{2+} increases due to its lower EC_{50} relative to Syt VI. Thus, to determine if Syt VIII has a functional role in the AR, I introduced IgG purified from antisera raised against recombinant GST-Syt VIII and a separate, previously-characterized anti-Syt VIII peptide antiserum (Figure 33) (Hutt et al., 2002) into SLO-permeabilized capacitated sperm and assessed the extent of AR following stimulation with saturating (1 mM) Ca^{2+}. In order to optimize the experimental conditions, I first performed a titration of the amount of recombinant SLO (rSLO) needed to induce AR in the sample population while minimizing the extent of spontaneous AR seen in sample not stimulated with Ca^{2+}. The titration revealed that 43.6 % of sperm treated with 5 μg/ml of rSLO and 1mM Ca^{2+} underwent AR, referred to as stimulated AR, compared to 24.3% of sperm in the sample treated with the same concentration of rSLO but not supplemented with Ca^{2+}, referred to as spontaneous AR (Figure 32). Lower concentrations of rSLO resulted in a significant decrease in stimulated AR with minimal effect on spontaneous AR while higher concentrations caused significant increases in spontaneous AR with a minimal increase in stimulated AR. Therefore, a concentration of 5 μg/ml of rSLO was used for all SLO-permeabilization of capacitated sperm.

I found that SLO-permeabilized capacitated sperm treated with 100 μg/ml of purified anti-GST-Syt VIII IgG exhibited a 58% inhibition in AR relative to buffer treated sperm or sperm treated with 100 μg/ml of pre-immune IgG (Figure 33). Similarly, SLO-permeabilized capacitated sperm treated with 100 μg/ml of anti-Syt VIII (peptide) IgG exhibited an 83% inhibition in AR relative to the buffer treated or an equal amount of pre-immune IgG treated

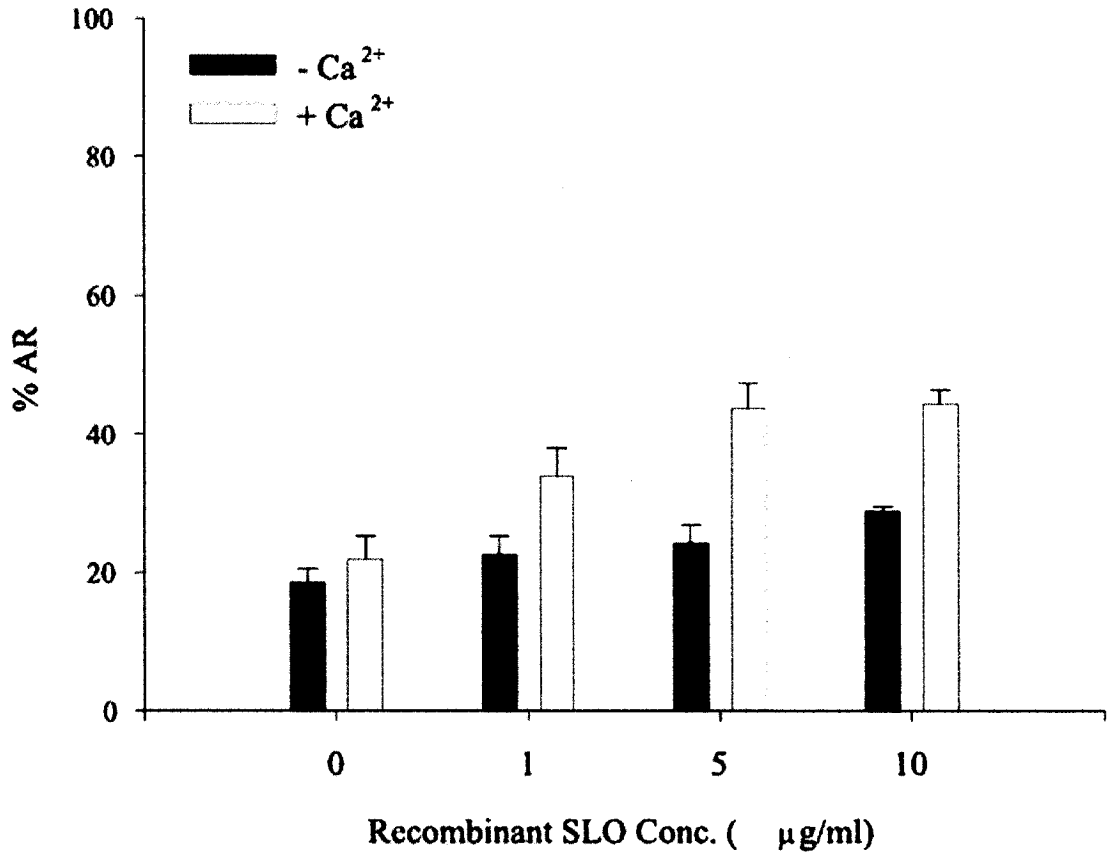

Figure 32. Titration of recombinant Streptolysin O for the permeabilization of capacitated sperm. Capacitated sperm were incubated in Ca^{2+}-free KRB containing the indicated concentration of recombinant SLO for 5 min at 37°C / 5%CO_2. The samples were then supplemented with buffer (open bars) or Ca^{2+} to a final concentration of 1mM (solid bars) and incubated for an additional 20 min at 37°C / 5%CO_2. The extent of AR was determined by Coomassie Brilliant Blue Staining and counting a minimum of 200 sperm per slide. The results are expressed as a percentage of AR ± SEM ($n \geq 3$).

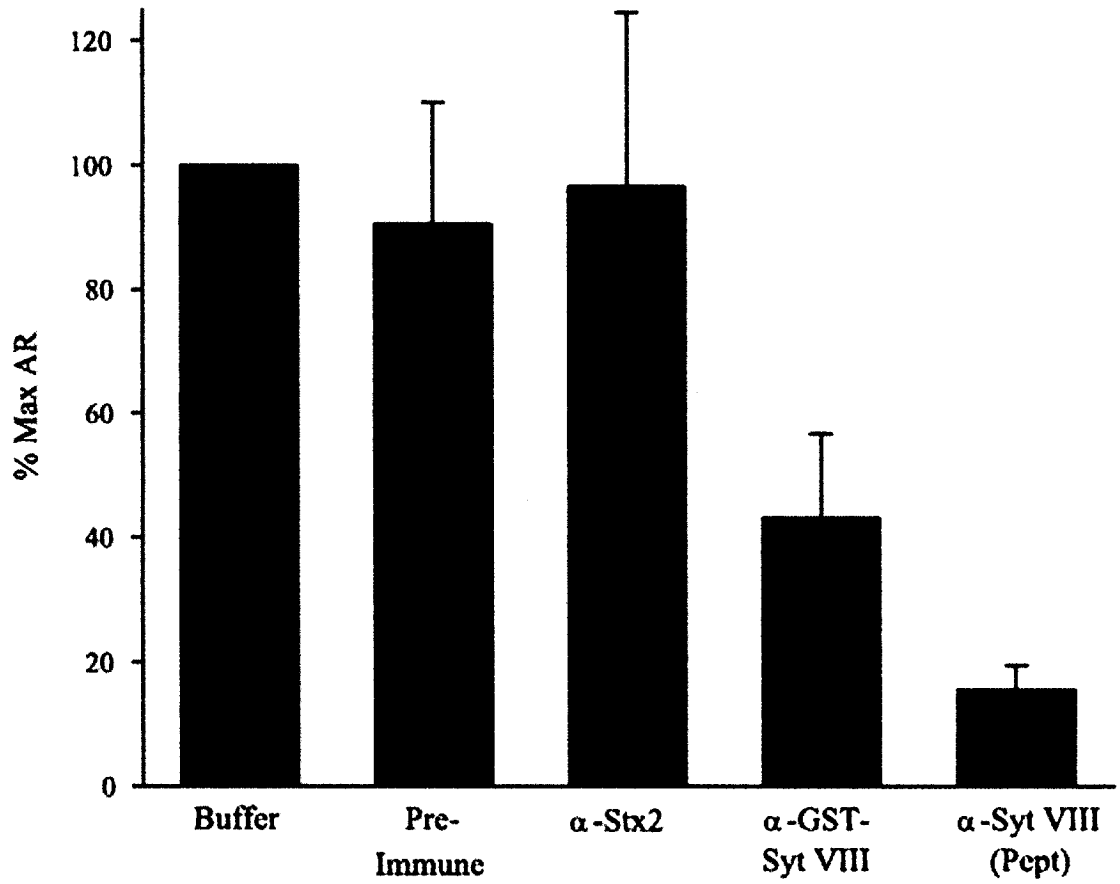

Figure 33. Inhibition of the acrosome reaction with synaptotagmin VIII antibodies. SLO-permeabilized capacitated sperm were incubated with 100 μg/ml of pre-immune, anti-GST Syt VIII or Syt VIII peptide IgG or 10 μg/ml of affinity purified anti-Stx2 antibody and challenged with 1 mM Ca^{2+}. The extent of AR was determined by counting a minimum of 200 sperm per slide, and the results are expressed as a percentage of maximal AR ± SEM ($n \geq 3$). The presence of anti-Syt VIII IgG resulted in inhibition of the AR relative to untreated sperm or sperm incubated with equal amount of pre-immune IgG. The addition of anti-Stx2 antibody had no-inhibitory effect on the ability of the sperm to undergo AR. The actual extent of AR seen for the SLO-permeabilized sperm with the different antisera was 47.7 ± 4.2%, 40.2 ± 3.7% and 42.9 ± 8.7% in the presence of the non-inhibitory compounds such as buffer, pre-immune serum and anti-Stx2 respectively as compared to 19.8 ± 3.8% for the non-permeabilized sperm. The extent of AR seen with the Syt VIII antisera was 31.3 ± 3.9% and 25.3 ± 3.2% in the presence of the GST-Syt VIII and the Syt VIII peptide antisera respectively.

sperm (Figure 33). I also assayed the effect of a commercially available, affinity-purified anti-Stx2 antibody (Stressgen; 10 μg/ml) on the AR. Contrary to the inhibitory effect seen with the Syt VIII antisera, addition of the Stx2 antibody did not result in inhibition of the AR (Figure 33). This inability of the anti-Stx2 antibody to block the AR suggests that either the antigen does not span a functional region, hence the antibody is non-neutralizing or that the antigen is not accessible due to Stx2 being sequestered into a preformed multi-protein complex.

Inhibition of the Acrosome Reaction by Anti-Synaptotagmin and Anti-Syntaxin Antibodies in Non-Capacitated Sperm. In order to address the possibility that incubation of sperm under capacitating conditions leads to the formation of a Stx2-containing SNARE complex or other multi-protein complex, I tested the ability of anti-Stx2 antibodies to inhibit the AR in SLO-permeabilized sperm, which had not been incubated under capacitating conditions. Since non-capacitated sperm exhibit different properties than capacitated sperm, I first performed a titration of rSLO required to obtain optimal AR as shown for capacitated sperm in Figure 32. This titration suggested that 1 μg/ml of rSLO is the optimal concentration for non-capacitated sperm (Figure 34) compared to 5 μg/ml for sperm which had been incubated under capacitating conditions (Figure 32).

The addition of 10 μg/ml of anti-Stx2 antibody to SLO-permeabilized non-capacitated sperm resulted in an 86.6% inhibition of the AR relative to sperm treated with buffer of an equal amount of pre-immune IgG (Figure 35). A 78.9% inhibition of the AR was also seen with the addition of 100 μg/ml of anti-Syt VIII peptide IgG relative to sperm treated with

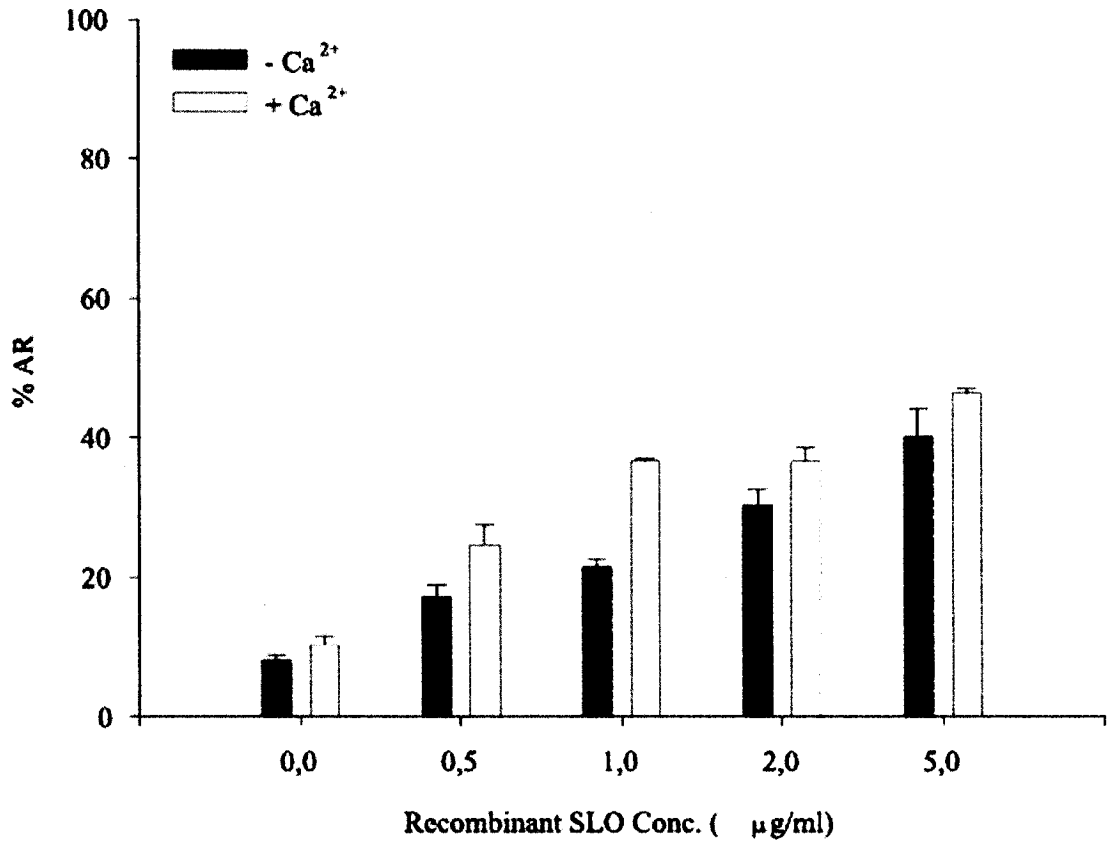

Figure 34. Titration of recombinant Streptolysin O for the permeabilization of non-capacitated sperm. Non-capacitated sperm were incubated in Ca^{2+}-free KRB containing the indicated concentration of recombinant SLO for 5 min at 37°C / 5%CO_2. The samples were then supplemented with buffer (open bars) or Ca^{2+} to a final concentration of 1mM (solid bars) and incubated for an additional 20 min at 37°C / 5%CO_2. The extent of AR was determined by Coomassie Brilliant Blue Staining and counting a minimum of 200 sperm per slide. The results are expressed as a percentage of AR ± SEM (n = 3).

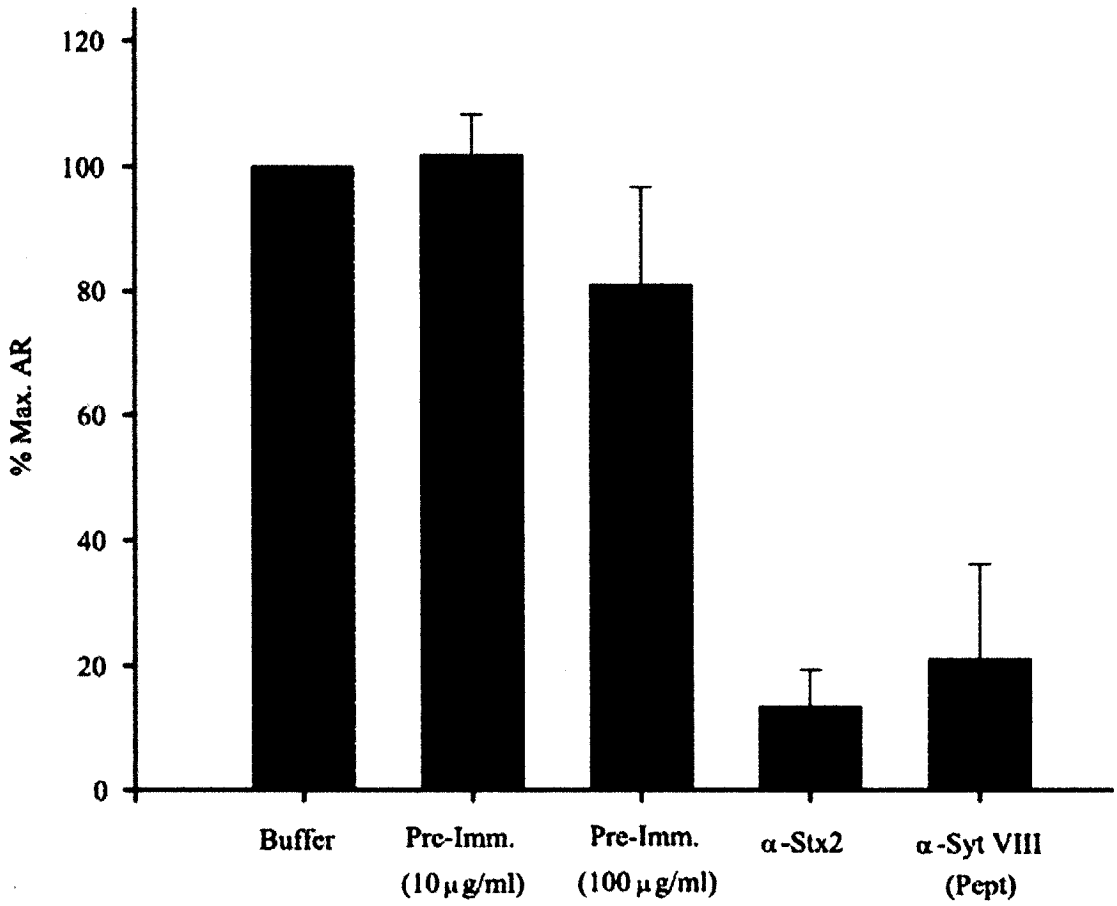

Figure 35. Inhibition of the acrosome reaction with Stx2 antibodies in non-capacitated sperm. SLO-permeabilized, non-capacitated sperm were incubated with 10 μg/ml of affinity purified anti-Stx2 antibody (Stressgen), 100 μg/ml Syt VIII peptide IgG or an equal amount of pre-immune IgG and challenged with 1 mM Ca^{2+}. The extent of AR was determined by counting a minimum of 200 sperm per slide, and the results are expressed as a percentage of maximal AR ± SEM ($n \geq 3$). The presence of anti-Stx2 or anti-Syt VIII IgG resulted in inhibition of the AR relative to untreated sperm or sperm incubated with equal amount of pre-immune IgG. The true extent of AR seen in the non-capacitated SLO permeabilized sperm treated with the different antisera was 30.7 ± 1.1% in the presence of buffer, 30.5 ± 1.0% in the presence of P.I antiserum and 21.8 ± 1.3% in the presence of anti-stx2.

buffer or an equal amount of pre-immune IgG (Figure 35). This suggests that Stx2 is an important component of the fusion machinery mediating the AR in mouse sperm.

Inhibition of the Acrosome Reaction by Recombinant Synaptotagmin. In order to further confirm a functional role of Syt in the AR, I introduced varying amounts of the bacterially expressed 6xHis/HA-tagged cytoplasmic region of Syt (C2AB) into SLO-permeabilized capacitated sperm. The addition of the C2AB of Syt VIII resulted in a dose dependent inhibition of the AR. Increasing the amount of recombinant C2AB from 5 μg/ml to 10 and 20 μg/ml resulted in 36.8, 49.1 and 73.6% inhibition of the AR, respectively (Figure 36). The addition of an amount equal to the highest concentrations tested for SNARE proteins, 20 μg/ml, of an irrelevant protein (bacterially-expressed 6xHis/HA tagged Abstrakt (Abs), a DEAD-box helicase with no known role in membrane fusion) (Irion and Leptin, 1999), had no measurable effect (Figure 36). The addition of the C2AB of Syt VI to the sperm also resulted in a dose dependent inhibition of the AR that appears to saturate at approximately 10 μg/ml (Figure 36). However, the addition of the C2AB region of Syt I had no significant inhibitory effect on the AR at either 5 or 10 μg/ml but resulted in a 54.4% inhibition of the AR at the maximal dose tested, 20 μg/ml (Figure 36). The inhibitory effect of Syt I, VI and VIII seen at 20 μg/ml was eliminated when the protein was denatured by heating for 5 minutes at 90°C prior to its addition to the sperm (Figure 38). These observations suggest that one or more Syt isoform is involved in the regulation of the AR and lends further support of a role for Syt VIII in the AR.

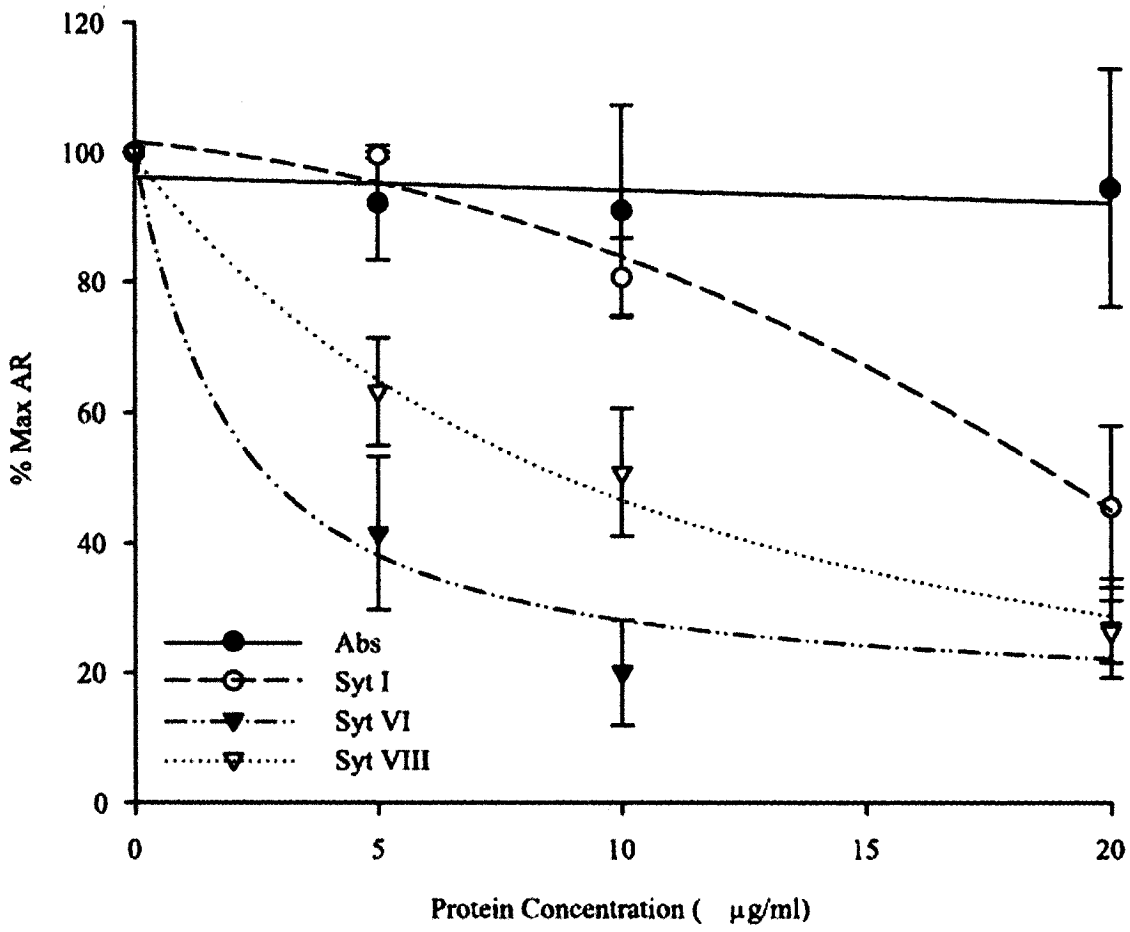

Figure 36. Inhibitory effect of recombinant synaptotagmin on the acrosome reaction. SLO-permeabilized sperm were incubated with the indicated amount of recombinant 6xHis/HA-tagged Abs (● / solid line), Syt I (○ / hatched line), Syt VI (▼/ double hatched) or Syt VIII (▽/ dotted) and the extent of AR was assessed following challenge with 1 mM free Ca^{2+}. The results are expressed as a percentage of maximal AR ± SEM (n = 4).

Inhibition of the Acrosome Reaction with Recombinant Syntaxin. In order to assess the role of Stx in the regulation of the AR, I introduced varying amounts of the bacterially expressed 6xHis/HA-tagged cytoplasmic region of Stx1 or 2 into SLO-permeabilized capacitated sperm and examined their ability to interfere with the AR. Treatment of sperm with Stx2 resulted in >65% inhibition of AR at all concentrations tested relative to sperm treated with equal amount of Abs (Figure 37). The addition of 5 μg/ml of Stx1 resulted in 25.7% inhibition of AR relative to mock treated sperm. Increasing the Stx1 concentration to 10 and 20 μg/ml resulted in a 55.1% and 48.6% inhibition of AR, respectively, relative to sperm treated with Abs, where no inhibition was observed (Figure 37). As seen with the recombinant Syts, the addition of 20 μg/ml of denatured Stx1 or 2 completely abrogated the inhibitory effect seen with equal concentration of the native recombinant protein (Figure 38). These observations suggest that both Stx1 and 2 may be important components of the fusion machinery involved in mediating the AR.

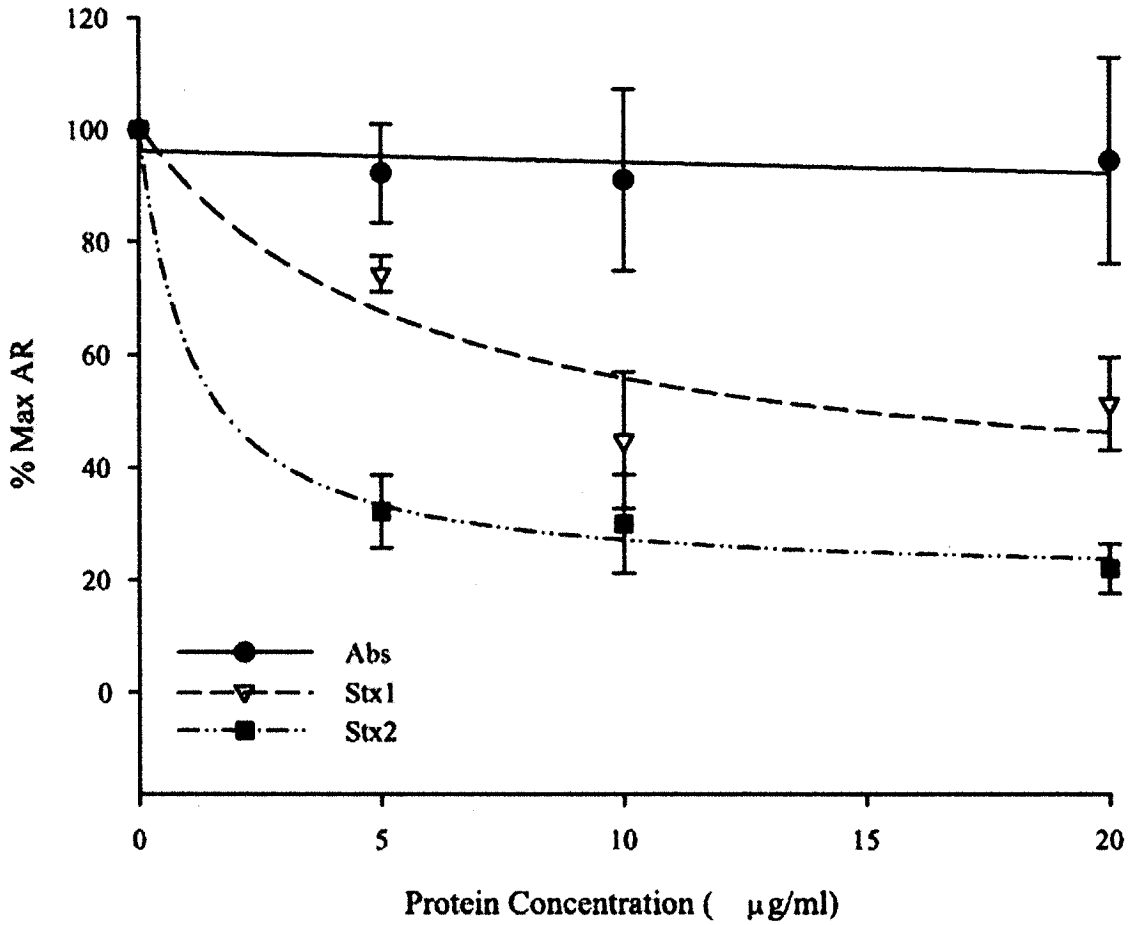

Figure 37. Inhibitory effect of recombinant syntaxin on the acrosome reaction. SLO-permeabilized sperm were incubated with the indicated amount of recombinant 6xHis/HA-tagged Abs (● / solid), Stx1 (▽/ hatched) or Stx2 (■ / double hatched) and the extent of AR was assessed following challenge with 1 mM free Ca^{2+}. The results are expressed as a percentage of maximal AR ± SEM (n = 4).

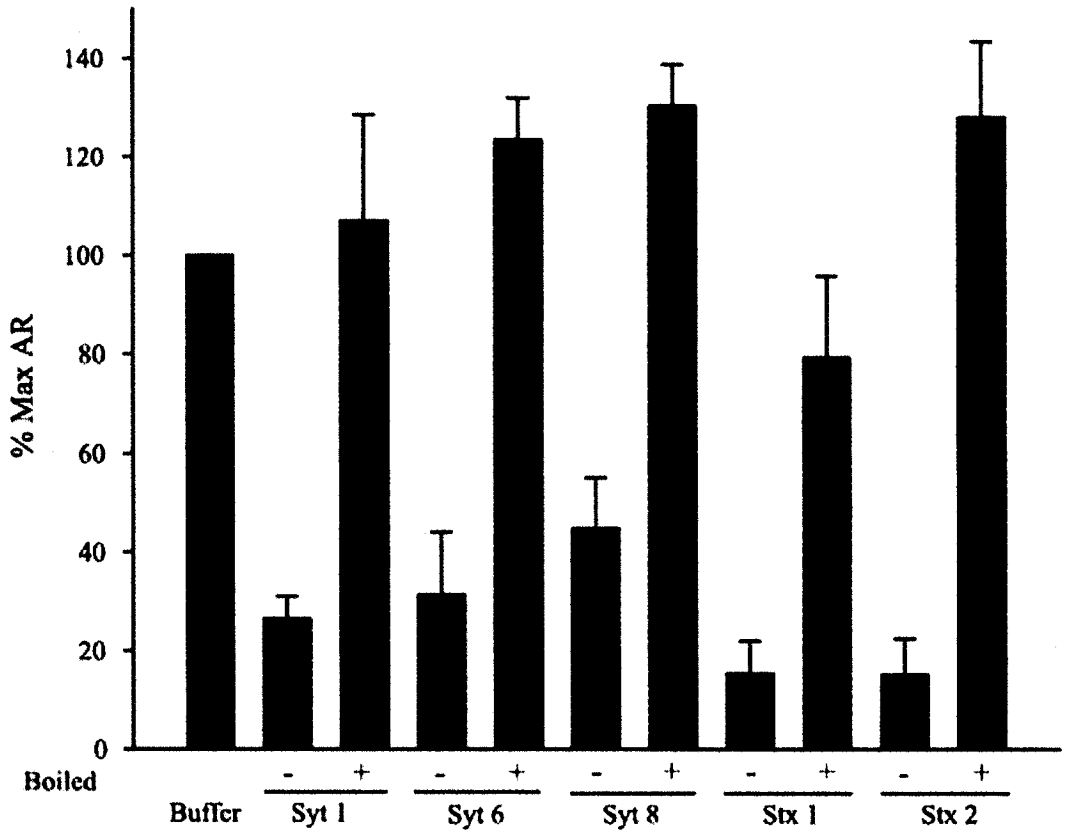

Figure 38. Inhibition of the acrosome reaction in the presence of native and denatured recombinant synaptotagmin and syntaxin. SLO-permeabilized sperm were incubated with 20 μg/ml native or heat denatured recombinant 6xHis/HA-tagged Syt I, VI or VIII or Stx1 or 2 and the extent of AR was assessed following challenge with 1 mM free Ca^{2+}. The results are expressed as a percentage of maximal AR ± SEM (n = 3). The true extent of AR seen in SLO permeabilized sperm was 51.2 ± 3.5% compared to that seen non-permeabilized sperm which was 20.2 ± 1.6%. Sperm treated with native Syt1, 6 and 8 exhibited 37.9 ± 2.9%, 36.1 ± 1.2% and 36.2 ± 2.3% respectively. While boiling the protein prior to addition resulted in 50.9 ± 3.4%, 52.4 ± 3.0% and 53.6 ± 2.3% AR for Syt1, 6 and 8 respectively. The addition of native Stx1 or Stx2 resulted in 34.8 ± 2.5% and 30.3 ± 3.0% AR while the addition of boiled Stx1 or 2 resulted in 47.6 ± 3.0% and 55.1 ± 1.7% respectively.

DISCUSSION

PRA1 is a Rab GTPase Interacting Protein

Prenylated Rab acceptor 1 (PRA1) is a 21 kDa protein which was originally identified as a Rab3A interacting protein through a yeast two-hybrid screen of a rat brain cDNA library (Martincic et al., 1997). Since then it has been shown to interact with other Rab GTPases such as Rab4a, 4b, 5a, 5c, 6, 7, 17 and 22 (Bucci et al., 1999) as well as other small GTPases such as Ha-Ras, TC21, RhoA and Rap1a (Figueroa et al., 2001) and a number of other proteins unrelated to the Ras superfamily(Enouf et al., 2003; Evans et al., 2002; Li et al., 2001). Because of its two extensive hydrophobic domains, structural prediction programs suggest that PRA1 is most likely a type III integral membrane protein with its amino- and carboxy-terminal tails exposed to the cytoplasmic face of a membrane. Recent evidence supports the hypothesis that PRA1 is an intrinsic membrane protein since it fractionates to the detergent phase following solubilization of membranes with Triton X-114 (Liang and Li, 2000).

PRA1 is associated with the Golgi complex

In order to characterize which membranous compartment PRA1 is associated with, I performed immunohistochemical analysis of BHK cells transfected with the mammalian expression vector pIRES-HA-PRA1. The full length PRA1 exhibited a punctate perinuclear and vesicular staining pattern indicative of membrane association (Figure 16A & C). In these cells, the membrane-bound wild-type PRA1 was preferentially associated with the Golgi complex based on extensive co-localization with mannosidase II, a Golgi membrane protein (Figure 16A & B). This Golgi localization for PRA1 has been corroborated by others using a number of different cell lines and expression vectors (Abdul-Ghani et al., 2001; Figueroa et

al., 2001; Li et al., 2001; Liang and Li, 2000; Liang et al., 2004). In contrast to the subcellular localization of the full length PRA1, I have observed that deletions within the carboxy-terminus of PRA1 results in mislocalization of the protein, a conclusion which is corroborated by other laboratories (Abdul-Ghani et al., 2001; Liang and Li, 2000; Liang et al., 2004). When I deleted the carboxy-terminal 21 amino acids of PRA1, I observed a reticular staining pattern in transfected BHK cells which exhibited extensive co-localization with the ER marker calnexin (Figure 16G & H). Thus, the carboxy-terminal domain of PRA1 appears to contain a Golgi localization signal and deletion of this sequence results either in retention of PRA1 in the ER or its retrograde transport from the Golgi complex due to the absence of a Golgi retention signal. Further analysis of the carboxy-terminal domain of PRA1 by Abdul-Ghani *et al.* identified a DXEE motif, spanning residues 176-179, at the carboxy-terminus (Figure 5) which appears to act as an ER exit signal and that mutation of any of these residues resulted in retention of PRA1 in the ER as exemplified by extensive co-localization with calnexin (Abdul-Ghani et al., 2001).

GDI1 binds to PRA1

Since PRA1 was identified as a Rab3A GTPase interacting protein, its localization to the Golgi compartment seemed appropriate since Rab3A is involved in the trafficking of secretory granules from the Golgi to the PM. I therefore sought to examine if PRA1 was able to interact with any known Rab3A effectors in the hopes of unraveling its functional role in the Rab cycle (Figure 2). I found that a small fraction of the cytosolic GDI1 could co-precipitate with recombinant PRA1 by affinity chromatography (Figure 17A). This small amount most likely represents free GDI1 because most, if not all, of the cytosolic GDI1 exists as a Rab-GDI complex. This interaction between PRA1 and GDI1 was confirmed by *in vitro*

binding assay using recombinant GDI1, which does not contain bound Rab GTPase. The interaction between PRA1 and GDI1 requires an intact PRA1 carboxy-terminus since only the full length PRA1 but not the truncated PRA1 (1-164) was able to bind to GDI1 (Figure 17C). I was unable to detect the presence of a stable complex consisting of Rab3A, PRA1 and GDI1 in either the *in vitro* binding or the affinity chromatography assays. This result was not surprising since truncation of PRA1 after the HD2 resulted in a loss of binding to both Rab3A and GDI1, suggesting that both proteins share a common binding region on PRA1. Alternatively, the trimeric complex may be extremely unstable or transient, making its isolation very difficult.

PRA1 inhibits the GDI1-mediated extraction of Rab3A

Proper functioning of Rab involves reversible membrane translocation and cycling to the cytosol with the latter dependent upon GDI (Ullrich et al., 1993) (Figure 2). I have shown that purified recombinant GDI1 can effectively remove Rab3A from PC12 membranes (Figure 18A), and that this activity can be blocked by the addition of recombinant PRA1 (Figure 18B & 19B) but not the carboxy-terminal truncation of PRA1 (1-164) (Figure 19C) (Hutt et al., 2000). Thus, the membrane and cytosolic distribution of Rab depends on the opposing action of PRA1 and GDI1 with PRA1 favoring membrane retention of Rab and GDI1 maintaining Rab soluble in the cytosol. Although membrane detachment is not obligatory for Rab function in yeast (Ossig et al., 1995), it nevertheless is required and that the loss of protein such as GDI1 in X-linked mental retardation can clearly disrupt membrane trafficking (D'Adamo et al., 1998). Therefore, there is a requirement for the proper function of the various regulatory proteins of the Rab cycle on intracellular trafficking. In fact, Gougeon *et al.*(Gougeon et al., 2002) have shown that point mutations in PRA1 can have

severe effects on intracellular trafficking. Trafficking of proteins through the membranous compartments of a cell is often monitored by tracking a fluorescently tagged protein. A commonly used marker for intracellular trafficking assays is the vesicular stomatitis virus envelope glycoprotein G (VSVG), a type I membrane protein that traffics through the constitutive secretory pathway of the cell. A temperature sensitive mutation, $VSVG^{ts045}$, results in misfolding of the protein at the non-permissive temperature of 45°C and its accumulation in the ER. Once the cells are returned to the permissive temperature of 37°C, the protein is properly folded and normal trafficking resumes. Mutations in key proteins involved in the trafficking of vesicles would result in alterations in the localization of VSVG or kinetics of trafficking relative to cells expressing a wild type isoform. Class A PRA1 mutants, which result in the loss of Rab3A binding and ER localization of PRA1, caused a delay in ER exit of $VSVG^{ts045}$ resulting in a delay in PM localization of the protein relative to cells expressing wild type PRA1 (Gougeon et al., 2002). Conversely, class B PRA1 mutants, which cause an increased binding to Rab3A and a morphologic alterations of the Golgi to a more condensed structure, do not affect ER exit of the $VSVG^{ts045}$, but prevent its exit from the Golgi complex (Gougeon et al., 2002). This suggests that proper intracellular trafficking requires correct subcellular localization of PRA1 and tight regulation of its binding to Rab GTPases.

Because both PRA1 and GDI1 are known to bind to a number of Rab GTPases, my results suggest that these two proteins may ultimately determine the level of membrane association of Rab GTPases in general. It is not clear whether PRA1 binding to Rab GTPase occurs before or after GDP/GTP exchange. However, it is likely that PRA1 binds the Rab GTPases upon membrane insertion since it showed little preference for either the GDP- or

GTP-bound form (Abdul-Ghani et al., 2001). The fact that the binding of PRA1 to Rab and VAMP2 is mutually exclusive (Hutt et al., 2000) suggests that PRA1 may influence the availability of these two proteins to interact with other regulatory proteins at the membrane. Upon completion of vesicle fusion, recycling of GDP-bound Rab to the cytosol may require prior dissociation of the PRA1-Rab complex, a step that might be facilitated by the availability of VAMP2 at the membrane. The interaction between PRA1 and GDI1 may also serve to recruit the cytosolic GDI-Rab3A complex to the Golgi membrane thereby facilitating the insertion of the Rab GTPase into the donor membrane compartment. The presence of PRA1 and PRA2 in the Golgi and the ER, respectively (Abdul-Ghani et al., 2001), could therefore serve as a marker of the target membrane for a given Rab GTPase, thus directing a specific Rab protein bound to GDI to the proper membrane to complete the Rab cycle (Figure 2). Recent evidence has suggested that PRA1 can function as a GDI dissociation factor (GDF) for the early endosome Rab5 and the late endosome Rab7 and Rab9, but was inactive for the ER Rab1a and the early Golgi Rab2 (Sivars et al., 2003). This selectivity is not surprising since neither the Rab1a nor Rab2 are likely to encounter PRA1 *in vivo* due to its Golgi localization, while Rabs 5, 7 and 9 are involved in transport and fusion of vesicles between the endosomal compartments and the Golgi complex. Whether the GDF activity of PRA1 also exists for other Rab proteins involved in anterograde transport from the Golgi, such as the Rab3 subfamily, which mediates the trafficking of secretory vesicles and granules from the Golgi to the PM remains to be determined. This model would account for my observations that PRA1 prevents membrane extraction of Rab3A by GDI1. In this system, PRA1 would interact with GDP-bound Rab3A and mediate GDP/GTP exchange, thus preventing its extraction by GDI1, which only recognizes GDP-bound Rab3A (Figure 2).

Furthermore, the establishment of a PRA2 GDF activity for ER to Golgi Rab GTPases also needs to be established.

Conclusions for the PRA1 Project

In conclusion, it appears that PRA1 localizes to the Golgi complex and that this subcellular distribution is dependent on a carboxy terminal localization motif. This Golgi association of PRA1 supports its proposed role of mediating the membrane retention of post-Golgi and endosomal Rab GTPases by preventing their extraction by GDI1. This role is further supported by observations that PRA1 functions as a GDI dissociation factor for the endosomal Rab5, 7 and 9, but not for the ER and early Golgi Rab1 and 2. Whether, PRA1 exhibits a similar function for the secretory vesicle Rab3A, remains to be determined. Therefore, PRA1 may serve as a recognition molecule for the proper trafficking of vesicles to and from the Golgi compartment by serving as a GDI/Rab receptor and mediates the reactivation of Rab GTPases for further trafficking cycles.

The results above provide evidence that the trafficking of vesicles between the intracellular organelles is tightly regulated and the disruption of these regulatory steps can result in a diseased state. Nowhere is this more evident than in the final step of trafficking of a secretory vesicle, the fusion with the plasma membrane. The calcium-regulated fusion of secretory vesicles is mediated by a family of proteins commonly referred to as the SNAREs (Terrian and White, 1997; Weimbs et al., 1997; Weimbs et al., 1998). The SNARE hypothesis states that, for vesicle fusion to be possible, SNARE proteins must first assemble into a stable ternary core complex composed of syntaxin (Stx) (Bennett et al., 1992), SNAP-

25 (Oyler et al., 1989), and VAMP (Baumert et al., 1989; Trimble et al., 1990). Formation of the SNARE complex brings the fusing membranes into close apposition and is a prerequisite for fusion. Despite the critical role the SNARE proteins are proposed to play in modulating vesicle fusion, they are not themselves sufficient to account for the precise regulation of vesicle fusion by calcium. Ca^{2+}-mediated secretion instead requires an additional regulatory mechanism that can transduce the increase in cytoplasmic Ca^{2+} to the SNARE fusion machinery, and induce the conformational changes that cause fusion. The established candidates for this calcium sensor are members of the Syt family.

Sperm as a Model System for Membrane Fusion

There is increasing evidence that the AR in mammalian sperm is mediated by a SNARE complex acting in concert with the Ca^{2+} sensor, Syt (Brahmaraju et al., 2004; Katafuchi et al., 2000; Kierszenbaum, 2000; Ramalho-Santos et al., 2000; Ramalho-Santos et al., 2001; Tomes et al., 2002), similar to stimulated secretion in other secretory cells such as neurons. A number of isoforms of the SNAREs Stx and VAMP have been reported to be present at the protein level in sperm (Ramalho-Santos et al., 2000; Tomes et al., 2002). However, their roles in the AR are not yet clear. In addition, the nature of the synaptotagmin isoforms, which are functionally important for the AR, remain elusive. The AR is a singular event, in contrast to the exocytic-endocytic cycles that occurs in other systems. Thus, it is a good model system to study the direct role of a protein in the fusion step of the vesicle life cycle. Also, the secretory machinery, which mediates such an unforgiving system, may exhibit different constraints from that in other cells in order to prevent spontaneous exocytosis, which suggests that non-conventional Syt isoforms or a combination of isoforms,

which confer a distinct Ca^{2+} sensitivity, may be involved. To date only Syt VI and VIII have been shown to be present in mammalian testis and spermatozoa (Hutt et al., 2002; Li et al., 1995; Michaut et al., 2001), suggesting that these are the isoforms of interest which could serve as the Ca^{2+} sensor to regulate the AR. However, the interactions of Stx with these Syt isoforms have been reported as Ca^{2+} insensitive (Li et al., 1995), while the AR is clearly triggered by Ca^{2+}. Thus, it was unclear how acrosomal exocytosis was regulated downstream of Ca^{2+}.

Synaptotagmin VIII is present is sperm

I have presented several lines of evidence above to confirm that synaptotagmin VIII is expressed in murine sperm. Southern blot analysis of murine spermatogenic cDNA libraries from pachytene spermatocytes and round spermatids have revealed that Syt VIII is expressed in these germ cells while Syt I was not detected (Figure 20). I utilized spermatogenic cell cDNA for this amplification in order to discount the possibility that the synaptotagmin message seen in the testis by Li *et al.* was originating from the neural plexus which overlays the testis, rather than from the germ cells themselves. The amplification of Syt VIII from both these spermatogenic cell lines suggests that it is expressed in sperm. In order to confirm that Syt VIII is expressed in mature sperm, I needed to raise an isoform specific antibody to distinguish it from other Syt family members since most commercially available antisera are raised against Syt I and the epitopes used for the various commercial antibodies span conserved regions to all Syts. In order to overcome this obstacle, I raised an antiserum against a peptide corresponding to the linker region between the two C2 domains of Syt VIII, which shows the highest degree of divergence amongst the known Syt isoforms. This

antiserum specifically detected Syt VIII and did not cross-react with Syt I through VII (Figure 21A). Due to the lack of availability of clones for Syt IX through XV, I could not conclusively exclude the possibility that our antiserum might cross-react with these Syt isoforms. However, sequence comparisons revealed a lack of significant sequence similarity between any other known Syt isoforms and Syt VIII within the region used to generate the peptide antibody, rendering cross-reactivity highly unlikely. Using this newly raised antiserum, I have shown that Syt VIII is present in whole sperm homogenate (Figure 22), therefore confirming that the protein is expressed in sperm. However, its expression alone does not allow us to assign a role for Syt VIII in the AR since it may be inappropriately localized to participate in such an event. Therefore, in order to determine the subcellular localization of the protein, I performed immunocytochemical analysis of fixed and permeabilized sperm using anti-Syt VIII antiserum. My results confirmed the presence of Syt VIII in mature mouse spermatozoa and localized it to the acrosomal region of the sperm head (Figure 24). This localization was also supported by data from subcellular fractionation of murine sperm membranes (Figure 23) which revealed that Syt VIII localizes to a membrane fraction positive for the sperm membrane proteins β-1,4 galactosyltransferase and PH20/hyaluronidase (Baker et al., 2002). The establishment of Syt VIII being associated with either the PM or the OAM would require an analysis by electron microscopy to distinguish between these two compartments. However, the role of Syt VIII as a calcium sensor for membrane fusion could be accomplish in association with either membranous compartment. Proteins that are localized to the PM or the OAM should be shed along with the acrosomal vesicles, as has been established for the SNARE molecules VAMP and Syntaxin in sea urchin and hamster sperm (Ramalho-Santos et al., 2000; Schulz et al., 1997) as well as for the small

GTPase Rab3A in rat sperm (Iida et al., 1999). I have determined by immunofluorescence and Western immunoblot that Syt VIII is indeed lost following the AR. When sperm were induced to undergo the AR using the Ca^{2+} ionophore A23187, there was a large increase in the number of sperm showing little or no Syt VIII immunofluorescence (Figure 25B & C) on the head. Quantitative analysis of Syt VIII immunoreactivity in fixed sperm and Western blot densitometric analysis of Syt VIII from sperm homogenate (Figure 26A & B) showed that Syt VIII is lost following acrosome reaction and correlated well with the amount of sperm undergoing acrosomal exocytosis as determined by Coomassie Blue staining (Figure 25A & C).

Ramalho-Santos *et al.* have previously reported that synaptotagmin is present in the heads of mammalian sperm of several species, using antiserum raised against a conserved region of Syt isoforms. Their subsequent analysis identified the isoform in sperm as Syt I based on immunocytochemical and immunoblot analysis using a commercial anti-Syt antibody from Transduction Laboratories. In contrast, I have determined that the commercial antibody that they used in this study is not specific for Syt I but instead cross-reacts with Syt I and Syt VIII (Figure 21B) as well as with other isoforms tested (Syt II to VII, data not shown). This is likely due to the fact that the epitope used to generate this antibody spans residues 72-223 which encompasses a large portion of the C2A domain of Syt I. This region contains the highest degree of conservation among the Syt family and therefore cross-reactivity of this antibody is not surprising. This raised the strong possibility that the immunoreactivity in sperm using this commercial antibody might have been due to the presence of a Syt isoform other than Syt I. Closer examination of the immunoblot probed with the commercial antibody also supports the presence of other Syt isoforms in the brain

homogenate (Figure 22). Since Syt I and II are the major isoforms in the brain, I believe that they are represented by the faster-migrating band since they are detected with the brightest intensity (Figure 22). The latter also differ from any band detected in the sperm homogenate (Figure 22). Therefore, our data indicate that Syt VIII is present in mouse sperm while Syt I is not.

Taken as a whole, these observations confirm that Syt VIII is expressed in murine sperm and is lost following AR while Syt I is not expressed in mouse sperm. These conclusions are supported by my Southern blot analysis described above, where no Syt I was detected in spermatogenic cell cDNA libraries and the study by Li *et al.* which showed that only Syt VI and Syt VIII are expressed in the testis, while Syt I is expressed exclusively in the brain, cerebellum and olfactory bulb (Li et al., 1995)

Calcium Sensitivity of the Acrosome Reaction in Streptolysin O-Permeabilized Sperm.

Confirming the role of specific gene products requires inhibiting the function of the endogenous proteins. However, sperm are transcriptionally and translationally silent, and therefore conventional molecular biological approaches such as transfection of dominant negative mutants and gene silencing cannot be easily performed. In order to accomplish such inhibition, myself and others have employed the bacterial pore toxin, SLO, to permeabilize the plasma membrane of the sperm and gain access to the cytoplasm (Martin-Moutot et al., 1996; Michaut et al., 2000; Tomes et al., 2002; Yunes et al., 2000) (Figure 27). The protocol I used results in the creation of pores in the plasma membrane that are large enough to allow for the introduction of macromolecules which could block the endogenous activity of proteins of interest, but which do not breach the acrosome (Figure 27). The SLO oligomer assembles

into a ring structure with an internal diameter of 24 nm (Sekiya et al., 1993) and allows introduction of molecules ≤ 260 000 daltons (Walev et al., 2001). In a first instance I employed this protocol to assess the Ca^{2+} requirements of the AR in order to establish a range of concentration in which a Ca^{2+} sensor would need to operate. I have confirmed here that increased Ca^{2+} in the buffer results in an increase in the number of capacitated sperm undergoing AR in the SLO-permeabilized sperm system, with an EC_{50} of 87 μM (Figure 28). This suggests that the calcium sensor involved in the regulation of the AR is active at calcium concentrations at or near this value. This value is comparable to the EC_{50} of about 20 μM obtained by measuring the calcium dependence of fusion between sperm plasma membrane and OAM vesicles (Spungin et al., 1995), especially when taking into account the wide spacing between Ca^{2+} concentrations employed in that study. However, in vivo measurements of Ca^{2+}_i in sperm using the Ca^{2+}-sensitive fluorophore, fura-2, yielded much lower values for free Ca^{2+}_i of about 0.16 μM before AR, which rose to only about 0.40 μM when the AR was triggered (O'Toole et al., 2000). This discrepancy of two orders of magnitude may be due to fura-2 measurements lacking the resolution to detect locally high Ca^{2+} concentrations near the site of fusion. Indeed, it has been proposed that, in general, the local Ca^{2+} concentrations in secretory cells at the site of fusion is actually several orders of magnitude higher than the global increase measured in the bulk cytoplasm, due to the co-localization of the SNAREs, Ca^{2+} sensor, and the plasma membrane-based Ca^{2+} channels that mediate Ca^{2+} influx (Martin-Moutot et al., 1996). However, the much higher Ca^{2+} needed to cause AR in permeabilized sperm or isolated vesicles might alternatively reflect a loss of sensitivity of the exocytotic apparatus after such manipulations. The EC_{50} value of 87 μM Ca^{2+} obtained for the mouse sperm AR resembles the half-maximal calcium requirements for neuronal secretion which is

of the order of hundreds of μM (Adler et al., 1991; Heidelberger et al., 1994; Llinas et al., 1992; Yamada and Zucker, 1992). This suggests that the same Ca^{2+} sensor, which mediates the fusion of synaptic vesicles, namely Syt I, could mediate the fusion of the OAM and PM in sperm. However, as mentioned above, no evidence for the expression of Syt I in sperm exists. Rather, Li *et al.* have shown that only Syt VI and VIII are expressed in the rat testis, which suggests that either of these isoforms or both would serve as Ca^{2+} sensor in this system (Li et al., 1995).

Calcium Titration of Synaptotagmin Binding to Syntaxin

I assumed that, like in other secretory cells, one or more Syt isoforms serve as the Ca^{2+} sensor(s) in the sperm AR and transmits the increase in cytoplasmic Ca^{2+} to the SNARE core complex via binding to syntaxin. However, the evidence presented to date suggest that the sperm isoforms of Syt, namely Syt VI and VIII, do not exhibit Ca^{2+}-dependent Stx binding and therefore would not likely act as Ca^{2+} sensors for the AR. Closer examination of the Ca^{2+} sensitivity of binding for Syt VIII performed by Li *et al.* revealed that Ca^{2+}-dependent binding was only assessed for Stx1 and only its C2A domain was used (Li et al., 1995). Subsequent evidence has suggested that both C2 domains are required for proper Stx binding (Chapman et al., 1996). Furthermore, Syt VI was shown to bind to Stx1-4 in this study, however, the Ca^{2+} sensitivity of these interactions proved inconclusive. It is of note that the evidence supporting the expression of Stx1 in mouse sperm is controversial. The antibody used for the analysis reveals strong staining of the acrosome in immunohistochemical analysis, but the western blot reveals bands which do not migrate to the expected 35kDa size of the protein (Ramalho-Santos et al., 2000). Also, Katafuchi *et al.* have shown convincingly that Stx2 is expressed in

mouse sperm, suggesting that it may be the Stx isoform of interest for the AR (Katafuchi et al., 2000). Therefore, I undertook an analysis of the Ca^{2+} sensitivity of binding among sperm isoforms of Syt and Stx.

Using recombinant cytoplasmic regions of each isoform, and the well-characterized Stx1 and Syt I as controls, in an *in vitro* pull-down assay, I have shown that both Syt VI and Syt VIII exhibit Ca^{2+}-dependent binding with Stx1 and Stx2 (Figure 29A & B and 30A & B). The hierarchy for Stx1 binding upon stimulation by Ca^{2+} was Syt I $\approx$ Syt VIII < Syt VI, indicating that binding occurred at a lower Ca^{2+} concentration for Syt I and VIII than for Syt VI (Figure 30A). When Syt binding to the Stx isoform proposed to be present in sperm, Stx2, was assessed, the hierarchy was Syt VIII < Syt I < Syt VI, indicating that, as Ca^{2+} increases, Syt VIII-Stx2 binding would occur first (Figure 30B). If this corresponds to the situation *in vivo*, the initial trigger of AR could thus be Syt VIII, with Syt VI playing a secondary role. The stimulation of AR by Ca^{2+} in SLO-permeabilized sperm (Figure 28) occurred with an EC_{50} that closely matched that which produced half-maximal binding between Syt VIII and Stx isoforms (Figure 30B). This close match may strengthen the case that these isoforms have a role in the sperm AR. However, such data must be interpreted with caution given the difficulties of determining whether data obtained with SLO-permeabilized sperm reflect transduction in intact sperm, and the possibility that binding between cytoplasmic portions of Syt and Stx isoforms occurs with different affinity from intact, transmembrane proteins. Nonetheless, the coincidence of the Ca^{2+} dependence of AR and Syt VIII-Stx2 binding under the conditions used is consistent with a role in the AR. I have attempted to confirm this interaction *in vivo* by immunoprecipitation of either Syt VIII or Stx2 from sperm lysate, but neither the GST-Syt VIII, the Syt VIII peptide nor the commercial Stx2 antibodies were

effective in precipitating there respective antigen. The results above reveal that, contrary to a previous report (Li et al., 1995), Syt VIII does exhibit Ca^{2+}-dependent binding to Stx1 and 2, which supports its possible role as a Ca^{2+} sensor in the murine AR.

Antibodies to Synaptotagmin VIII Inhibit the Acrosome Reaction in Mouse Sperm

Confirming the role of specific gene products requires inhibiting the function of the endogenous proteins. However, as previously mentioned, conventional molecular biological approaches cannot be easily performed in sperm. I have employed the SLO-permeabilization protocol described above, to gain access to the sperm cytoplasm and introduce macromolecules which could block the endogenous activity of proteins of interest, but which do not breach the acrosome (Figure 27). To address whether Syt VIII has a functional role in the AR, I used IgG purified from an antiserum raised against a non-conserved Syt VIII-derived peptide, which I have shown above to not cross-react with other Syt isoforms. In addition, I also used IgG from antiserum raised against a GST-tagged C2AB construct of Syt VIII; this antiserum likely does cross-react with other Syt isoforms, although I have not fully assessed its specificity. The addition of either anti-Syt VIII peptide or anti-GST-C2AB Syt VIII IgG to SLO-permeabilized sperm resulted in an 83 and 58% inhibition of the Ca^{2+}-stimulated AR, respectively, relative to buffer treated sperm or sperm treated with the equal amount of pre-immune IgG (Figure 33). This inhibition, especially by the anti-peptide antiserum, which is Syt VIII-specific, indicates that Syt VIII is required for the AR in mouse sperm. I could not similarly assess a role for Syt VI, as no specific antisera were available.

Recombinant Synaptotagmin C2AB Inhibits the Acrosome Reaction

In order to confirm the observations seen with the Syt VIII antibodies, I introduced increasing amounts of recombinant Syt cytoplasmic region (C2AB) into SLO-permeabilized sperm. Since the C2AB Syts lack their membrane anchor, they should behave in a dominant negative manner by chelating away binding partners for the endogenous Syt(s). I observed a similar dose-dependent inhibition of the Ca^{2+}-stimulated AR in SLO-permeabilized capacitated sperm by the addition of recombinant 6xHis/HA-tagged Syt VI or VIII cytoplasmic regions (Figure 36). Both recombinant Syt proteins neared maximal inhibition at a concentration of 10 μg/ml, while the addition of 6xHis/HA-tagged Syt I had little effect until the dosage was elevated to 20 μg/ml, suggesting that Syt VI and Syt VIII may be the preferred isoforms to bind to the sperm SNARE complex. The simplest interpretation of these data is that the inhibition of AR by recombinant C2AB of Syt I, VI or VIII is due to their acting as dominant negative inhibitors, disrupting endogenous Syt binding to target sperm SNAREs or other effectors. The inhibition was specific, as the addition of equal amount of an irrelevant protein, 6xHis/HA-tagged Abs, had no effect on AR, and the inhibitory effect seen with recombinant C2AB of Syt I, VI and VIII was eliminated when the proteins were first denatured by heating (Figure 38).

The inhibition of AR by both Syt VIII antisera and recombinant C2AB suggests that Syt VIII is critical component of the membrane fusion apparatus. The results also suggest that Syt VI is important for the AR since its C2AB also had an inhibitory effect. The expression of multiple Syt isoforms in various cell lines has often been thought to be a redundancy mechanism to prevent a loss of signaling in the event of a defect in one of the proteins. However, if this hypothesis were accurate, inhibiting a single Syt isoform in the experiments described above would not have resulted in inhibition of the AR, since the "back

up" pathway would have compensated for the inhibition. This suggests that both Syts are critical for the AR where they may mediate different steps of the pathway or they may interact with each other to mediate membrane fusion by conferring a distinct Ca^{2+} sensitivity to the process. The latter hypothesis is likely since Syts have been shown to exhibit Ca^{2+}-dependent and independent dimerization (Fukuda and Mikoshiba, 2000). The distinct or concerted roles of Syt VI and VIII remains to be determined, but it is clear that both are required for the mouse sperm AR.

Antibody to Syntaxin 2 does not inhibit the Acrosome Reaction in Capacitated Sperm

In contrast to my results for Syt VIII above, the addition of a commercial anti-Stx2 antibody to SLO-permeabilized capacitated sperm did not result in inhibition of the AR (Figure 33). One interpretation is that Stx2 is not critical for the AR. Alternatively, this inability of the anti-Stx2 antibody to inhibit the AR could suggest that either the antigen does not span a functional region, hence the antibody is non-neutralizing or that the antigen is not accessible. The former is possible since the Stressgen anti-Stx2 antibody epitope spans residues 1-19, which is located in the H_{abc} domain (Figure 7), and is not directly involved in formation of the SNARE core complex or Syt binding. However, simple steric hindrance of an antibody binding to the N-terminus of such a small protein would be predicted to inhibit binding to SNARE partners given the tight association which occurs in core complex formation, thus suggesting the latter alternative of antigen inaccessibility due to Stx2 being sequestered into a preformed protein complex, possibly the SNARE core complex.

Recombinant Cytoplasmic Region of Syntaxin Inhibits the Acrosome Reaction

In contrast, the addition of recombinant cytoplasmic domain of Stx2 to SLO-permeabilized capacitated sperm resulted in 77.9% inhibition of AR relative to sperm treated with a non-specific protein, with its inhibitory effect saturated at the lowest dose of 5 μg/ml that was tested (Figure 37). The addition of recombinant Stx1 also resulted in inhibition of AR, but required 10 μg/ml to saturate and caused a maximal inhibition of 55.1% relative to sperm treated with a control protein (Figure 37). Thus, under these conditions, the Stx2 cytoplasmic domain was a more potent inhibitor of the AR than Stx1. As was seen with the addition of recombinant Syt C2AB, the inhibition was specific, as denatured Stx1 or 2 had no effect (Figure 38). The simplest interpretation of these data is that the interaction of the endogenous Stx2 with the endogenous Syt or other SNARE proteins in sperm is disrupted by the presence of added cytoplasmic region of Stx isoforms, thus blocking transduction of the Ca^{2+} signal to the SNARE complex. The higher potency of Stx2, and its presence in sperm, suggests that it is a likely candidate for the endogenous Stx in sperm.

Antibody to Syntaxin 2 inhibits the Acrosome Reaction in Non-Capacitated Sperm

The hypothesis that Stx2 was inaccessible to its antibody in capacitated sperm suggested that the process of capacitation might cause the assembly of the core complex, or other multi-protein complex, and sequester Stx2. The addition of 10 μg/ml of anti-Stx2 antibody to non-capacitated, SLO-permeabilized sperm resulted in an 86.6% inhibition of AR relative to sperm treated with buffer or an equal amount of pre-immune IgG (Figure 35). The addition of the Syt VIII peptide antibody (100 μg/ml) to these non-capacitated, SLO-permeabilized sperm also resulted in inhibition of the AR to a similar extent of that seen in capacitated sperm described above (Figure 33 & 35). This suggests that non-capacitated

sperm undergo AR by a similar Ca^{2+}-dependent pathway as their capacitated counterparts. In addition, it appears that Stx2 is critical for the AR and that capacitation results in the assembly of a Stx2 containing complex, possibly the core complex, which may prime the sperm for fusion prior to Ca^{2+} influx.

Is Synaptotagmin VIII the only synaptotagmin isoform in sperm?

Although it appears highly likely that Syt VIII is present in mouse sperm, my results do not preclude the presence of other Syt isoforms. mRNA encoding the Syt isoforms Syt VI (Li et al., 1995) and Syt XIII (von Poser and Sudhof, 2000) is expressed in the testis, while Syt IV has been sequenced from a mouse testis cDNA library (GenBank accession number BB070672). In addition, it has been reported that Syt VI is localized to the OAM of human sperm and is essential for acrosomal exocytosis (Michaut et al., 2001). Furthermore, the addition of recombinant Syt VI C2AB into SLO-permeabilized mouse sperm resulted in inhibition of the AR (Figure 36). Thus, assuming Syt VI is also expressed in mouse sperm, it appears that there may be at least two Syt isoforms present in sperm. Whether both function in synergy as the Ca^{2+} sensors during the AR or whether the separate isoforms might have distinct functions remains to be determined. Moreover, the Syt isoforms are known to form hetero-oligomers (Fukuda and Mikoshiba, 2000), raising the possibility that such different combinatorial interactions might confer a broader repertoire of Ca^{2+} sensitivity to the AR. Other Syt isoforms expressed in the testis, such as Syt IV and XIII, may also be expressed in spermatogenic cells or instead may only be expressed in other compartments of the testis. Thus, the total number of Syt isoforms present in sperm, and their functions, remains to be determined.

Model of Synaptotagmin VI and VIII Action in the Sperm Acrosome Reaction

Based on the observations above and other known properties of the synaptotagmin and SNARE family of proteins, I have proposed a model of action for Syt VI and VIII in the AR (Figure 39). Syt isoforms interact with a number of effectors all of which mediate its function in regulating vesicle fusion. Upon an increase in cytoplasmic Ca^{2+}, the earliest Syt interaction would be its PL binding property since this interaction exhibits an EC_{50} of 5-20 μM Ca^{2+} (Davis et al., 1999; Nalefski et al., 2001). Prior investigation of this property for Syt VI and VIII has revealed that only Syt VI exhibits Ca^{2+}-dependent PL binding while Syt VIII exhibits a weak Ca^{2+}-independent PL binding property. Therefore, I propose that upon Ca^{2+} influx in the sperm cytoplasm, Syt VI would interact with anionic PL, such as PS or PI3,4P on the inner leaflet of the PM. Since Syt VI has been localized to both the PM and the vesicle membrane, it is possible that the PL interaction occurs in cis, in the case of a PM localization (Figure 39A (I)), or in trans, in the case of an OAM localization, which has been shown for human sperm (Michaut et al., 2001) (Figure 39A (II)). As the Ca^{2+} concentration increases to the hundred micromolar range, Syt VIII would interact with the pre-formed SNARE complex which assembles during the capacitation step (Figure 39B). The hetero-dimerization of Syt VI and VIII would serve, in conjunction with the core SNARE complex to pull the membranes into close apposition therefore overcoming the repulsive energy barrier, which prevents membrane fusion (Figure 39C). The homo-dimerization of Syt VI and Syt VIII would pull multiple SNARE-Syt complexes together through lateral diffusion and a cause the assembly of a ring of SNARE complexes to allow for the formation of the fusion pore (Figure 39D).

Conclusion of Synaptotagmin VIII Project

In conclusion, I have shown here that Syt VIII is expressed in spermatogenic cells and that it localizes to the acrosomal region of the mouse sperm appropriately placed to participate

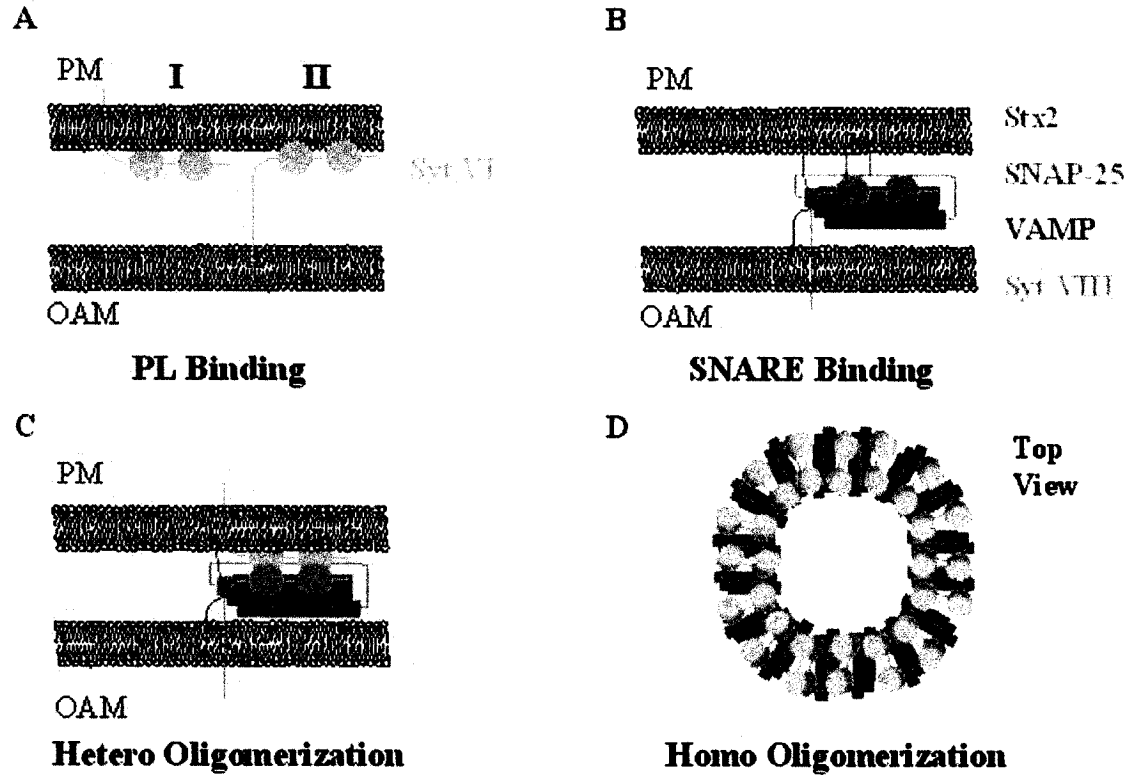

Figure 39. Model of the possible interaction between Syt isoforms and the SNARE complex mediating the acrosome reaction. A. The earliest Ca^{2+}-mediated interaction known for Syt isoforms is the phospholipids (PL) binding property, which occurs at low micromolar Ca^{2+}. Syt VI has been shown to exhibit Ca^{2+}-dependent PL-binding while Syt VIII is not thought to possess this property. Evidence also suggests that Syt VI could be localized to either the PM (I) or the vesicle membrane (II) where it is likely to preferentially associate with the PM which specifically contains phosphatidylinositol 3, 4 phosphate (PI3,4P). **B.** As the cytoplasmic Ca^{2+}-concentration increases to the hundred micromolar range, Syt VIII binds to the pre-assembled SNARE complex. **C.** The heteroligomerization of Syt VI and VIII, along with the core SNARE complex, serves to bring the fusing membranes into close apposition. **D.** The complex shown in C must be present in a ring structure around the site of fusion to mediate the formation of the fusion pore. The view from above suggests that the homo-oligomerization property of Syt VIII and Syt VI could serve to assemble and hold multiple SNARE complexes to mediate the fusion.

in the AR as a Ca^{2+} sensor. Like other components of the fusion machinery, Syt VIII is shed with the acrosomal vesicles following AR, suggesting that it may be an active participant in the membrane fusion event. Furthermore, I have established here that two Syt isoforms, Syt VI and Syt VIII, can exhibit Ca^{2+}-dependent binding to Stx isoforms, contrary to previous reports, and thus can potentially mediate Ca^{2+}-stimulated membrane fusion and exocytosis. The EC_{50} for Ca^{2+} of the Syt VIII / Stx2 binding resembles the EC_{50} value for Ca^{2+} of the AR, suggesting that this pairing may mediate the fusion of the OAM with the PM in sperm. Furthermore, my data suggest that Syt VIII has a required role in the AR, while my observations also support previous data suggesting that Syt VI may also participate, but cannot substitute in the role of Syt VIII. The Stx isoform that binds to one or both of these Syts is most likely to be Stx2 among the candidates thus far identified. Like Syt VIII, Stx2 has a critical role in the AR. I propose that this particular combination of SNARE proteins and putative Ca^{2+}-sensors may help account for the unique character of the sperm exocytotic event.

References

Abdul-Ghani, M., Gougeon, P. Y., Prosser, D. C., Da-Silva, L. F., and Ngsee, J. K. (2001). PRA isoforms are targeted to distinct membrane compartments. J Biol Chem *276*, 6225-6233.

Adler, E. M., Augustine, G. J., Duffy, S. N., and Charlton, M. P. (1991). Alien intracellular calcium chelators attenuate neurotransmitter release at the squid giant synapse. J Neurosci *11*, 1496-1507.

Advani, R. J., Bae, H. R., Bock, J. B., Chao, D. S., Doung, Y. C., Prekeris, R., Yoo, J. S., and Scheller, R. H. (1998). Seven novel mammalian SNARE proteins localize to distinct membrane compartments. J Biol Chem *273*, 10317-10324.

Albert, S., Will, E., and Gallwitz, D. (1999). Identification of the catalytic domains and their functionally critical arginine residues of two yeast GTPase-activating proteins specific for Ypt/Rab transport GTPases. EMBO J *18*, 5216-5225.

Allan, B. B., Moyer, B. D., and Balch, W. E. (2000). Rab1 recruitment of p115 into a cis-SNARE complex: programming budding COPII vesicles for fusion. Science *289*, 444-448.

Andrews, N. W. (2000). Regulated secretion of conventional lysosomes. Trends Cell Biol *10*, 316-321.

Aravamudan, B., Fergestad, T., Davis, W. S., Rodesch, C. K., and Broadie, K. (1999). Drosophila UNC-13 is essential for synaptic transmission. Nat Neurosci *2*, 965-971.

Arnoult, C., Cardullo, R. A., Lemos, J. R., and Florman, H. M. (1996). Activation of mouse sperm T-type Ca2+ channels by adhesion to the egg zona pellucida. Proc Natl Acad Sci U S A *93*, 13004-13009.

Babity, J. M., Armstrong, J. N., Plumier, J. C., Currie, R. W., and Robertson, H. A. (1997). A novel seizure-induced synaptotagmin gene identified by differential display. Proc Natl Acad Sci U S A *94*, 2638-2641.

Bailey, J. L., and Storey, B. T. (1994). Calcium influx into mouse spermatozoa activated by solubilized mouse zona pellucida, monitored with the calcium fluorescent indicator, fluo-3. Inhibition of the influx by three inhibitors of the zona pellucida induced acrosome reaction: tyrphostin A48, pertussis toxin, and 3-quinuclidinyl benzilate. Mol Reprod Dev *39*, 297-308.

Baker, S. S., Cardullo, R. A., and Thaler, C. D. (2002). Sonication of mouse sperm membranes reveals distinct protein domains. Biol Reprod *66*, 57-64.

Baumert, M., Maycox, P. R., Navone, F., De Camilli, P., and Jahn, R. (1989). Synaptobrevin: an integral membrane protein of 18,000 daltons present in small synaptic vesicles of rat brain. EMBO J *8*, 379-384.

Bennett, M. K., Calakos, N., and Scheller, R. H. (1992). Syntaxin: a synaptic protein implicated in docking of synaptic vesicles at presynaptic active zones. Science *257*, 255-259.

Binz, T., Blasi, J., Yamasaki, S., Baumeister, A., Link, E., Sudhof, T. C., Jahn, R., and Niemann, H. (1994). Proteolysis of SNAP-25 by types E and A botulinal neurotoxins. J Biol Chem *269*, 1617-1620.

Blasi, J., Chapman, E. R., Link, E., Binz, T., Yamasaki, S., De Camilli, P., Sudhof, T. C., Niemann, H., and Jahn, R. (1993a). Botulinum neurotoxin A selectively cleaves the synaptic protein SNAP-25. Nature *365*, 160-163.

Blasi, J., Chapman, E. R., Yamasaki, S., Binz, T., Niemann, H., and Jahn, R. (1993b). Botulinum neurotoxin C1 blocks neurotransmitter release by means of cleaving HPC-1/syntaxin. Embo J *12*, 4821-4828.

Bock, J. B., Matern, H. T., Peden, A. A., and Scheller, R. H. (2001). A genomic perspective on membrane compartment organization. Nature *409*, 839-841.

Bommert, K., Charlton, M. P., DeBello, W. M., Chin, G. J., Betz, H., and Augustine, G. J. (1993). Inhibition of neurotransmitter release by C2-domain peptides implicates synaptotagmin in exocytosis. Nature *363*, 163-165.

Brahmaraju, M., Shoeb, M., Laloraya, M., and Kumar, P. G. (2004). Spatio-temporal organization of Vam6P and SNAP on mouse spermatozoa and their involvement in sperm-zona pellucida interactions. Biochem Biophys Res Commun *318*, 148-155.

Brennwald, P., Kearns, B., Champion, K., Keranen, S., Bankaitis, V., and Novick, P. (1994). Sec9 is a SNAP-25-like component of a yeast SNARE complex that may be the effector of Sec4 function in exocytosis. Cell *79*, 245-258.

Broadie, K., Bellen, H. J., DiAntonio, A., Littleton, J. T., and Schwarz, T. L. (1994). Absence of synaptotagmin disrupts excitation-secretion coupling during synaptic transmission. Proc Natl Acad Sci U S A *91*, 10727-10731.

Brose, N., Petrenko, A. G., Sudhof, T. C., and Jahn, R. (1992). Synaptotagmin: a calcium sensor on the synaptic vesicle surface. Science *256*, 1021-1025.

Bruns, D., Engers, S., Yang, C., Ossig, R., Jeromin, A., and Jahn, R. (1997). Inhibition of transmitter release correlates with the proteolytic activity of tetanus toxin and botulinus toxin A in individual cultured synapses of Hirudo medicinalis. J Neurosci *17*, 1898-1910.

Bucci, C., Chiariello, M., Lattero, D., Maiorano, M., and Bruni, C. B. (1999). Interaction cloning and characterization of the cDNA encoding the human prenylated rab acceptor (PRA1). Biochem Biophys Res Commun *258*, 657-662.

Bucci, C., Parton, R. G., Mather, I. H., Stunnenberg, H., Simons, K., Hoflack, B., and Zerial, M. (1992). The small GTPase rab5 functions as a regulatory factor in the early endocytic pathway. Cell *70*, 715-728.

Burns, M. E., Sasaki, T., Takai, Y., and Augustine, G. J. (1998). Rabphilin-3A: a multifunctional regulator of synaptic vesicle traffic. J Gen Physiol *111*, 243-255.

Burton, J. L., Burns, M. E., Gatti, E., Augustine, G. J., and De Camilli, P. (1994). Specific interactions of mss4 with members of the rab GTPase subfamily. EMBO J *13*, 5547-5558.

Butz, S., Fernandez-Chacon, R., Schmitz, F., Jahn, R., and Sudhof, T. C. (1999). The subcellular localizations of atypical synaptotagmins III and VI. Synaptotagmin III is enriched in synapses and synaptic plasma membranes but not in synaptic vesicles. J Biol Chem *274*, 18290-18296.

Cao, X., Ballew, N., and Barlowe, C. (1998). Initial docking of ER-derived vesicles requires Uso1p and Ypt1p but is independent of SNARE proteins. EMBO J *17*, 2156-2165.

Chapman, E. R., An, S., Edwardson, J. M., and Jahn, R. (1996). A novel function for the second C2 domain of synaptotagmin. Ca2+-triggered dimerization. J Biol Chem *271*, 5844-5849.

Chapman, E. R., Hanson, P. I., An, S., and Jahn, R. (1995). Ca2+ regulates the interaction between synaptotagmin and syntaxin 1. J Biol Chem *270*, 23667-23671.

Chapman, E. R., and Jahn, R. (1994). Calcium-dependent interaction of the cytoplasmic region of synaptotagmin with membranes. Autonomous function of a single C2-homologous domain. J Biol Chem *269*, 5735-5741.

Christoforidis, S., Miaczynska, M., Ashman, K., Wilm, M., Zhao, L., Yip, S. C., Waterfield, M. D., Backer, J. M., and Zerial, M. (1999). Phosphatidylinositol-3-OH kinases are Rab5 effectors. Nat Cell Biol *1*, 249-252.

Chung, S. H., Song, W. J., Kim, K., Bednarski, J. J., Chen, J., Prestwich, G. D., and Holz, R. W. (1998). The C2 domains of Rabphilin3A specifically bind phosphatidylinositol 4,5-bisphosphate containing vesicles in a Ca2+-dependent manner. In vitro characteristics and possible significance. J Biol Chem *273*, 10240-10248.

Chung, S. H., Takai, Y., and Holz, R. W. (1995). Evidence that the Rab3a-binding protein, rabphilin3a, enhances regulated secretion. Studies in adrenal chromaffin cells. J Biol Chem *270*, 16714-16718.

Clary, D. O., Griff, I. C., and Rothman, J. E. (1990). SNAPs, a family of NSF attachment proteins involved in intracellular membrane fusion in animals and yeast. Cell *61*, 709-721.

Coppola, T., Perret-Menoud, V., Luthi, S., Farnsworth, C. C., Glomset, J. A., and Regazzi, R. (1999). Disruption of Rab3-calmodulin interaction, but not other effector interactions, prevents Rab3 inhibition of exocytosis. Embo J *18*, 5885-5891.

Cornille, F., Martin, L., Lenoir, C., Cussac, D., Roques, B. P., and Fournie-Zaluski, M. C. (1997). Cooperative exosite-dependent cleavage of synaptobrevin by tetanus toxin light chain. J Biol Chem *272*, 3459-3464.

D'Adamo, P., Menegon, A., Lo Nigro, C., Grasso, M., Gulisano, M., Tamanini, F., Bienvenu, T., Gedeon, A. K., Oostra, B., Wu, S. K., *et al.* (1998). Mutations in GDI1 are responsible for X-linked non-specific mental retardation. Nat Genet *19*, 134-139.

Davis, A. F., Bai, J., Fasshauer, D., Wolowick, M. J., Lewis, J. L., and Chapman, E. R. (1999). Kinetics of synaptotagmin responses to Ca2+ and assembly with the core SNARE complex onto membranes. Neuron *24*, 363-376.

De Blas, G., Michaut, M., Trevino, C. L., Tomes, C. N., Yunes, R., Darszon, A., and Mayorga, L. S. (2002). The intraacrosomal calcium pool plays a direct role in acrosomal exocytosis. J Biol Chem *277*, 49326-49331.

DiAntonio, A., Parfitt, K. D., and Schwarz, T. L. (1993). Synaptic transmission persists in synaptotagmin mutants of Drosophila. Cell *73*, 1281-1290.

Dirac-Svejstrup, A. B., Soldati, T., Shapiro, A. D., and Pfeffer, S. R. (1994). Rab-GDI presents functional rab9 to the intracellular transport machinery and contributes selectivity to rab9 membrane recruitment. J Biol Chem *269*, 15427-15430.

Dulubova, I., Sugita, S., Hill, S., Hosaka, M., Fernandez, I., Sudhof, T. C., and Rizo, J. (1999). A conformational switch in syntaxin during exocytosis: role of munc18. Embo J *18*, 4372-4382.

Echard, A., Jollivet, F., Martinez, O., Lacapere, J. J., Rousselet, A., Janoueix-Lerosey, I., and Goud, B. (1998). Interaction of a Golgi-associated kinesin-like protein with Rab6. Science *279*, 580-585.

Elferink, L. A., Peterson, M. R., and Scheller, R. H. (1993). A role for synaptotagmin (p65) in regulated exocytosis. Cell *72*, 153-159.

Elferink, L. A., Trimble, W. S., and Scheller, R. H. (1989). Two vesicle-associated membrane protein genes are differentially expressed in the rat central nervous system. J Biol Chem *264*, 11061-11064.

Enouf, V., Chwetzoff, S., Trugnan, G., and Cohen, J. (2003). Interactions of rotavirus VP4 spike protein with the endosomal protein Rab5 and the prenylated Rab acceptor PRA1. J Virol *77*, 7041-7047.

Evans, D. T., Tillman, K. C., and Desrosiers, R. C. (2002). Envelope glycoprotein cytoplasmic domains from diverse lentiviruses interact with the prenylated Rab acceptor. J Virol *76*, 327-337.

Fasshauer, D., Otto, H., Eliason, W. K., Jahn, R., and Brunger, A. T. (1997). Structural changes are associated with soluble N-ethylmaleimide-sensitive fusion protein attachment protein receptor complex formation. J Biol Chem *272*, 28036-28041.

Fatt, P., and Katz, B. (1952). Spontaneous subthreshold activity at motor nerve endings. J Physiol *117*, 109-128.

Fernandez, I., Arac, D., Ubach, J., Gerber, S. H., Shin, O., Gao, Y., Anderson, R. G., Sudhof, T. C., and Rizo, J. (2001). Three-dimensional structure of the synaptotagmin 1 C2B-domain: synaptotagmin 1 as a phospholipid binding machine. Neuron *32*, 1057-1069.

Fernandez-Chacon, R., Konigstorfer, A., Gerber, S. H., Garcia, J., Matos, M. F., Stevens, C. F., Brose, N., Rizo, J., Rosenmund, C., and Sudhof, T. C. (2001). Synaptotagmin I functions as a calcium regulator of release probability. Nature *410*, 41-49.

Figueroa, C., Taylor, J., and Vojtek, A. B. (2001). Prenylated Rab acceptor protein is a receptor for prenylated small GTPases. J Biol Chem *276*, 28219-28225.

Florman, H. M. (1994). Sequential focal and global elevations of sperm intracellular Ca2+ are initiated by the zona pellucida during acrosomal exocytosis. Dev Biol *165*, 152-164.

Foran, P., Lawrence, G. W., Shone, C. C., Foster, K. A., and Dolly, J. O. (1996). Botulinum neurotoxin C1 cleaves both syntaxin and SNAP-25 in intact and permeabilized chromaffin cells: correlation with its blockade of catecholamine release. Biochemistry *35*, 2630-2636.

Foran, P., Shone, C. C., and Dolly, J. O. (1994). Differences in the protease activities of tetanus and botulinum B toxins revealed by the cleavage of vesicle-associated membrane protein and various sized fragments. Biochemistry *33*, 15365-15374.

Fukuda, M. (2003a). Molecular cloning and characterization of human, rat, and mouse synaptotagmin XV. Biochem Biophys Res Commun *306*, 64-71.

Fukuda, M. (2003b). Molecular cloning, expression, and characterization of a novel class of synaptotagmin (Syt XIV) conserved from Drosophila to humans. J Biochem (Tokyo) *133*, 641-649.

Fukuda, M., Kabayama, H., and Mikoshiba, K. (2000). Drosophila AD3 mutation of synaptotagmin impairs calcium-dependent self-oligomerization activity. FEBS Lett *482*, 269-272.

Fukuda, M., Kojima, T., and Mikoshiba, K. (1996). Phospholipid composition dependence of Ca2+-dependent phospholipid binding to the C2A domain of synaptotagmin IV. J Biol Chem *271*, 8430-8434.

Fukuda, M., Kuroda, T. S., and Mikoshiba, K. (2002). Slac2-a/melanophilin, the missing link between Rab27 and myosin Va: implications of a tripartite protein complex for melanosome transport. J Biol Chem *277*, 12432-12436.

Fukuda, M., and Mikoshiba, K. (2000). Calcium-dependent and -independent hetero-oligomerization in the synaptotagmin family. J Biochem (Tokyo) *128*, 637-645.

Fukuda, M., Moreira, J. E., Lewis, F. M., Sugimori, M., Niinobe, M., Mikoshiba, K., and Llinas, R. (1995). Role of the C2B domain of synaptotagmin in vesicular release and recycling as determined by specific antibody injection into the squid giant synapse preterminal. Proc Natl Acad Sci U S A *92*, 10708-10712.

Fukui, K., Sasaki, T., Imazumi, K., Matsuura, Y., Nakanishi, H., and Takai, Y. (1997). Isolation and characterization of a GTPase activating protein specific for the rab3 subfamily of small G proteins. J Biol Chem *272*, 4655-4658.

Gao, Z., Reavey-Cantwell, J., Young, R. A., Jegier, P., and Wolf, B. A. (2000). Synaptotagmin III/VII isoforms mediate Ca2+-induced insulin secretion in pancreatic islet beta -cells. J Biol Chem *275*, 36079-36085.

Geppert, M., Archer, B. T., 3rd, and Sudhof, T. C. (1991). Synaptotagmin II. A novel differentially distributed form of synaptotagmin. J Biol Chem *266*, 13548-13552.

Geppert, M., Goda, Y., Hammer, R. E., Li, C., Rosahl, T. W., Stevens, C. F., and Sudhof, T. C. (1994). Synaptotagmin I: a major Ca2+ sensor for transmitter release at a central synapse. Cell *79*, 717-727.

Geppert, M., Goda, Y., Stevens, C. F., and Sudhof, T. C. (1997). The small GTP-binding protein Rab3A regulates a late step in synaptic vesicle fusion. Nature *387*, 810-814.

Gerona, R. R., Larsen, E. C., Kowalchyk, J. A., and Martin, T. F. (2000). The C terminus of SNAP25 is essential for Ca(2+)-dependent binding of synaptotagmin to SNARE complexes. J Biol Chem *275*, 6328-6336.

Gerst, J. E. (1997). Conserved alpha-helical segments on yeast homologs of the synaptobrevin/VAMP family of v-SNAREs mediate exocytic function. J Biol Chem *272*, 16591-16598.

Gerst, J. E., Rodgers, L., Riggs, M., and Wigler, M. (1992). SNC1, a yeast homolog of the synaptic vesicle-associated membrane protein/synaptobrevin gene family: genetic interactions with the RAS and CAP genes. Proc Natl Acad Sci U S A *89*, 4338-4342.

Gietz, R. D., Schiestl, R. H., Willems, A. R., and Woods, R. A. (1995). Studies on the transformation of intact yeast cells by the LiAc/SS- DNA/PEG procedure. Yeast *11*, 355-360.

Gorvel, J. P., Chavrier, P., Zerial, M., and Gruenberg, J. (1991). rab5 controls early endosome fusion in vitro. Cell *64*, 915-925.

Gougeon, P. Y., Prosser, D. C., Da-Silva, L. F., and Ngsee, J. K. (2002). Disruption of Golgi morphology and trafficking in cells expressing mutant prenylated rab acceptor-1. J Biol Chem *277*, 36408-36414.

Gournier, H., Stenmark, H., Rybin, V., Lippe, R., and Zerial, M. (1998). Two distinct effectors of the small GTPase Rab5 cooperate in endocytic membrane fusion. EMBO J *17*, 1930-1940.

Green, D. P. (1978). The osmotic properties of the acrosome of guinea-pig sperm. J Cell Sci *32*, 165-176.

Griscelli, C., and Prunieras, M. (1978). Pigment dilution and immunodeficiency: a new syndrome. Int J Dermatol *17*, 788-791.

Grote, E., Hao, J. C., Bennett, M. K., and Kelly, R. B. (1995). A targeting signal in VAMP regulating transport to synaptic vesicles. Cell *81*, 581-589.

Hansen, N. J., Antonin, W., and Edwardson, J. M. (1999). Identification of SNAREs involved in regulated exocytosis in the pancreatic acinar cell. J Biol Chem *274*, 22871-22876.

Hao, J. C., Salem, N., Peng, X. R., Kelly, R. B., and Bennett, M. K. (1997). Effect of mutations in vesicle-associated membrane protein (VAMP) on the assembly of multimeric protein complexes. J Neurosci *17*, 1596-1603.

Hayashi, T., McMahon, H., Yamasaki, S., Binz, T., Hata, Y., Sudhof, T. C., and Niemann, H. (1994). Synaptic vesicle membrane fusion complex: action of clostridial neurotoxins on assembly. Embo J *13*, 5051-5061.

Heidelberger, R., Heinemann, C., Neher, E., and Matthews, G. (1994). Calcium dependence of the rate of exocytosis in a synaptic terminal. Nature *371*, 513-515.

Hilbush, B. S., and Morgan, J. I. (1994). A third synaptotagmin gene, Syt3, in the mouse. Proc Natl Acad Sci U S A *91*, 8195-8199.

Holz, R. W., Senter, R. A., and Uhler, M. D. (1995). Investigation by transient transfection of the effects on regulated exocytosis of Rab3a. Methods Enzymol *257*, 221-231.

Horiuchi, H., Lippe, R., McBride, H. M., Rubino, M., Woodman, P., Stenmark, H., Rybin, V., Wilm, M., Ashman, K., Mann, M., and Zerial, M. (1997). A novel Rab5

GDP/GTP exchange factor complexed to Rabaptin-5 links nucleotide exchange to effector recruitment and function. Cell *90*, 1149-1159.

Hutt, D. M., Cardullo, R. A., Baltz, J. M., and Ngsee, J. K. (2002). Synaptotagmin VIII is localized to the mouse sperm head and may function in acrosomal exocytosis. Biol Reprod *66*, 50-56.

Hutt, D. M., Da-Silva, L. F., Chang, L. H., Prosser, D. C., and Ngsee, J. K. (2000). PRA1 inhibits the extraction of membrane-bound rab GTPase by GDI1. J Biol Chem *275*, 18511-18519.

Iida, H., Yoshinaga, Y., Tanaka, S., Toshimori, K., and Mori, T. (1999). Identification of Rab3A GTPase as an acrosome-associated small GTP-binding protein in rat sperm. Dev Biol *211*, 144-155.

Irion, U., and Leptin, M. (1999). Developmental and cell biological functions of the Drosophila DEAD-box protein abstrakt. Curr Biol *9*, 1373-1381.

Johnson, L. R., Moss, S. B., and Gerton, G. L. (1999). Maintenance of motility in mouse sperm permeabilized with streptolysin O. Biol Reprod *60*, 683-690.

Katafuchi, K., Mori, T., Toshimori, K., and Iida, H. (2000). Localization of a syntaxin isoform, syntaxin 2, to the acrosomal region of rodent spermatozoa. Mol Reprod Dev *57*, 375-383.

Kierszenbaum, A. L. (2000). Fusion of membranes during the acrosome reaction: a tale of two SNAREs. Mol Reprod Dev *57*, 309-310.

Klein, C., Philippe, N., Le Deist, F., Fraitag, S., Prost, C., Durandy, A., Fischer, A., and Griscelli, C. (1994). Partial albinism with immunodeficiency (Griscelli syndrome). J Pediatr *125*, 886-895.

Kobori, H., Miyazaki, S., and Kuwabara, Y. (2000). Characterization of intracellular Ca(2+) increase in response to progesterone and cyclic nucleotides in mouse spermatozoa. Biol Reprod *63*, 113-120.

Komuro, R., Sasaki, T., Orita, S., Maeda, M., and Takai, Y. (1996). Involvement of rabphilin-3A in Ca2+-dependent exocytosis from PC12 cells. Biochem Biophys Res Commun *219*, 435-440.

Lane, S. R., and Liu, Y. (1997). Characterization of the palmitoylation domain of SNAP-25. J Neurochem *69*, 1864-1869.

Larson, J. L., and Miller, D. J. (1999). Simple histochemical stain for acrosomes on sperm from several species. Mol Reprod Dev *52*, 445-449.

Lazar, T., Gotte, M., and Gallwitz, D. (1997). Vesicular transport: how many Ypt/Rab-GTPases make a eukaryotic cell? Trends Biochem Sci *22*, 468-472.

Lerman, J. C., Robblee, J., Fairman, R., and Hughson, F. M. (2000). Structural analysis of the neuronal SNARE protein syntaxin-1A. Biochemistry *39*, 8470-8479.

Leveque, C., el Far, O., Martin-Moutot, N., Sato, K., Kato, R., Takahashi, M., and Seagar, M. J. (1994). Purification of the N-type calcium channel associated with syntaxin and synaptotagmin. A complex implicated in synaptic vesicle exocytosis. J Biol Chem *269*, 6306-6312.

Li, C., Ullrich, B., Zhang, J. Z., Anderson, R. G., Brose, N., and Sudhof, T. C. (1995). Ca(2+)-dependent and -independent activities of neural and non-neural synaptotagmins. Nature *375*, 594-599.

Li, L. Y., Shih, H. M., Liu, M. Y., and Chen, J. Y. (2001). The cellular protein PRA1 modulates the anti-apoptotic activity of Epstein-Barr virus BHRF1, a homologue of Bcl-2, through direct interaction. J Biol Chem *276*, 27354-27362.

Liang, Z., and Li, G. (2000). Mouse prenylated Rab acceptor is a novel Golgi membrane protein. Biochem Biophys Res Commun *275*, 509-516.

Liang, Z., Veeraprame, H., Bayan, N., and Li, G. (2004). The C-terminus of prenylin is important in forming a dimer conformation necessary for endoplasmic-reticulum-to-Golgi transport. Biochem J *380*, 43-49.

Lin, J., and Addison, R. (1995). A novel integration signal that is composed of two transmembrane segments is required to integrate the Neurospora plasma membrane H(+)-ATPase into microsomes. J Biol Chem *270*, 6935-6941.

Lin, J., Liang, Z., Zhang, Z., and Li, G. (2001). Membrane topography and topogenesis of prenylated Rab acceptor (PRA1). J Biol Chem *276*, 41733-41741.

Link, E., Edelmann, L., Chou, J. H., Binz, T., Yamasaki, S., Eisel, U., Baumert, M., Sudhof, T. C., Niemann, H., and Jahn, R. (1992). Tetanus toxin action: inhibition of neurotransmitter release linked to synaptobrevin proteolysis. Biochem Biophys Res Commun *189*, 1017-1023.

Littleton, J. T., Bai, J., Vyas, B., Desai, R., Baltus, A. E., Garment, M. B., Carlson, S. D., Ganetzky, B., and Chapman, E. R. (2001). synaptotagmin mutants reveal essential functions for the C2B domain in Ca2+-triggered fusion and recycling of synaptic vesicles in vivo. J Neurosci *21*, 1421-1433.

Littleton, J. T., Stern, M., Schulze, K., Perin, M., and Bellen, H. J. (1993). Mutational analysis of Drosophila synaptotagmin demonstrates its essential role in Ca(2+)-activated neurotransmitter release. Cell *74*, 1125-1134.

Llinas, R., Sugimori, M., and Silver, R. B. (1992). Microdomains of high calcium concentration in a presynaptic terminal. Science *256*, 677-679.

Marsal, J., Ruiz-Montasell, B., Blasi, J., Moreira, J. E., Contreras, D., Sugimori, M., and Llinas, R. (1997). Block of transmitter release by botulinum C1 action on syntaxin at the squid giant synapse. Proc Natl Acad Sci U S A *94*, 14871-14876.

Martincic, I., Peralta, M. E., and Ngsee, J. K. (1997). Isolation and characterization of a dual prenylated Rab and VAMP2 receptor. J Biol Chem *272*, 26991-26998.

Martinez, I., Chakrabarti, S., Hellevik, T., Morehead, J., Fowler, K., and Andrews, N. W. (2000). Synaptotagmin VII regulates Ca(2+)-dependent exocytosis of lysosomes in fibroblasts. J Cell Biol *148*, 1141-1149.

Martinez, O., and Goud, B. (1998). Rab proteins. Biochim Biophys ACTA *1404*, 101-112.

Martin-Moutot, N., Charvin, N., Leveque, C., Sato, K., Nishiki, T., Kozaki, S., Takahashi, M., and Seagar, M. (1996). Interaction of SNARE complexes with P/Q-type calcium channels in rat cerebellar synaptosomes. J Biol Chem *271*, 6567-6570.

McMahon, H. T., Ushkaryov, Y. A., Edelmann, L., Link, E., Binz, T., Niemann, H., Jahn, R., and Sudhof, T. C. (1993). Cellubrevin is a ubiquitous tetanus-toxin substrate homologous to a putative synaptic vesicle fusion protein. Nature *364*, 346-349.

Meizel, S., Turner, K. O., and Nuccitelli, R. (1997). Progesterone triggers a wave of increased free calcium during the human sperm acrosome reaction. Dev Biol *182*, 67-75.

Menasche, G., Pastural, E., Feldmann, J., Certain, S., Ersoy, F., Dupuis, S., Wulffraat, N., Bianchi, D., Fischer, A., Le Deist, F., and de Saint Basile, G. (2000). Mutations in RAB27A cause Griscelli syndrome associated with haemophagocytic syndrome. Nat Genet *25*, 173-176.

Mercer, J. A., Seperack, P. K., Strobel, M. C., Copeland, N. G., and Jenkins, N. A. (1991). Novel myosin heavy chain encoded by murine dilute coat colour locus. Nature *349*, 709-713.

Michaut, M., De Blas, G., Tomes, C. N., Yunes, R., Fukuda, M., and Mayorga, L. S. (2001). Synaptotagmin VI Participates in the Acrosome Reaction of Human Spermatozoa. Dev Biol *235*, 521-529.

Michaut, M., Tomes, C. N., De Blas, G., Yunes, R., and Mayorga, L. S. (2000). Calcium-triggered acrosomal exocytosis in human spermatozoa requires the coordinated activation of Rab3A and N-ethylmaleimide-sensitive factor. Proc Natl Acad Sci U S A *97*, 9996-10001.

Mikoshiba, K., Fukuda, M., Moreira, J. E., Lewis, F. M., Sugimori, M., Niinobe, M., and Llinas, R. (1995). Role of the C2A domain of synaptotagmin in transmitter release as determined by specific antibody injection into the squid giant synapse preterminal. Proc Natl Acad Sci U S A *92*, 10703-10707.

Mizoguchi, A., Yano, Y., Hamaguchi, H., Yanagida, H., Ide, C., Zahraoui, A., Shirataki, H., Sasaki, T., and Takai, Y. (1994). Localization of Rabphilin-3A on the synaptic vesicle. Biochem Biophys Res Commun *202*, 1235-1243.

Mizuta, M., Inagaki, N., Nemoto, Y., Matsukura, S., Takahashi, M., and Seino, S. (1994). Synaptotagmin III is a novel isoform of rat synaptotagmin expressed in endocrine and neuronal cells. J Biol Chem *269*, 11675-11678.

Montecucco, C., and Schiavo, G. (1995). Structure and function of tetanus and botulinum neurotoxins. Q Rev Biophys *28*, 423-472.

Moyer, B. D., Allan, B. B., and Balch, W. E. (2001). Rab1 interaction with a GM130 effector complex regulates COPII vesicle cis--Golgi tethering. Traffic *2*, 268-276.

Murase, T., and Roldan, E. R. (1996). Progesterone and the zona pellucida activate different transducing pathways in the sequence of events leading to diacylglycerol generation during mouse sperm acrosomal exocytosis. Biochem J *320 (Pt 3)*, 1017-1023.

Nalefski, E. A., Wisner, M. A., Chen, J. Z., Sprang, S. R., Fukuda, M., Mikoshiba, K., and Falke, J. J. (2001). C2 domains from different Ca2+ signaling pathways display functional and mechanistic diversity. Biochemistry *40*, 3089-3100.

Nonet, M. L., Grundahl, K., Meyer, B. J., and Rand, J. B. (1993). Synaptic function is impaired but not eliminated in C. elegans mutants lacking synaptotagmin. Cell *73*, 1291-1305.

Novick, P., and Zerial, M. (1997). The diversity of Rab proteins in vesicle transport. Curr Opin Cell Biol *9*, 496-504.

Nuoffer, C., Wu, S. K., Dascher, C., and Balch, W. E. (1997). Mss4 does not function as an exchange factor for Rab in endoplasmic reticulum to Golgi transport. Molec Biol Cell *8*, 1305-1316.

O'Connor, V., Heuss, C., De Bello, W. M., Dresbach, T., Charlton, M. P., Hunt, J. H., Pellegrini, L. L., Hodel, A., Burger, M. M., Betz, H., *et al.* (1997). Disruption of syntaxin-mediated protein interactions blocks neurotransmitter secretion. Proc Natl Acad Sci U S A *94*, 12186-12191.

Ossig, R., Laufer, W., Schmitt, H. D., and Gallwitz, D. (1995). Functionality and specific membrane localization of transport GTPases carrying C-terminal membrane anchors of synaptobrevin-like proteins. EMBO J *14*, 3645-3653.

O'Toole, C. M., Arnoult, C., Darszon, A., Steinhardt, R. A., and Florman, H. M. (2000). Ca(2+) entry through store-operated channels in mouse sperm is initiated by egg ZP3 and drives the acrosome reaction. Mol Biol Cell *11*, 1571-1584.

Oyler, G. A., Higgins, G. A., Hart, R. A., Battenberg, E., Billingsley, M., Bloom, F. E., and Wilson, M. C. (1989). The identification of a novel synaptosomal-associated protein,

SNAP-25, differentially expressed by neuronal subpopulations. J Cell Biol *109*, 3039-3052.

Parlati, F., Weber, T., McNew, J. A., Westermann, B., Sollner, T. H., and Rothman, J. E. (1999). Rapid and efficient fusion of phospholipid vesicles by the alpha-helical core of a SNARE complex in the absence of an N-terminal regulatory domain. Proc Natl Acad Sci U S A *96*, 12565-12570.

Pastural, E., Barrat, F. J., Dufourcq-Lagelouse, R., Certain, S., Sanal, O., Jabado, N., Seger, R., Griscelli, C., Fischer, A., and de Saint Basile, G. (1997). Griscelli disease maps to chromosome 15q21 and is associated with mutations in the myosin-Va gene. Nat Genet *16*, 289-292.

Pereira-Leal, J. B., and Seabra, M. C. (2000). The mammalian Rab family of small GTPases: definition of family and subfamily sequence motifs suggests a mechanism for functional specificity in the Ras superfamily. J Mol Biol *301*, 1077-1087.

Perin, M. S., Brose, N., Jahn, R., and Sudhof, T. C. (1991). Domain structure of synaptotagmin (p65). J Biol Chem *266*, 623-629.

Perin, M. S., Fried, V. A., Mignery, G. A., Jahn, R., and Sudhof, T. C. (1990). Phospholipid binding by a synaptic vesicle protein homologous to the regulatory region of protein kinase C. Nature *345*, 260-263.

Peter, F., Nuoffer, C., Pind, S. N., and Balch, W. E. (1994). Guanine nucleotide dissociation inhibitor is essential for rab1 function in budding from the endoplasmic reticulum and transport through the Golgi stack. J Cell Biol *126*, 1393-1406.

Pind, S. N., Nuoffer, C., McCaffery, J. M., Plutner, H., Davidson, H. W., Farquhar, M. G., and Balch, W. E. (1994). Rab1 and Ca2+ are required for the fusion of carrier vesicles mediating endoplasmic reticulum to Golgi transport. J Cell Biol *125*, 239-252.

Ponting, C. P., and Parker, P. J. (1996). Extending the C2 domain family: C2s in PKCs delta, epsilon, eta, theta, phospholipases, GAPs, and perforin. Protein Sci *5*, 162-166.

Protopopov, V., Govindan, B., Novick, P., and Gerst, J. E. (1993). Homologs of the synaptobrevin/VAMP family of synaptic vesicle proteins function on the late secretory pathway in S. cerevisiae. Cell *74*, 855-861.

Ramalho-Santos, J., Moreno, R. D., Sutovsky, P., Chan, A. W., Hewitson, L., Wessel, G. M., Simerly, C. R., and Schatten, G. (2000). SNAREs in mammalian sperm: possible implications for fertilization. Dev Biol *223*, 54-69.

Ramalho-Santos, J., Moreno, R. D., Wessel, G. M., Chan, E. K., and Schatten, G. (2001). Membrane trafficking machinery components associated with the mammalian acrosome during spermiogenesis. Exp Cell Res *267*, 45-60.

Rao, S. K., Huynh, C., Proux-Gillardeaux, V., Galli, T., and Andrews, N. W. (2004). Identification of SNAREs involved in synaptotagmin VII-regulated lysosomal exocytosis. J Biol Chem *279*, 20471-20479.

Ravichandran, V., Chawla, A., and Roche, P. A. (1996). Identification of a novel syntaxin- and synaptobrevin/VAMP-binding protein, SNAP-23, expressed in non-neuronal tissues. J Biol Chem *271*, 13300-13303.

Reddy, A., Caler, E. V., and Andrews, N. W. (2001). Plasma membrane repair is mediated by Ca(2+)-regulated exocytosis of lysosomes. Cell *106*, 157-169.

Regazzi, R., Sadoul, K., Meda, P., Kelly, R. B., Halban, P. A., and Wollheim, C. B. (1996). Mutational analysis of VAMP domains implicated in Ca2+-induced insulin exocytosis. Embo J *15*, 6951-6959.

Rickman, C., Craxton, M., Osborne, S., and Davletov, B. (2004). Comparative analysis of tandem C2 domains from the mammalian synaptotagmin family. Biochem J *378*, 681-686.

Rodriguez, A., Martinez, I., Chung, A., Berlot, C. H., and Andrews, N. W. (1999). cAMP regulates Ca2+-dependent exocytosis of lysosomes and lysosome-mediated cell invasion by trypanosomes. J Biol Chem *274*, 16754-16759.

Rodriguez, A., Webster, P., Ortego, J., and Andrews, N. W. (1997). Lysosomes behave as Ca2+-regulated exocytic vesicles in fibroblasts and epithelial cells. J Cell Biol *137*, 93-104.

Roldan, E. R., Murase, T., and Shi, Q. X. (1994). Exocytosis in spermatozoa in response to progesterone and zona pellucida. Science *266*, 1578-1581.

Rybin, V., Ullrich, O., Rubino, M., Alexandrov, K., Simon, I., Seabra, C., Goody, R., and Zerial, M. (1996). GTPase activity of Rab5 acts as a timer for endocytic membrane fusion. Nature *383*, 266-269.

Sasaki, T., Kikuchi, A., Araki, S., Hata, Y., Isomura, M., Kuroda, S., and Takai, Y. (1990). Purification and characterization from bovine brain cytosol of a protein that inhibits the dissociation of GDP from and the subsequent binding of GTP to smg p25A, a ras p21-like GTP-binding protein. J Biol Chem *265*, 2333-2337.

Schiavo, G., Benfenati, F., Poulain, B., Rossetto, O., Polverino de Laureto, P., DasGupta, B. R., and Montecucco, C. (1992a). Tetanus and botulinum-B neurotoxins block neurotransmitter release by proteolytic cleavage of synaptobrevin. Nature *359*, 832-835.

Schiavo, G., Malizio, C., Trimble, W. S., Polverino de Laureto, P., Milan, G., Sugiyama, H., Johnson, E. A., and Montecucco, C. (1994). Botulinum G neurotoxin cleaves VAMP/synaptobrevin at a single Ala-Ala peptide bond. J Biol Chem *269*, 20213-20216.

Schiavo, G., Poulain, B., Rossetto, O., Benfenati, F., Tauc, L., and Montecucco, C. (1992b). Tetanus toxin is a zinc protein and its inhibition of neurotransmitter release and protease activity depend on zinc. Embo J *11*, 3577-3583.

Schiavo, G., Rossetto, O., Catsicas, S., Polverino de Laureto, P., DasGupta, B. R., Benfenati, F., and Montecucco, C. (1993a). Identification of the nerve terminal targets of botulinum neurotoxin serotypes A, D, and E. J Biol Chem *268*, 23784-23787.

Schiavo, G., Shone, C. C., Bennett, M. K., Scheller, R. H., and Montecucco, C. (1995). Botulinum neurotoxin type C cleaves a single Lys-Ala bond within the carboxyl-terminal region of syntaxins. J Biol Chem *270*, 10566-10570.

Schiavo, G., Shone, C. C., Rossetto, O., Alexander, F. C., and Montecucco, C. (1993b). Botulinum neurotoxin serotype F is a zinc endopeptidase specific for VAMP/synaptobrevin. J Biol Chem *268*, 11516-11519.

Schiavo, G., Stenbeck, G., Rothman, J. E., and Sollner, T. H. (1997). Binding of the synaptic vesicle v-SNARE, synaptotagmin, to the plasma membrane t-SNARE, SNAP-25, can explain docked vesicles at neurotoxin-treated synapses. Proc Natl Acad Sci U S A *94*, 997-1001.

Schimmoller, F., Simon, I., and Pfeffer, S. R. (1998). Rab GTPases, directors of vesicle docking. J Biol Chem *273*, 22161-22164.

Schluter, O. M., Schnell, E., Verhage, M., Tzonopoulos, T., Nicoll, R. A., Janz, R., Malenka, R. C., Geppert, M., and Sudhof, T. C. (1999). Rabphilin knock-out mice reveal that rabphilin is not required for rab3 function in regulating neurotransmitter release. J Neurosci *19*, 5834-5846.

Schoch, S., Castillo, P. E., Jo, T., Mukherjee, K., Geppert, M., Wang, Y., Schmitz, F., Malenka, R. C., and Sudhof, T. C. (2002). RIM1alpha forms a protein scaffold for regulating neurotransmitter release at the active zone. Nature *415*, 321-326.

Schoch, S., Deak, F., Konigstorfer, A., Mozhayeva, M., Sara, Y., Sudhof, T. C., and Kavalali, E. T. (2001). SNARE function analyzed in synaptobrevin/VAMP knockout mice. Science *294*, 1117-1122.

Schu, P. V., Takegawa, K., Fry, M. J., Stack, J. H., Waterfield, M. D., and Emr, S. D. (1993). Phosphatidylinositol 3-kinase encoded by yeast VPS34 gene essential for protein sorting. Science *260*, 88-91.

Schulz, J. R., Sasaki, J. D., and Vacquier, V. D. (1998). Increased association of synaptosome-associated protein of 25 kDa with syntaxin and vesicle-associated membrane protein following acrosomal exocytosis of sea urchin sperm. J Biol Chem *273*, 24355-24359.

Schulz, J. R., Wessel, G. M., and Vacquier, V. D. (1997). The exocytosis regulatory proteins syntaxin and VAMP are shed from sea urchin sperm during the acrosome reaction. Dev Biol *191*, 80-87.

Segev, N. (2001a). Ypt and Rab GTPases: insight into functions through novel interactions. Curr Opin Cell Biol *13*, 500-511.

Segev, N. (2001b). Ypt/rab gtpases: regulators of protein trafficking. Sci STKE *2001*, RE11.

Sekiya, K., Satoh, R., Danbara, H., and Futaesaku, Y. (1993). A ring-shaped structure with a crown formed by streptolysin O on the erythrocyte membrane. J Bacteriol *175*, 5953-5961.

Shao, X., Li, C., Fernandez, I., Zhang, X., Sudhof, T. C., and Rizo, J. (1997). Synaptotagmin-syntaxin interaction: the C2 domain as a Ca2+-dependent electrostatic switch. Neuron *18*, 133-142.

Sheng, Z. H., Rettig, J., Cook, T., and Catterall, W. A. (1996). Calcium-dependent interaction of N-type calcium channels with the synaptic core complex. Nature *379*, 451-454.

Shi, Q. X., and Roldan, E. R. (1995). Evidence that a GABAA-like receptor is involved in progesterone-induced acrosomal exocytosis in mouse spermatozoa. Biol Reprod *52*, 373-381.

Shirataki, H., Kaibuchi, K., Sakoda, T., Kishida, S., Yamaguchi, T., Wada, K., Miyazaki, M., and Takai, Y. (1993). Rabphilin-3A, a putative target protein for smg p25A/rab3A p25 small GTP-binding protein related to synaptotagmin. Mol Cell Biol *13*, 2061-2068.

Shone, C. C., and Roberts, A. K. (1994). Peptide substrate specificity and properties of the zinc-endopeptidase activity of botulinum type B neurotoxin. Eur J Biochem *225*, 263-270.

Sivars, U., Aivazian, D., and Pfeffer, S. R. (2003). Yip3 catalyses the dissociation of endosomal Rab-GDI complexes. Nature *425*, 856-859.

Skach, W. R., and Lingappa, V. R. (1993). Amino-terminal assembly of human P-glycoprotein at the endoplasmic reticulum is directed by cooperative actions of two internal sequences. J Biol Chem *268*, 23552-23561.

Sollner, T., Bennett, M. K., Whiteheart, S. W., Scheller, R. H., and Rothman, J. E. (1993). A protein assembly-disassembly pathway in vitro that may correspond to sequential steps of synaptic vesicle docking, activation, and fusion. Cell *75*, 409-418.

Spungin, B., Margalit, I., and Breitbart, H. (1995). Sperm exocytosis reconstructed in a cell-free system: evidence for the involvement of phospholipase C and actin filaments in membrane fusion. J Cell Sci *108 (Pt 6)*, 2525-2535.

Steegmaier, M., Yang, B., Yoo, J. S., Huang, B., Shen, M., Yu, S., Luo, Y., and Scheller, R. H. (1998). Three novel proteins of the syntaxin/SNAP-25 family. J Biol Chem *273*, 34171-34179.

Stenmark, H., Vitale, G., Ullrich, O., and Zerial, M. (1995). Rabaptin-5 is a direct effector of the small GTPase Rab5 in endocytic membrane fusion. Cell *83*, 423-432.

Sudhof, T. C., De Camilli, P., Niemann, H., and Jahn, R. (1993). Membrane fusion machinery: insights from synaptic proteins. Cell *75*, 1-4.

Sutton, R. B., Fasshauer, D., Jahn, R., and Brunger, A. T. (1998). Crystal structure of a SNARE complex involved in synaptic exocytosis at 2.4 A resolution. Nature *395*, 347-353.

Takai, Y., Kaibuchi, K., Kikuchi, A., Sasaki, T., and Shirataki, H. (1993). Regulators of small GTPases. Ciba Found Symp *176*, 128--146.

Teng, F. Y., Wang, Y., and Tang, B. L. (2001). The syntaxins. Genome Biol *2*, REVIEWS3012.

Terrian, D. M., and White, M. K. (1997). Phylogenetic analysis of membrane trafficking proteins: a family reunion and secondary structure predictions. Eur J Cell Biol *73*, 198-204.

Thompson, C. C. (1996). Thyroid hormone-responsive genes in developing cerebellum include a novel synaptotagmin and a hairless homolog. J Neurosci *16*, 7832-7840.

Thorne-Tjomsland, G., Clermont, Y., and Hermo, L. (1988). Contribution of the Golgi apparatus components to the formation of the acrosomic system and chromatoid body in rat spermatids. Anat Rec *221*, 591-598.

Tomes, C. N., Michaut, M., De Blas, G., Visconti, P., Matti, U., and Mayorga, L. S. (2002). SNARE complex assembly is required for human sperm acrosome reaction. Dev Biol *243*, 326-338.

Trimble, W. S., Gray, T. S., Elferink, L. A., Wilson, M. C., and Scheller, R. H. (1990). Distinct patterns of expression of two VAMP genes within the rat brain. J Neurosci *10*, 1380-1387.

Tulsiani, D. R., Abou-Haila, A., Loeser, C. R., and Pereira, B. M. (1998). The biological and functional significance of the sperm acrosome and acrosomal enzymes in mammalian fertilization. Exp Cell Res *240*, 151-164.

Turner, M. D., Plutner, H., and Balch, W. E. (1997). A rab GTPase is required for homotypic assembly of the endoplasmic reticulum. J Biol Chem *272*, 13479-13483.

Ubach, J., Lao, Y., Fernandez, I., Arac, D., Sudhof, T. C., and Rizo, J. (2001). The C2B domain of synaptotagmin I is a Ca2+-binding module. Biochemistry *40*, 5854-5860.

Ubach, J., Zhang, X., Shao, X., Sudhof, T. C., and Rizo, J. (1998). Ca2+ binding to synaptotagmin: how many Ca2+ ions bind to the tip of a C2-domain? Embo J *17*, 3921-3930.

Ullrich, O., Stenmark, H., Alexandrov, K., Huber, L. A., Kaibuchi, K., Sasaki, T., Takai, Y., and Zerial, M. (1993). Rab GDP dissociation inhibitor as a general regulator for the membrane association of rab proteins. J Biol Chem *268*, 18143-18150.

Vaidyanathan, V. V., Yoshino, K., Jahnz, M., Dorries, C., Bade, S., Nauenburg, S., Niemann, H., and Binz, T. (1999). Proteolysis of SNAP-25 isoforms by botulinum neurotoxin types A, C, and E: domains and amino acid residues controlling the formation of enzyme-substrate complexes and cleavage. J Neurochem *72*, 327-337.

Veit, M., Sollner, T. H., and Rothman, J. E. (1996). Multiple palmitoylation of synaptotagmin and the t-SNARE SNAP-25. FEBS Lett *385*, 119-123.

Velasco, A., Hendricks, L., Moremen, K. W., Tulsiani, D. R., Touster, O., and Farquhar, M. G. (1993). Cell type-dependent variations in the subcellular distribution of alpha-mannosidase I and II. J Cell Biol *122*, 39-51.

Volinia, S., Dhand, R., Vanhaesebroeck, B., MacDougall, L. K., Stein, R., Zvelebil, M. J., Domin, J., Panaretou, C., and Waterfield, M. D. (1995). A human phosphatidylinositol 3-kinase complex related to the yeast Vps34p-Vps15p protein sorting system. Embo J *14*, 3339-3348.

von Poser, C., Ichtchenko, K., Shao, X., Rizo, J., and Sudhof, T. C. (1997). The evolutionary pressure to inactivate. A subclass of synaptotagmins with an amino acid substitution that abolishes Ca2+ binding. Journal of Biological Chemistry *272*, 14314-14319.

von Poser, C., and Sudhof, T. C. (2000). Synaptotagmin 13: structure and expression of a novel synaptotagmin. Eur J Cell Biol *80*, 41-47.

von Poser, C., and Sudhof, T. C. (2001). Synaptotagmin 13: structure and expression of a novel synaptotagmin. Eur J Cell Biol *80*, 41-47.

Wada, I., Rindress, D., Cameron, P. H., Ou, W. J., Doherty, J. J. d., Louvard, D., Bell, A. W., Dignard, D., Thomas, D. Y., and Bergeron, J. J. (1991). SSR alpha and associated calnexin are major calcium binding proteins of the endoplasmic reticulum membrane. J Biol Chem *266*, 19599-19610.

Wada, M., Nakanishi, H., Satoh, A., Hirano, H., Obaishi, H., Matsuura, Y., and Takai, Y. (1997). Isolation and characterization of a GDP/GTP exchange protein specific for the Rab3 subfamily small G proteins. J Biol Chem *272*, 3875-3878.

Walev, I., Bhakdi, S. C., Hofmann, F., Djonder, N., Valeva, A., Aktories, K., and Bhakdi, S. (2001). Delivery of proteins into living cells by reversible membrane permeabilization with streptolysin-O. Proc Natl Acad Sci U S A *98*, 3185-3190.

Wang, Y., Okamoto, M., Schmitz, F., Hofmann, K., and Sudhof, T. C. (1997). Rim is a putative Rab3 effector in regulating synaptic-vesicle fusion. Nature *388*, 593-598.

Washbourne, P., Pellizzari, R., Baldini, G., Wilson, M. C., and Montecucco, C. (1997). Botulinum neurotoxin types A and E require the SNARE motif in SNAP-25 for proteolysis. FEBS Lett *418*, 1-5.

Wassarman, P. M., Jovine, L., and Litscher, E. S. (2001). A profile of fertilization in mammals. Nat Cell Biol *3*, E59-64.

Weber, T., Zemelman, B. V., McNew, J. A., Westermann, B., Gmachl, M., Parlati, F., Sollner, T. H., and Rothman, J. E. (1998). SNAREpins: minimal machinery for membrane fusion. Cell *92*, 759-772.

Weimbs, T., Low, S. H., Chapin, S. J., Mostov, K. E., Bucher, P., and Hofmann, K. (1997). A conserved domain is present in different families of vesicular fusion proteins: a new superfamily. Proc Natl Acad Sci U S A *94*, 3046-3051.

Weimbs, T., Mostov, K., Low, S. H., and Hofmann, K. (1998). A model for structural similarity between different SNARE complexes based on sequence relationships. Trends Cell Biol *8*, 260-262.

Whiteheart, S. W., Griff, I. C., Brunner, M., Clary, D. O., Mayer, T., Buhrow, S. A., and Rothman, J. E. (1993). SNAP family of NSF attachment proteins includes a brain-specific isoform. Nature *362*, 353-355.

Williamson, L. C., Halpern, J. L., Montecucco, C., Brown, J. E., and Neale, E. A. (1996). Clostridial neurotoxins and substrate proteolysis in intact neurons: botulinum neurotoxin C acts on synaptosomal-associated protein of 25 kDa. J Biol Chem *271*, 7694-7699.

Wilson, S. M., Yip, R., Swing, D. A., O'Sullivan, T. N., Zhang, Y., Novak, E. K., Swank, R. T., Russell, L. B., Copeland, N. G., and Jenkins, N. A. (2000). A mutation in Rab27a causes the vesicle transport defects observed in ashen mice. Proc Natl Acad Sci U S A *97*, 7933-7938.

Wiser, O., Tobi, D., Trus, M., and Atlas, D. (1997). Synaptotagmin restores kinetic properties of a syntaxin-associated N-type voltage sensitive calcium channel. FEBS Lett *404*, 203-207.

Yamada, W. M., and Zucker, R. S. (1992). Time course of transmitter release calculated from simulations of a calcium diffusion model. Biophys J *61*, 671-682.

Yamasaki, S., Baumeister, A., Binz, T., Blasi, J., Link, E., Cornille, F., Roques, B., Fykse, E. M., Sudhof, T. C., Jahn, R., and et al. (1994a). Cleavage of members of the synaptobrevin/VAMP family by types D and F botulinal neurotoxins and tetanus toxin. J Biol Chem *269*, 12764-12772.

Yamasaki, S., Binz, T., Hayashi, T., Szabo, E., Yamasaki, N., Eklund, M., Jahn, R., and Niemann, H. (1994b). Botulinum neurotoxin type G proteolyses the Ala81-Ala82 bond of rat synaptobrevin 2. Biochem Biophys Res Commun *200*, 829-835.

Yang, X., Matern, H. T., and Gallwitz, D. (1998). Specific binding to a novel and essential Golgi membrane protein (Yip1p) functionally links the transport GTPases Ypt1p and Ypt31p. EMBO J *17*, 4954-4963.

Yunes, R., Michaut, M., Tomes, C., and Mayorga, L. S. (2000). Rab3A triggers the acrosome reaction in permeabilized human spermatozoa. Biol Reprod *62*, 1084-1089.

Zaneveld, L. J. D. a. d. J., C. J. (1991). A Comparative Overview of Mammalian Fertilization. In, B. a. O. R. Dunbar, M., ed. (New York, Plenum Press), pp. 1265-1274.

Zerial, M., and McBride, H. (2001). Rab proteins as membrane organizers. Nat Rev Mol Cell Biol *2*, 107-117.